UNIVERSITY OF CALIFORNIA, SAN DIEGO

Control and Optimization of Wave-Induced Motion of Ramp-Interconnected Craft for Cargo Transfer

A Thesis submitted in partial satisfaction of the requirements
for the degree Master of Science

in

Engineering Sciences (Mechanical Engineering)

by

Jacob Toubi

Committee in charge:

Professor Miroslav Krstic, Chair
Professor Kenneth Kreutz-Delgado
Professor Raymond de Callafon

2009

The Thesis of Jacob Toubi is approved and it is acceptable in quality form for publication on microfilm and electronically:

Chair

University of California, San Diego

2009

Dedication

I want to dedicate this thesis to my parents, Moshe and Yaffa Toubi, who have encouraged me throughout my childhood to pursue a higher education after high school and eventually a master's degree following my bachelor's degree in mechanical engineering.

Table of Contents

List of Figures

List of Tables

Acknowledgements

I would like to acknowledge Professor Miroslav Krstic for giving me the opportunity to be involved in this research endeavor and his guidance throughout my graduate schooling.

I would like to acknowledge Stephen Oonk for his preliminary work on this research topic by building the foundation of the various models, which my thesis expands on and uses for control applications. For instance, the figures of the half cylinder and rectangular ramp with their respective moment of inertia equations were taken directly from his thesis, in addition to all other geometry related values used in the model. Also the phase calculations of section 2.3 were summarized from Stephen's thesis, although I derived them independently as well.

I would like to acknowledge Joseph Doblack for his work on the multiple parameter extremum seeking results of section 4.3 and included in this thesis for the sake of completion.

ABSTRACT OF THE THESIS

Control and Optimization of Wave-Induced Motion of Ramp-Interconnected Craft for Cargo Transfer

by

Jacob Toubi

Master of Science in Engineering Sciences (Mechanical Engineering)

University of California, San Diego, 2009

Professor Miroslav Krstic, Chair

A two vessel interconnected by a ramp system was modeled using SimMechanics toolbox in Simulink. Both vessels were modeled as half cylinders and the ramp as a rectangular solid. Although the equations of motion for the system were derived, the SimMechanics model proved to be more efficient to implement certain control and optimization techniques and is emphasized throughout the thesis. This thesis documents different attempts to control and optimize the various motions of the system using passive and active methods. The passive methods include extremum seeking tuning of two parameters namely the ramp length and wave heading angle to reduce the pitch angle amplitude at the joint connecting the ramp and T-Craft. The

second method employed mimics automotive shock absorbers to reduce relative motion between each vessel and ramp to reduce overall ramp motions. In both methods the results concur with the goal of the problem statement of stabilizing ramp/vessel motions. Applying the ES algorithm to tune the ramp length and wave heading angle reduced the pitch amplitude by 67% (from approx. 15 to 5 degrees) and applying the shock absorbers in the pitch joint case of the system reduced the pitch angle amplitude by two orders of magnitude (from approx. 10 to 0.1 degrees).

The active method explored is installing a control moment gyroscope on the T-Craft to stabilize its roll motion. The results show that roll motion is decreased to lie within the stability region of one degree in amplitude and have a feasible size and weight requirement.

Introduction

The transfer of cargo over a ramp from a LMSR (large, medium-speed, roll-on/roll-off) vessel to a connector vessel in high sea states represents significant challenges for ship and control system designers. The goal of this project is to determine the actuation/sensing requirements and to devise control and real-time optimization algorithms to minimize the amplitude of oscillation of the interconnected ramp primarily in the roll, pitch and heave degree of freedoms (DOF).

The system investigated consists of a Sea Base (LMSR) and a T-Craft (the connector vessel) connected by a ramp in a bow to stern configuration. Due to the nonlinear nature of the three interconnected dynamical model the resulting motions are quite complex and as the initial effort the system was modeled non-analytically in MATLAB, Simulink, and SimMechanics. In order to simplify the problem, yet maintain a reasonable level of complexity, a few assumptions and simplifications were made. For example, the simplification of the ocean surface is modeled as linear waves which are a superposition of sine waves with differing phase that exert surface forces through a spring-damper connection at various points on the vessels. This model is based on the ocean behaving like a second order differential equation system. The vessels were modeled as half cylinders and the ramp as a rectangular solid with three joint cases explored that connect each ship to the ramp, which influence the amplitude of the angle oscillations per degree of freedom considered as discussed below.

Following the initial SimMechanics model implementation the equations of motion were derived for the system using Lagrangian mechanics. However, the

SimMechanics model proved to be a simpler way to perform control and optimization techniques without the need to alter the equations of motion. The solution to the equations of motion provides a cross reference with the results of the rigid body simulations which validate each other.

One of the approaches used to minimize the amplitude of the ramp angles involved applying the extremum seeking algorithm to optimize the ramp length and wave heading angle. Extremum Seeking (ES) was first implemented in a 2D sense to optimize the ramp length for a set wave heading angle to achieve the desired minimum angle amplitudes. It is named 2D to correspond to the amount of directions the system moves namely heave (z-axis) and surge (x-axis). The 3D case refers to optimizing both ramp length and wave heading to achieve the minimum values for a given cost function on the desired parameters. In our case the cost function was a function of ramp length and pitch angle amplitude between T-Craft and ramp. The three motions accounted for in the 3D case are heave, surge, and yaw (rotation about z-axis).

To predict the neighborhood of a local minimum off line 3D cost plots were produced, which show the dependence of the angle amplitudes to ramp length and wave orientation. A longer ramp has been found to decrease the magnitude of the pitch angle oscillation, but fails to decrease the roll angle magnitudes. In addition if the ramp length is increased beyond a reasonable range it introduces an undesirable weight issue and infeasibility in the design. In order to force the ES algorithm to optimize to a feasible ramp length a penalty on the ramp length was introduced. This ramp penalty multiplied by the pitch angle amplitude per time step of simulation comprised the cost function. The penalty and multiplication of the terms in the cost

function increased the convexity of the cost plots, making the local minimum more pronounced.

Another approach to decrease the amplitude of angle oscillations was to implement passive control techniques into the system. Passive control is integrated into the system by mimicking automotive shock absorbers with springs and dampers in the joints between each vessel and the ramp. The results confirmed the intuition and showed a decrease in angle oscillations for the three DOFs in the joints (pitch, roll, yaw) considered.

The final method of control implemented on the T-Craft is the active control moment gyroscope, which is designed to stabilize roll motion. The roll motion of the T-Craft, coupled with the precession motion of the gyroscope is modeled using the equations of motion derived from the conservation of angular momentum law. A linear controller is then designed to influence the gyroscope's precession rate, which provides an opposing moment in the roll DOF. The results successfully show that a control moment gyroscope can reduce the roll angle amplitudes of the T-Craft to allow for safe cargo transfer between the Sea Base.

Chapter 1. System Models

1.1. Ship Model

The SimMechanics model consists of a series of rigid bodies acted on by a wave force model at the corners of each vessel. Each ship is modeled as a monohull as shown in Figure 1.1 meaning there is only one hull submerged beneath the water. Although this is an over simplifying assumption of the actual shape, the control techniques executed can be readily applied to any vessel model desired. Figure 1.2 shows the SimMechanics representation of the system model. The specific mass and dimensions of the system's individual components are given in Table 1.1.

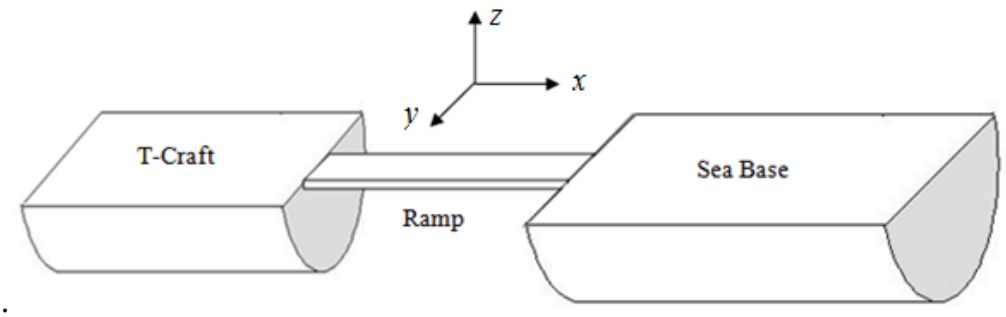

Figure 1.1: System model using half-cylinder ships and rectangular ramp

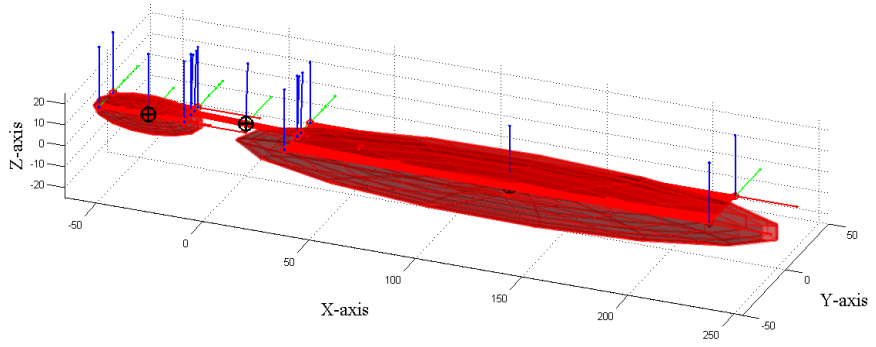

Figure 1.2: SimMechanics representation of the system model

Table 1.1: Vessel dimensions and mass used in SimMechanics model

Variable	T-Craft	Sea Base	Ramp	Abrams Tank
Length [m]	40	200	10	7.9
Width [m]	16	30	4	3.7
Height [m]	8	15	0.05	2.4
Radius [m]	8	15	---	---
Mass [metric ton]	2,721	45,359	16	6

After picking the shape of the ship models we need to calculate the moment of inertia for the half-cylinder and rectangular prism about the three axes. Note: in the SimMechanics model, the coordinate system is rotated with respect to the figures below.

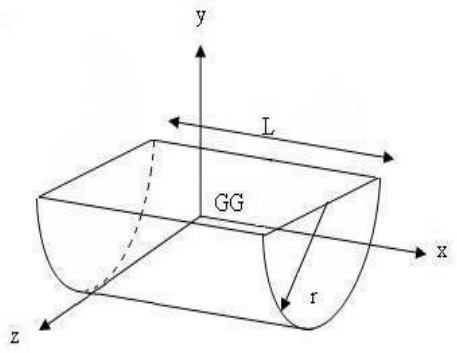

Figure 1.3: Half-cylinder model of ships

Moments of inertia through center of gravity:

$$I_{XX} = \left(\frac{1}{2} - \frac{16}{9\pi^2}\right) mr^2$$

$$I_{YY} = \frac{1}{4} mr^2 + \frac{1}{12} mL^2$$

$$I_{ZZ} = \left(\frac{1}{4} - \frac{16}{9\pi^2}\right) mr^2 + \frac{1}{12} mL^2$$

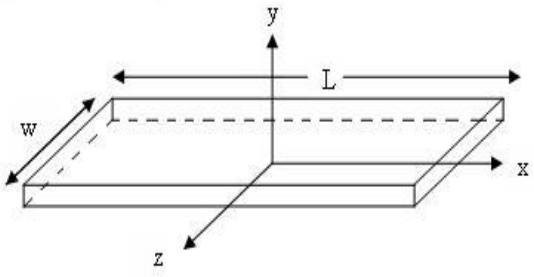

Figure 1.4: Rectangular prism model of ramp

Moments of inertia through center of gravity (*negligable thickness*):

$$I_{XX} = \frac{1}{12} mw^2$$

$$I_{YY} = \frac{1}{4} m\left(w^2 + L^2\right)$$

$$I_{ZZ} = \frac{1}{12} mL^2$$

The forthcoming terms and calculations are essential in the study of ship hydrostatics and are adapted from Biran [2]. The waterplane area A_w is a horizontal slice of a ship's hull at the water level and equals the length of the ship multiplied by the horizontal distance (c) from the starboard (right) to port (left) measured at the water level. The length of the vessel goes into the paper in Figure 1.5. The vertical distance from the water level to the bottom of the hull defines the drought (T) and can be determined from the drought scale that usually exists on the side of the hull. Figure 1.5 depicts the cross section of a half cylinder ship with the relevant variables to calculate the waterplane area.

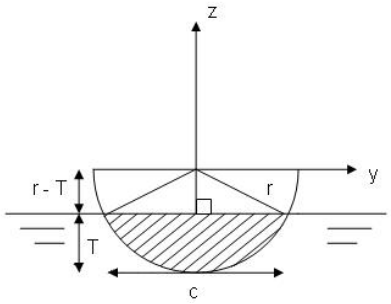

Figure 1.5: Cross section of half cylinder ship submerged in water

To express the variable c in terms of the drought, T and radius of the cylinder (r), we apply the Pythagorean Theorem on one of the right triangles above the waterline.

$$\left(\frac{c}{2}\right)^2 + \left(r-T\right)^2 = r^2 \Rightarrow c = 2\sqrt{r^2 - \left(r-T\right)^2} = 2\sqrt{2Tr - T^2} \qquad (1.1)$$

The waterplane area is then expressed as

$$A_W = cL = 2L\sqrt{2Tr - T^2} = 2L\sqrt{r^2 - \left(r - T\right)^2} \tag{1.2}$$

Another important metric is the metacentric height, $\overline{GM}_i$ and greatly influences the stability of the ship. The variable i differentiates between the transverse and longitudinal metacentric heights, which apply to roll and pitch motions and are denoted $\overline{GM}_R$ and $\overline{GM}_P$ respectively. The transverse metacentric height equals the distance from the ship's center of gravity (G) to its metacenter (M) for heel (roll) motion. The longitudinal metacentric height is computed the same way except the metacenter used corresponds to pitch motion. For small angles of heel, the metacenter is assumed to be a fixed point thus allowing us to use the aforementioned definition of metacentric height. To describe the metacenter we first need to define the center of buoyancy. The center of buoyancy (B) defines the center of the volume of water displaced by the vessel's hull and lies below the center of gravity for stable ship geometries. When a ship heels (rotates about the x-axis) clockwise, the point B displaces laterally, which is to the right in Figure 1.6. The metacenter (M) is the intersection point between the original vertical line through the center of buoyancy, and the new vertical line through the translated center of buoyancy.

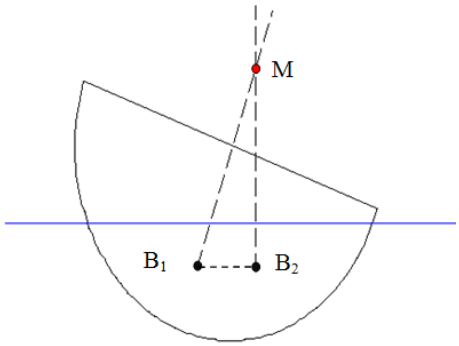

Figure 1.6: Ship heeling to show metacenter

The metacentric height is also given by the equation

$$\overline{GM} = \overline{KB} + \overline{BM} - \overline{KG} \tag{1.3}$$

where $\overline{KB}$ is the distance from the keel to the center of buoyancy, $\overline{BM}$ is the distance from center of buoyancy to the metacenter, and $\overline{KG}$ is the distance from the keel to the center of gravity. These terms were calculated for the half cylinder model in Oonk [6] and only the results are presented here. Note for the calculations below the keel is located at z = 0.

$$\overline{KB}_R = r - \frac{\frac{2}{3}r^3 \sin^3\left(\cos^{-1}\left(\frac{r-T}{r}\right)\right)}{r^2 \cos^{-1}\left(\frac{r-T}{r}\right) - (r-T)\sqrt{r^2-(r-T)^2}} \tag{1.4}$$

$$\overline{KB}_P = \frac{1}{2}T \tag{1.5}$$

$$\overline{BM}_R = \frac{I_R}{\nabla} = \frac{\frac{Lw^3}{12}}{L\left[r^2 \cos^{-1}\left(\frac{r-T}{r}\right) - (r-T)\sqrt{r^2-(r-T)^2}\right]} \tag{1.6}$$

$$\overline{BM}_P = \frac{I_P}{\nabla} = \frac{\frac{wL^3}{12}}{L\left[r^2 \cos^{-1}\left(\frac{r-T}{r}\right) - (r-T)\sqrt{r^2-(r-T)^2}\right]} \tag{1.7}$$

where I_P and I_R are the moment of inertias of the waterplane area about the respective axis of inclination, and ∇ is the volume of the immersed part of the ship. The volume is the area of the submerged hull multiplied by the length of the ship and is given as

$$\nabla = L\left[r^2 \cos^{-1}\left(\frac{r-T}{r}\right) - (r-T)\sqrt{r^2-(r-T)^2}\right] \tag{1.8}$$

After combining the individual terms we arrive at the final metacentric height values. These values are used to calculate the roll and pitch spring constants for the SimMechanics model as will be expanded on below.

$$\overline{GM}_R = \overline{KB}_R + \overline{BM}_R - \overline{KG}_R \tag{1.9}$$

$$\overline{GM}_R = r - \frac{\frac{2}{3}r^3 \sin^3\left(\cos^{-1}\left(\frac{r-T}{r}\right)\right)}{r^2 \cos^{-1}\left(\frac{r-T}{r}\right) - (r-T)\sqrt{r^2-(r-T)^2}} + \frac{\frac{Lw^3}{12}}{L\left[r^2 \cos^{-1}\left(\frac{r-T}{r}\right) - (r-T)\sqrt{r^2-(r-T)^2}\right]} - \left(r - \frac{4r}{3\pi}\right) \tag{1.10}$$

$$\overline{GM}_P = \overline{KB}_P + \overline{BM}_P - \overline{KG}_P \tag{1.11}$$

$$\overline{GM}_P = \frac{1}{2}T + \frac{\frac{wL^3}{12}}{L\left[r^2\cos^{-1}\left(\frac{r-T}{r}\right) - (r-T)\sqrt{r^2-(r-T)^2}\right]} - \frac{r}{2} \qquad (1.12)$$

1.2. **Joint Models**

There are three joint models proposed to connect each vessel with the ramp; they include: pitch (P) joint, pitch-roll (PR) joint, and pitch-roll-yaw (PRY) joint. The complexity of implementing each joint increases with each DOF. The simplest is the pitch joint, which acts like a door hinge and is the one emphasized throughout the research. Figure 1.7 shows each DOF separately to visualize its motion; however the above joint types go from one to three DOF per joint.

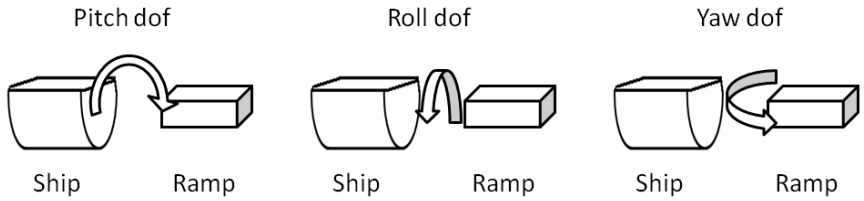

Figure 1.7: Degree of freedoms in joints between ship and ramp

If the system's equations of motion are derived for each joint model, the number of first order differential equations describing its motion would be: 16 for a pitch joint, 20 for a pitch-roll joint and 24 for a pitch-roll-yaw joint. Using the pitch joint system model, we have eight DOFs. If we first assume the ship-ramp-ship system to be a rigid body we arrive at the usual six DOFs of a rigid body: surge, sway, heave, roll, pitch and yaw. These correspond to all translational and rotary motion along a Euclidean coordinate system. The pitch joint introduces two more DOFs where the T-

Craft and Sea Base can pitch independently of the system at large. Summing the two, gives eight DOFs and since each DOF can be thought of as a 2^{nd} order differential equation, given the proper change of variables can be expressed as a system of 16 first order differential equations as shown below. The same process can be used to arrive at number of equations required for the other two joint models.

1.3. **Open Loop Response of System**

Using the above calculated ship parameters in the SimMechanics model and applying the wave force inputs gives the open loop response of the system. The responses are considered baseline values of the state variables, which through control and optimization can be reduced or stabilized. The most important state variables to consider for our goal of safe cargo transfer are roll, pitch and heave. The responses of these variables and their dependence on the three joint models are shown below separately for the T-Craft, Sea Base and ramp. The ramp length value used is 10 m and the heading angle is $\pi/4$ radians.

The results indicate that the joint type primary influence the roll DOF. As the top subplots in Figure 1.8 and Figure 1.10 shows, the roll amplitude is reduced for the PR and PRY-joint cases compared to the response for the P-joint. Note that the roll evolution of the ramp for the PRY-joint case (top subplot of Figure 1.10) has similar amplitude to that of the P-joint because springs were inserted between the roll and yaw DOFs due to unstable behavior. The bottom two subplots on the figures corresponding to pitch and heave motions do not vary much with the joint case as indicated by the overlap.

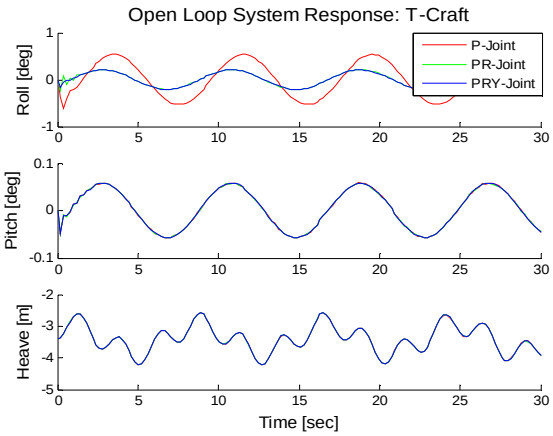

Figure 1.8: T-Craft open loop roll, pitch, heave

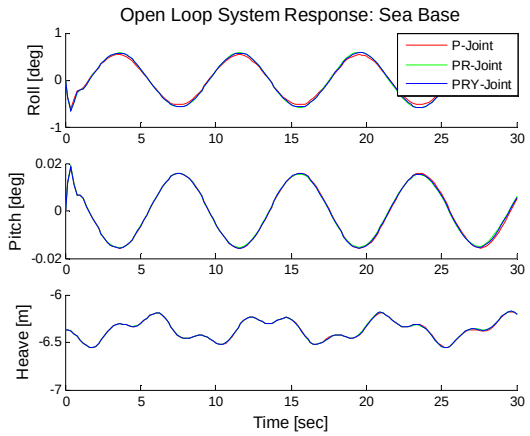

Figure 1.9: Sea Base open loop roll, pitch, heave

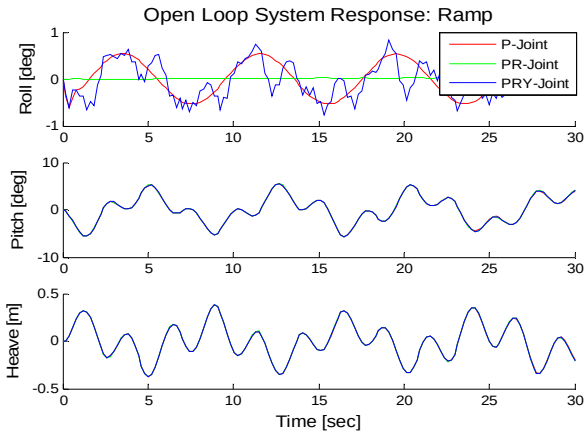

Figure 1.10: Ramp open loop roll, pitch, heave

Chapter 2. Ocean Wave Model

Environmental disturbances for ship modeling exist as waves, wind and ocean currents. In the forthcoming simulations we will neglect the direct effect of the wind and ocean current and instead only consider the wave disturbances that are modeled as linear plane waves. The basic assumptions of the linear wave theory are: the sea water is incompressible, inviscid, no surface tension, the fluid motion is irrotational, and the wave amplitude is significantly smaller than the wavelength. The linear wave theory allows us to express the wave model as a superposition of sine waves with differing frequencies distributed according to a spectrum. The resulting wave will produce an irregular pattern and is considered a useable approximation to model real seas [2]. We can represent the sea surface profile equation as a superposition of sine waves as

$$\zeta = \sum_{i=1}^{N} A_i \sin(\omega_i t - k_i x + \varepsilon_i) \tag{2.1}$$

where A_i is the wave amplitude, ω_i is the wave frequency, k_i is the wave number and ε_i is a random and uniformly distributed number between 0 and 2π. As the number of waves superimposed, N , increases this formulation produces an irregular sea pattern that marches both in time and 1-D space.

To characterize the waves according to standard sea state (SS) codes we need to formulate the concept of significant wave height H_S and define two types of wave heights. Figure 2.1 shows two types of trough-to-crest heights. H_1 measures the

trough-to-crest when they lie on opposite sides of the mean sea level, while H_2 measures the height on the same side of the sea level. Experimentation shows that the former height, H_1, follows a Raleigh distribution

$$f(H) = \frac{H}{4m_o} \exp\left(-\frac{H^2}{8m_o} \right) \tag{2.2}$$

with mean height of

$$H_m = \int_0^\infty H f(H) dH = \sqrt{2\pi m_o} \tag{2.3}$$

where m_o is the variance of the wave distribution. The mean of the highest third of the wave heights is called the *significant wave height*, H_S.

$$H_S = \int_{H_o}^\infty H f(H) dH \tag{2.4}$$

where H_o is given by $\int_{H_o}^\infty f(H) dH = \frac{1}{3}$

The significant wave height corresponds to the wave height estimated by a trained observer. The maximum wave height naturally depends on the number of waves superimposed and it was shown in Bonnefille (1992) that $H_{\max}/H_S$ varies from 1.2 for $N = 10$ to 1.9 for $N = 1000$. We have chosen arbitrarily to use $N = 100$ for the following sea elevation computations.

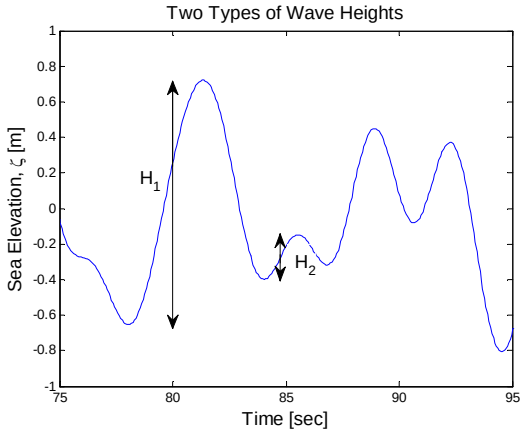

Figure 2.1: Two Types of Wave Height

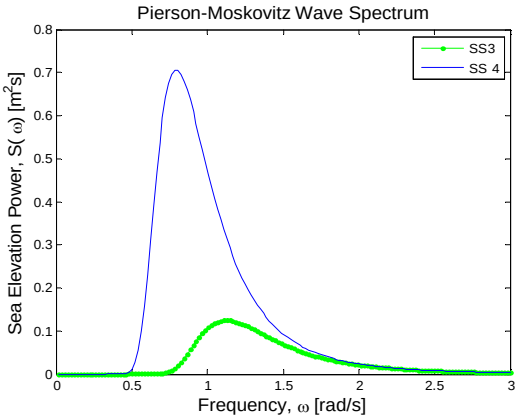

Figure 2.2: PM-Spectrum for Sea State 3, 4

The main result born from the significant wave height is the wave spectrum $S(\omega)$, which is a distribution of the wave energy verses angular frequency for a given sea state. In Figure 2.2 the Pierson-Moskowitz (PM) Spectrum is depicted for waves of SS 3 where $H_S = 0.5 - 1.25$ and SS 4 where $H_S = 1.25 - 2.5$ [3]. As shown, the larger the wave height the more the energy of the modal frequency wave is shifted to a lower frequency range. The PM-Spectrum is given by the following equation

$$S(\omega) = A\omega^{-5} \exp\left(-B\omega^{-4}\right) \mathrm{m}^2\mathrm{s} \tag{2.5}$$

where $\mathrm{A} = 8.1\times10^{-3} g^2\ \mathrm{m}^2\mathrm{s}^{-4}$ and $\mathrm{B} = 3.11/H_s^2\ \mathrm{s}^{-4}$.

We can find the modal frequency or peak frequency present in the PM-Spectrum by requiring that

$$\left(\frac{dS(\omega)}{d\omega}\right)_{\omega=\omega_o} = 0$$
$$\Downarrow \tag{2.6}$$
$$-5A\omega_o^{-6}\left[\exp\left(-B\omega_o^{-4}\right)\right] + A\omega_o^{-5}\left[\exp\left(-B\omega_o^{-4}\right)\right]4B\omega_o^{-5} = 0$$

Solving for ω_o yields

$$\omega_o = \sqrt[4]{\frac{4B}{5}} \tag{2.7}$$

Consequently the maximum spectrum value, which can be used to find a transfer function or state space model of the wave is found.

$$S_{max} = S\left(\omega_o\right) = \frac{5A}{4B\omega_o}\exp\left(-5/4\right) \tag{2.8}$$

The first moment or variance of the wave spectrum is used in designing linear wave response models and is given by m_o and σ can be thought of the RMS value of the wave spectrum.

$$m_o = \sigma^2 = \int_0^\infty S\left(\omega\right) d\omega = \frac{A}{4B} \tag{2.9}$$

The PM-Spectrum is empirically formulated using measured sea characteristics and corresponds to a first order approximation of fully developed seas in the North Atlantic with large depth, no swell and unlimited fetch, which means the wave shape moves but there is no mass transport [3]. For moving ships this approximation is sufficient, consequently a higher order approximation that predicts drift is necessary for static vessels.

It is known that the total energy of N wave components is half of the sum of all wave component amplitudes squared. Given how the spectrum is defined to

correspond to the wave energy, the amplitude of each wave component can be determined by

$$S(\omega_i)\Delta\omega = \frac{1}{2}A_i^2 \tag{2.10}$$

Figure 2.3 shows the result after plugging each amplitude value per time step into the sea elevation profile equation above while holding the space variable constant. This sea profile vector ζ is used below (section 2.2) to calculate the force term amplitudes for the respective DOFs acting on a floating body. Holding time constant and varying the space variable produces a similar irregular shape. The evolution of the wave in both space and time is shown in Figure 2.4. It is the space component of the wave profile that is used to determine the proper phase delay of the wave force acting on the ship. For instance, as the distance the wave travels increases, phase increases accordingly.

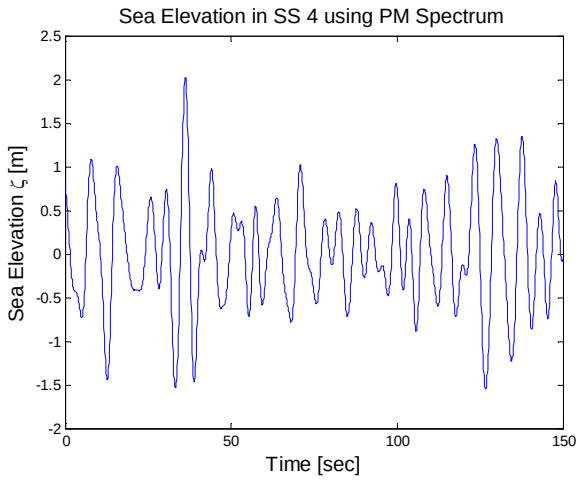

Figure 2.3: Sea elevation with time for SS 4

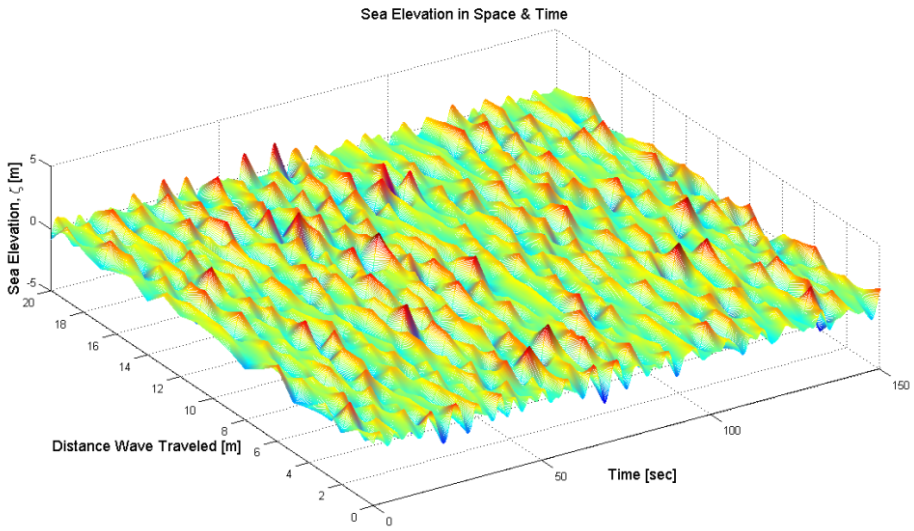

Figure 2.4: Sea elevation with space and time for SS 4

2.1. **Ocean Wave Response Model**

For closed loop systems and control analysis it is desired to form linear wave response models in transfer function or state space form and proves to be more practical than the spectrum representation of an ocean surface. This approach is based on determining the coefficients of the wave response transfer function by comparing its output to the spectral density function $S(\omega)$ of the empirical approach. A linear approximation can be found by expressing the output as a linear filter.

$$y(s) = h(s)\,w(s) \tag{2.11}$$

where $w(s)$ is zero mean Gaussian white noise process with unity power across the spectrum, $\Phi_w(\omega) = 1.0$, and $h(s)$ is a transfer function to be determined. The power spectral density functions for $y(s)$ can be written as

$$\Phi_y(\omega) = \left|h(j\omega)\right|^2 \Phi_w(\omega) = \left|h(j\omega)\right|^2 \tag{2.12}$$

The final 2nd order linear wave response transfer function approximation with a damping term was introduced by Saelid *et.al* (1983) as

$$h(s) = \frac{K_\omega s}{s^2 + 2\lambda\omega_o s + \omega_o^2} \tag{2.13}$$

The gain constant is defined as $K_\omega = 2\lambda\omega_o\sigma$, σ describes the wave intensity, λ is a damping coefficient and ω_o is the wave peak frequency. Hence, the power spectral density function of the output $y(s)$ can be written as

$$\Phi_y(\omega) = \left|h(j\omega)\right|^2 = \frac{4(\lambda\omega_o\sigma)^2\omega^2}{\left(\omega_o^2 + \omega^2\right)^2 + 4(\lambda\omega_o\sigma)^2} \tag{2.14}$$

The parameters λ and σ can be varied to better fit the Pierson-Moskowitz empirical spectrum. Since the ultimate goal is to design $\Phi_y(\omega)$ to approximate $S(\omega)$ and their respective maximum values are obtained for $\omega = \omega_o$ this yields

$$\begin{gathered} \Phi_y(\omega_o) = S(\omega_o) \\ \text{c} \\ \sigma^2 = \frac{5A}{4B\omega_o}\exp(-5/4) \end{gathered} \tag{2.15}$$

The damping coefficient λ can be determined by requiring the energy, that is the areas under $\Phi_y(\omega)$ and $S(\omega)$, to be equal. One method of doing this is to fit

$\Phi_y(\omega)$ on $S(\omega)$ in a least-squares sense, which results in $\lambda \approx 0.26$ for the PM-Spectrum and is independent of the significant wave height for fully developed sea models.

The 2nd order linear wave spectrum can also be transformed into the time domain and represented in state space form by defining $\dot{x}_1 = x_2$, $\dot{x}_2 = y_w$ which eventually yields

$$\begin{bmatrix} \dot{x}_1 \\ \dot{x}_2 \end{bmatrix} = \begin{bmatrix} 0 & 1 \\ -\omega_o^2 & -2\lambda\omega_o \end{bmatrix} \begin{bmatrix} x_1 \\ x_2 \end{bmatrix} + \begin{bmatrix} 0 \\ K_\omega \end{bmatrix} w$$
$$y_w = \begin{bmatrix} 0 & 1 \end{bmatrix} \begin{bmatrix} x_1 \\ x_2 \end{bmatrix} \tag{2.16}$$

As a further approximation to white noise filtered through a 2nd order transfer function we can use a sine wave with the same dominating frequency ω_o and a stochastic white noise additive component in the form

$$y(t) = A\sin(\omega_o t + \varphi) + w(t) \tag{2.17}$$

Representing the ocean wave as a sine wave allows us to define the time at which the wave meets each ship by modifying the phase delay and can be used to orient the wave front relative to the ship system axis. As seen from Figure 2.5 the sine wave model is an ad hoc approximation to the 2nd order transfer function model by differing in phase, frequency components and amplitude in certain regions. However, it is useful when implementing the model in SimMechanics for the reasons mentioned above.

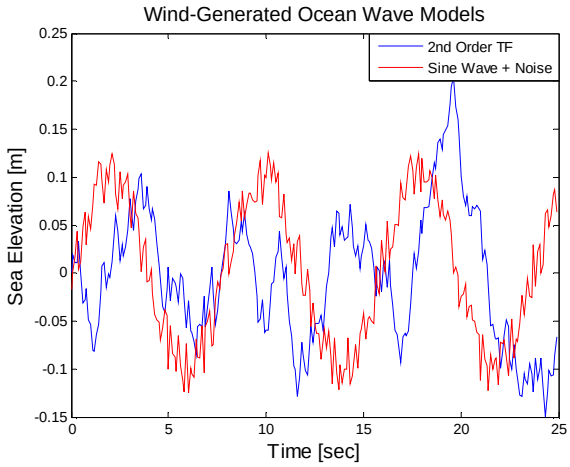

Figure 2.5: A transfer function and sine wave model for wind-generated ocean waves

Table 2.1: Parameter values of wave model

Parameter	Value
Peak Frequency, ω_o [rad/s]	0.79
Damping Coefficient, λ	0.26
RMS of Wave Spectrum, σ	0.63
A [m^2s^{-4}]	0.78
B [s^{-4}]	0.50

2.2. **Wave Induced Forces and Motions**

Instead of modeling the *motion* of an ocean vessel as influenced by the waves as described above, we can model the *forces* acting on the vessel, which ultimately affect the motion. The term used to describe the induced force caused by the waves that act on a semi-immersed body is restoring force [2]. These restoring forces arise from the buoyancy and gravity force, which both depend on the wave characteristics. Although generally a three dimensional body moves in six DOFs, we will only model the three relevant DOF's that are affected by the hydrostatic force and moments from the waves. The DOF considered in the model are: roll, pitch and heave. These

restoring forces tend to return a floating body to its initial position, while no opposing hydrostatic restoring forces exist in the surge, sway or yaw directions. In other words, since these motions are analogous to a spring-damper system their respective spring constants and damping coefficients are set to zero.

There are two primary effects that influence the forces acting on a vessel. There are the 1st order effects that are due to the wave frequency motion as described above and the 2nd order effects that comprise the wave drift forces, which tend to behave as slowly varying bias terms (Wiener process). The above transfer function wave motion model can be used to describe the forces in each DOF desired as

$$F_{wave} = \frac{K_\omega s}{s^2 + 2\lambda\omega_o s + \omega_o^2} w_1 + d_1$$
$$\dot{d}_1 = w_2 \tag{2.18}$$

where w_1 and w_2 are Gaussian white noise processes. However, in the forthcoming simulation results the transfer function force model is not used, rather the method below, which uses an approximating sine wave force.

An approximation to the equations of motion that govern the roll, pitch and heave take the form of an uncoupled second order dynamical system [2]. The symbols used follow the convention by Society of Naval Architects and Marine Engineers (SNAME) and International Towing Tank Conference (ITTC) *Dictionary of Ship Hydrodynamics*. The equation for roll motion with linear damping and linear waves is given as

$$\ddot{\phi} + 2b\dot{\phi} + \omega_\phi^2\phi = \omega_\phi^2 \frac{2\pi\zeta_o}{\lambda}\sin(\omega_W t),\ \omega_\phi = \frac{\sqrt{g\overline{GM}_R}}{i_R},\ i_R^2 = J_R/\Delta \tag{2.19}$$

where b is a linear damping coefficient, ω_ϕ is the ship natural frequency in roll, ζ_o is the wave amplitude, ω_W is the wave angular frequency, $\overline{GM}_R$ is the metacentric height in roll, i_R is the mass radius of gyration in roll and for a half cylinder equals $i_r = r\sqrt{\frac{1}{2}-\frac{16}{9\pi^2}} \approx w/\left(2\sqrt{3}\right)$ where w = width of half cylinder, J_R is the mass moment of inertia, Δ is the mass displacement from the floating body. The roll equation can be rearranged to:

$$J_R\ddot{\phi} + 2J_R b\dot{\phi} + g\Delta\overline{GM}_R\phi = g\Delta\overline{GM}_R\frac{2\pi\zeta_o}{\lambda}\sin\left(\omega_W t\right) \tag{2.20}$$

The undamped uncoupled pitch equation is:

$$\ddot{\theta} + \omega_\theta^2\theta = \omega_\theta^2\gamma\sin\left(\omega_E t\right),\ \omega_E = \frac{2\pi}{T_E},\ T_E = \frac{\lambda}{c - v\cos\left(\alpha\right)},\ \omega_\theta = \frac{\sqrt{g\overline{GM}_P}}{i_P} \tag{2.21}$$

where ω_θ is the ship natural frequency in pitch, γ is the maximum pitch amplitude, ω_E is the angular frequency of encounter (number of waves seen by the ship per unit time), i_P is the mass radius of gyration in pitch and equals $i_p = \sqrt{\left(\frac{1}{4}-\frac{16}{9\pi^2}\right)r^2 + \frac{1}{12}L^2} \approx L/\left(2\sqrt{3}\right)$ where L is length, v is the ship speed, c is the wave celerity, α is the angle between ship speed and wave celerity. The pitch equation can be rearranged to yield:

$$J_P\ddot{\theta} + g\Delta\overline{GM}_P\theta = g\Delta\overline{GM}_P\gamma\sin\left(\omega_E t\right) \tag{2.22}$$

The uncoupled heave equation is:

$$\left(m + A_{33}\right)\ddot{z} + b\dot{z} + \rho g A_w z = \rho g A_w \zeta_o \cos\left(\omega_E t\right) \tag{2.23}$$

where A_{33} is the added submerged mass in the heave DOF due to the heave motion, A_w is the waterplane area of the floating body, which both depend on the waves' frequency of oscillation.

The two metacentric heights and waterplane area used in the simulations were calculated for a half-cylinder model of the two ships. Since no explicit expression for the damping coefficients were available they were estimated in an ad hoc manner provided the result complied with intuitive ship motions. Summarizing the resulting spring and damping constants we get

$$\begin{gathered} k_{roll} = g\Delta\overline{GM}_R,\ k_{pitch} = g\Delta\overline{GM}_P,\ k_{heave} = \rho g A_w \\ b_\phi = 2J_R b,\ b_z = b,\ b = 0.01 \end{gathered} \tag{2.24}$$

Since the waves are modeled as linear plane waves the heave DOF force is used to model the wave forces. Hence, the final wave force form implemented in the SimMechanics model is

$$F_{wave} = \rho g A_w \zeta_o \cos\left(\omega_o t + \varphi\right) \tag{2.25}$$

where the phase delay depends on the distance the wave travels until reaching the reacting body.

The above expressions were used in the SimMechanics model to simulate the ocean wave and restoring force disturbances by its analogous spring damper system. Although these equations were derived for a single ship, rather than an interconnected ship-ramp-ship system, nevertheless the resulting spring and damper coefficients were used as an estimate for the system's motion. In reality there exists some coupling between the various DOFs, which these equations do not capture. For example, the combination of roll and pitch motions will induce yaw and heave motions. Also, during the roll motion, the center of buoyancy will move and cause some pitch motion. It is important to understand the limitations of these equations, which fall short at describing the full behavior of a floating body.

2.3. **Phases due to Approaching Wave Front**

Since the ocean surface is modeled as linear plane waves in the x-y plane, we assume there is some delay between when two points of the system feel the impact of the waves. This delay is accounted for in the phase term of the wave force and is proportional to the distance the wave travels. The line perpendicular to the direction of travel is called the wave front and the distance from the wave front to the points 1-8 is proportional to the phase by the equation

$$Phase = \frac{\text{Distance}}{\lambda} 2\pi \tag{2.26}$$

where λ is the wavelength of the ocean wave. This equation fits our intuition in that a distance that is a multiple of the wavelength has a 2π phase, which is equivalent to a zero phase. A floating body with length equal to the wavelength of a

wave and exposed to a wave front perpendicular to its direction of motion will not experience any rotary motion since the back and front of the body are struck by the wave with the same phase causing only translational heave to exist. The angle α is called the heading angle, which is the angle between the wave front and the horizontal line that is parallel to the ship-ramp-ship system. The heading angle ranges from 0 to π, and because of symmetry does not need to go a full circle. When $\alpha = 0$ the wave encounters the T-Craft first specifically points 1 and 2 and when $\alpha = \pi$ points 7 and 8 of the Sea Base encounter the wave first. The auxiliary angle $\varphi = \pi / 2 - \alpha$ is used for ease of analysis.

In Figure 2.6 the diagonal lines that originate at the wave front and end at each of the eight point of the system represent the distance the wave travels and is used to find the relative phase shifts of the wave forces. For ease of visualization the phases are derived for the two intermediate ranges of heading angle: $\alpha \in (0, \pi / 2)$ and $\alpha \in (\pi / 2, \pi)$, which corresponds to $\varphi \in (\pi / 2, 0)$ and $\varphi \in (0, -\pi / 2)$ respectively, where L'Hôpital's rule can be applied to arrive at the end point phase values. However, it is straight forward to arrive at the end point cases through inspection and only use L'Hôpital's for verification. It should be noted that this mathematical construction of modeling the phase holds under the assumption that the six degrees of freedom of the floating body are relatively small. The final phases are used in the SimMechanics model to represent the incoming waves.

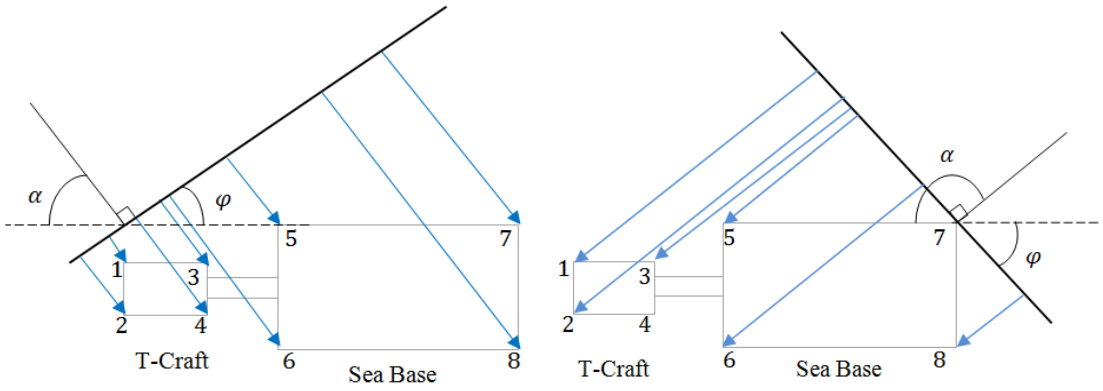

Figure 2.6: Wave front and system for $\alpha \in (0, \pi/2)$ (left) and $\alpha \in (\pi/2, \pi)$ (right)

In the first range of heading angles $\alpha \in (0, \pi/2)$ or $\varphi \in (\pi/2, 0)$ points 1, 2, 5, 7 have fairly obvious phase's using simple geometry and are given as

$$\text{Phase}(1) = \frac{(w_{sb}/2 - w_{tc}/2)\sin(\pi/2 - \varphi)}{\lambda} 2\pi \tag{2.27}$$

$$\text{Phase}(2) = \frac{(w_{tc}/2 + w_{sb}/2)\sin(\pi/2 - \varphi)}{\lambda} 2\pi \tag{2.28}$$

$$\text{Phase}(5) = \frac{(L_{tc} + L_{ramp})\sin\varphi}{\lambda} 2\pi \tag{2.29}$$

$$\text{Phase}(7) = \frac{(L_{tc} + L_{ramp} + L_{sb})\sin\varphi}{\lambda} 2\pi \tag{2.30}$$

At the end points these phases simplify to rational numbers thus circumventing the use of L'Hôpital's rule. We will now derive the phase shifts for points 3, 4, 6, 8 for the range $\alpha \in (0, \pi/2)$.

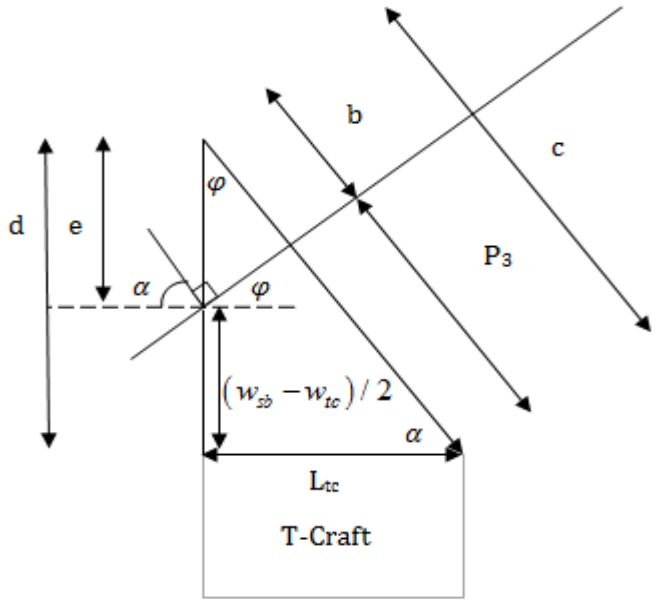

Figure 2.7: Geometry for deriving phase shift for point 3 (P_3)

Using Figure 2.7 we first solve for the following variables

$$c = \frac{L_{tc}}{\cos\alpha},\ d = L_{tc}\tan\alpha,\ e = L_{tc}\tan\alpha - \left(w_{sb} - w_{tc}\right)/2$$

We then solve for b, using the above expression

$$b = e\cos\varphi = \left[L_{tc}\tan\alpha - \left(w_{sb} - w_{tc}\right)/2\right]\cos\varphi$$

It is clear that P_3 = c - b, subtracting yields the formula for P_3 in terms of known quantities:

$$P_3 = \frac{L_{tc}}{\cos\left(\frac{\pi}{2} - \varphi\right)} - \left[L_{tc}\frac{\cos\varphi}{\sin\varphi} - \left(w_{sb} - w_{tc}\right)/2\right]\cos\varphi$$

The phase shift for point 3 then becomes

$$\text{Phase}(3)=\left\{\frac{L_{tc}}{\cos\left(\frac{\pi}{2}-\varphi\right)}-\left[L_{tc}\frac{\cos\varphi}{\sin\varphi}-\left(w_{sb}-w_{tc}\right)/2\right]\cos\varphi\right\}\frac{2\pi}{\lambda} \qquad (2.31)$$

In the geometry for point 4, only the expression for e changes by subtracting the T-Craft width term

$$e=L_{tc}\tan\alpha-\left(w_{sb}-w_{tc}\right)/2-w_{tc}\Rightarrow L_{tc}\tan\alpha-\left(w_{sb}+w_{tc}\right)/2$$

Plugging in the new expression for e, gives the following phase shift for point 4

$$\text{Phase}(4)=\left\{\frac{L_{tc}}{\cos\left(\frac{\pi}{2}-\varphi\right)}-\left[L_{tc}\frac{\cos\varphi}{\sin\varphi}-\left(w_{sb}+w_{tc}\right)/2\right]\cos\varphi\right\}\frac{2\pi}{\lambda} \qquad (2.32)$$

Deriving the above variable expressions for point 6 we have

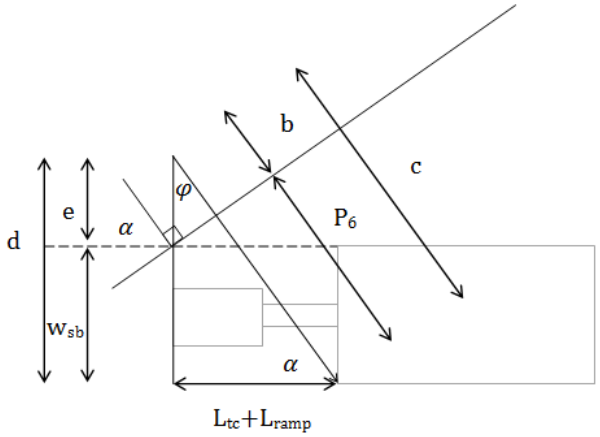

Figure 2.8: Geometry for deriving phase shift for point 6 (P_6)

$$c=\frac{L_{tc}+L_{ramp}}{\cos\alpha},\ d=\left(L_{tc}+L_{ramp}\right)\tan\alpha,\ e=\left(L_{tc}+L_{ramp}\right)\tan\alpha-w_{sb}$$

$$b=e\cos\varphi=\left[\left(L_{tc}+L_{ramp}\right)\tan\alpha-w_{sb}\right]\cos\varphi$$

Solving for the phase shift in the usual way gives

$$\text{Phase}(6)=\left\{\frac{L_{tc}+L_{ramp}}{\cos\left(\frac{\pi}{2}-\varphi\right)}-\left[\left(L_{tc}+L_{ramp}\right)\frac{\cos\varphi}{\sin\varphi}-w_{sb}\right]\cos\varphi\right\}\frac{2\pi}{\lambda} \qquad (2.33)$$

Deriving the above variable expressions for point 8 we have

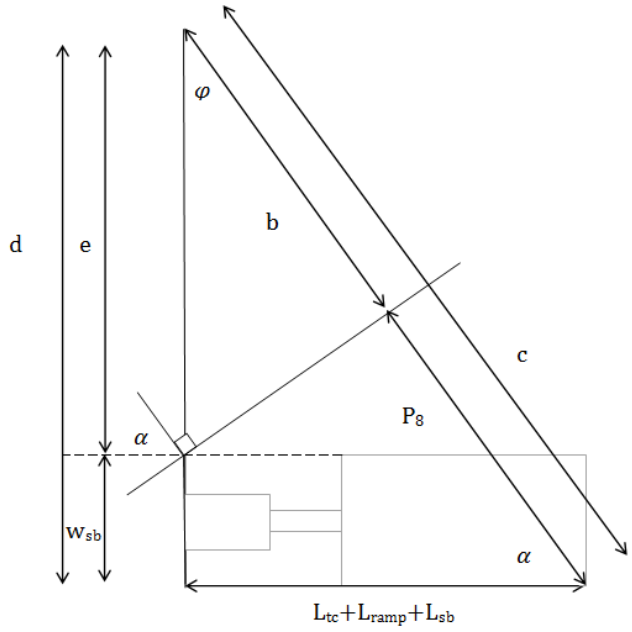

Figure 2.9: Geometry for deriving phase shift for point 8 (P_8)

$$c=\frac{L_{tc}+L_{ramp}+L_{sb}}{\cos\alpha},\ d=\left(L_{tc}+L_{ramp}+L_{sb}\right)\tan\alpha,\ e=\left(L_{tc}+L_{ramp}+L_{sb}\right)\tan\alpha-w_{sb}$$

$$b=e\cos\varphi=\left[\left(L_{tc}+L_{ramp}+L_{sb}\right)\tan\alpha-w_{sb}\right]\cos\varphi$$

$$\text{Phase}(8)=\left\{\frac{L_{tc}+L_{ramp}+L_{sb}}{\cos\left(\frac{\pi}{2}-\varphi\right)}-\left[\left(L_{tc}+L_{ramp}+L_{sb}\right)\frac{\cos\varphi}{\sin\varphi}-w_{sb}\right]\cos\varphi\right\}\frac{2\pi}{\lambda} \qquad (2.34)$$

A summary of the phases for the boundary condition $\varphi=\pi/2$ is given below

$$\begin{aligned}
&\text{Phase}(1) = \text{Phase}(2) = 0 \\
&\text{Phase}(3) = \text{Phase}(4) = L_{tc}\frac{2\pi}{\lambda} \\
&\text{Phase}(5) = \text{Phase}(6) = \left(L_{tc} + L_{ramp}\right)\frac{2\pi}{\lambda} \\
&\text{Phase}(7) = \text{Phase}(8) = \left(L_{tc} + L_{ramp} + L_{sb}\right)\frac{2\pi}{\lambda}
\end{aligned} \tag{2.35}$$

A summary of the phases for the boundary condition $\varphi = 0$ is given below. Note L'Hôpital's rule was used for points 3, 4, 6, 8 since plugging in $\varphi = 0$ would cause the not well defined expression $\infty - \infty$ to define the phase. L'Hôpital's rule circumvents this problem.

$$\begin{aligned}
&\text{Phase}(5) = \text{Phase}(7) = 0 \\
&\text{Phase}(6) = \text{Phase}(8) = w_{sb}\frac{2\pi}{\lambda} \\
&\text{Phase}(1) = \text{Phase}(3) = \left(\frac{w_{sb}}{2} - \frac{w_{tc}}{2}\right)\frac{2\pi}{\lambda} \\
&\text{Phase}(2) = \text{Phase}(4) = \left(\frac{w_{sb}}{2} + \frac{w_{tc}}{2}\right)\frac{2\pi}{\lambda}
\end{aligned} \tag{2.36}$$

A summary of the phases for the angle range $\varphi \in (\pi/2, 0)$ is given below

$$
\begin{aligned}
\text{Phase}(1) &= \left(w_{sb}/2 - w_{tc}/2\right)\sin\left(\pi/2-\varphi\right)\frac{2\pi}{\lambda} \\
\text{Phase}(2) &= \left(w_{tc}/2 + w_{sb}/2\right)\sin\left(\pi/2-\varphi\right)\frac{2\pi}{\lambda} \\
\text{Phase}(3) &= \left\{\frac{L_{tc}}{\cos\left(\frac{\pi}{2}-\varphi\right)} - \left[L_{tc}\frac{\cos\varphi}{\sin\varphi} - \left(w_{sb}-w_{tc}\right)/2\right]\cos\varphi\right\}\frac{2\pi}{\lambda} \\
\text{Phase}(4) &= \left\{\frac{L_{tc}}{\cos\left(\frac{\pi}{2}-\varphi\right)} - \left[L_{tc}\frac{\cos\varphi}{\sin\varphi} - \left(w_{sb}+w_{tc}\right)/2\right]\cos\varphi\right\}\frac{2\pi}{\lambda} \\
\text{Phase}(5) &= \left(L_{tc}+L_{ramp}\right)\sin\varphi\frac{2\pi}{\lambda} \\
\text{Phase}(6) &= \left\{\frac{L_{tc}+L_{ramp}}{\cos\left(\frac{\pi}{2}-\varphi\right)} - \left[\left(L_{tc}+L_{ramp}\right)\frac{\cos\varphi}{\sin\varphi} - w_{sb}\right]\cos\varphi\right\}\frac{2\pi}{\lambda} \\
\text{Phase}(7) &= \left(L_{tc}+L_{ramp}+L_{sb}\right)\sin\varphi\frac{2\pi}{\lambda} \\
\text{Phase}(8) &= \left\{\frac{L_{tc}+L_{ramp}+L_{sb}}{\cos\left(\frac{\pi}{2}-\varphi\right)} - \left[\left(L_{tc}+L_{ramp}+L_{sb}\right)\frac{\cos\varphi}{\sin\varphi} - w_{sb}\right]\cos\varphi\right\}\frac{2\pi}{\lambda}
\end{aligned}
\tag{2.37}
$$

The derivation for the heading angle range of $\varphi \in \left(0, -\pi/2\right]$ is not shown, but the final results are given below.

$$\text{Phase}(1)=\left\{\frac{L_{sb}+L_{ramp}+L_{tc}}{\cos\left(\frac{\pi}{2}-|\varphi|\right)}-\left[\left(L_{sb}+L_{ramp}+L_{tc}\right)\frac{\cos|\varphi|}{\sin|\varphi|}-\left(w_{sb}-w_{tc}\right)/2\right]\cos|\varphi|\right\}\frac{2\pi}{\lambda}$$

$$\text{Phase}(2)=\left\{\frac{L_{sb}+L_{ramp}+L_{tc}}{\cos\left(\frac{\pi}{2}-|\varphi|\right)}-\left[\left(L_{sb}+L_{ramp}+L_{tc}\right)\frac{\cos|\varphi|}{\sin|\varphi|}-\left(w_{tc}+w_{sb}\right)/2\right]\cos|\varphi|\right\}\frac{2\pi}{\lambda}$$

$$\text{Phase}(3)=\left\{\frac{L_{sb}+L_{ramp}}{\cos\left(\frac{\pi}{2}-|\varphi|\right)}-\left[\left(L_{sb}+L_{ramp}\right)\frac{\cos|\varphi|}{\sin|\varphi|}-\left(w_{sb}-w_{tc}\right)/2\right]\cos|\varphi|\right\}\frac{2\pi}{\lambda}$$

$$\text{Phase}(4)=\left\{\frac{L_{sb}+L_{ramp}}{\cos\left(\frac{\pi}{2}-|\varphi|\right)}-\left[\left(L_{sb}+L_{ramp}\right)\frac{\cos|\varphi|}{\sin|\varphi|}-\left(w_{sb}+w_{tc}\right)/2\right]\cos|\varphi|\right\}\frac{2\pi}{\lambda}$$

$$\text{Phase}(5)=L_{sb}\sin|\varphi|\frac{2\pi}{\lambda}$$

$$\text{Phase}(6)=\left\{\frac{L_{sb}}{\cos\left(\frac{\pi}{2}-|\varphi|\right)}-\left[L_{sb}\frac{\cos|\varphi|}{\sin|\varphi|}-w_{sb}\right]\cos|\varphi|\right\}\frac{2\pi}{\lambda}$$

$$\text{Phase}(7)=0$$

$$\text{Phase}(8)=w_{sb}\sin\left(\frac{\pi}{2}-|\varphi|\right)\frac{2\pi}{\lambda}$$

(2.38)

Chapter 3. Lagrangian Mechanics Approach to Deriving Equations of Motion of Ship System with Pitch Joint

Lagrangian mechanics is an approach used to derive the equations of motion of a dynamical system and is based on the principle of conservation of energy. The method can be modified to account for dissipative forces as well that are a function of the first derivative of a generalized coordinate. Since in our model the effects from gravity and buoyancy are modeled as a second order spring and damper system this modification is employed due to the damping. Generalized coordinates are the minimum amount of coordinates required to model the system and prove to significantly simplify the analysis and shown in Table 3.1. Counterclockwise angles are assumed positive in the derivation. The system modeled here includes a pitch joint between each ship and ramp resulting in $n = 8$ degree of freedoms.

We begin by defining the Lagrangian $L = T - V$ as the difference between the kinetic and potential energy of the system. Then we construct Rayleigh's dissipation function D to include all relevant terms to describe the system. Then we derive the work done by the generalized applied forces Q_A. Once the intermediate steps for each of the aforementioned items are complete the results are plugged into equation (3.1) and solved for the equations of motion in second order form. A simple change of coordinates can change it to a first order form as shown by equation (3.20). Following the resulting equations of motion, their respective solutions are given and include the position and velocity of the system states.

Throughout this section it is assumed the reader can follow the flow of the derivation by the order of equations being presented and is why only terse language is used for more guidance.

Table 3.1: Generalized coordinates for deriving equation of motion

Generalized Coordinate	Degree of Freedom	Units
q_1	Surge (x)	[m]
q_2	Sway (y)	[m]
q_3	Heave (z)	[m]
q_4	Roll (about x)	[rad]
q_5	Yaw (about z)	[rad]
q_6	Pitch (about y)	[rad]
q_7	Pitch of T-Craft	[rad]
q_8	Pitch of Sea Base	[rad]

Kinetic Energy = T

Potential Energy: $V = V_G + V_S$ (work done by gravity and by springs)

Work done by Applied Force: $Q_A = \sum_{i=1}^{n} \int_0^t Q_i(t)\dot{q}_i(t)dt$, where Q_i = generalized applied force/moment and $\dot{q}_i$ = generalized velocity coordinate

Lagrangian: $L = T - V$

Lagrange's Equation with Dissipation Function:

$$\frac{d}{dt}\left(\frac{\partial L}{\partial \dot{q}_i}\right) - \frac{\partial L}{\partial q_i} + \frac{\partial D}{\partial \dot{q}_i} = Q_i \tag{3.1}$$

Rayleigh's Dissipation Function (represents damping force): $D = \frac{1}{2}\sum_{i=1}^{n} b_i \dot{q}_i^2$

$b_i =$ damping coefficient of q_i DOF

$D = \sum D_{q_i}$, where $D_{q_i} =$ the dissipation function due to motion in the q_i DOF

Let $b_{Tot3} = 4b_{TC3} + 4b_{SB3}$, total damping in q_3 (heave) DOF

In the system model, damping is present only in the following DOFs: heave, roll and pitch.

$$D_{q_3} = \frac{\dot{q}_3^2}{2} b_{Tot3} \tag{3.2}$$

$$D_{q_4} = \frac{\dot{q}_4^2}{2} \cos^2 q_4 \left({w_{TC}}^2 b_{TC3} + {w_{SB}}^2 b_{SB3} \right) \tag{3.3}$$

$$D_{q_{7,8}} = \frac{\dot{q}_7^2}{2} 2b_{TC7} + \frac{\dot{q}_7^2}{2} 2b_{TC3} \left(L_{TC} \cos q_7 \right)^2 + \frac{\dot{q}_8^2}{2} 2b_{SB8} + \frac{\dot{q}_8^2}{2} 2b_{SB3} \left(L_{SB} \cos q_8 \right)^2 \tag{3.4}$$

$$D_{q_6} = \frac{\dot{q}_6^2}{2} \left\{ \begin{array}{l} 2b_{TC7} + 2b_{SB8} + \left(\frac{L_R}{2} \cos q_6 \right)^2 \left(2b_{TC3} + 2b_{SB3} \right) + \\ 2b_{TC3} \left(\cos q_6 \left(L_{TC} + \frac{L_R}{2} \right) \right)^2 + 2b_{SB3} \left(\cos q_6 \left(L_{SB} + \frac{L_R}{2} \right) \right)^2 \end{array} \right\} \tag{3.5}$$

Reduce dissipation function components by substituting the Taylor series expansion of $\sin x$ and $\cos x$ into previous form to get the following

$$D_{q_3} = \frac{\dot{q}_3^2}{2} b_{Tot3} \tag{3.6}$$

$$D_{q_4} = \frac{\dot{q}_4^2}{2} \left({w_{TC}}^2 b_{TC3} + {w_{SB}}^2 b_{SB3} \right) \tag{3.7}$$

$$D_{q_7} = \dot{q}_7^2 b_{TC7} \left(1 + {L_{TC}}^2 \right) \tag{3.8}$$

$$D_{q_6} = \frac{\dot{q}_6^2}{2}\left\{\left(2b_{TC7} + 2b_{SB8} + \left(\frac{L_R}{2}\right)^2\left(2b_{TC3} + 2b_{SB3}\right) + 2b_{TC3}L_{TCR}{}^2 + 2b_{SB3}L_{SBR}{}^2\right)\right\} \quad (3.9)$$

Let $m_{Tot} = m_{TC} + m_R + m_{SB}$

The first term in the kinetic energy equation is from the ramp surge velocity. The second term is the T-Craft's surge velocity, which also depends its rotation in its pitch DOF. The third term is similar to the previous T-Craft term but accounts for the Sea Base. The fourth term accounts for energy due to sway velocity. The fifth, sixth and seventh terms accounts for energy from the ramp, T-Craft and Sea Base heave motions respectively. The next two terms correspond to the rotational energy of the whole system in roll and yaw DOFs. The last three terms correspond to the pitch motion of the ramp, T-Craft and Sea Base respectively.

$$\begin{aligned} T = {} & \frac{1}{2}\left(m_R\dot{q}_1^2 + m_{TC}\left(\dot{q}_1 + \frac{L_{TC}}{2}\dot{q}_7\sin q_7\right)^2 + m_{SB}\left(\dot{q}_1 - \frac{L_{SB}}{2}\dot{q}_8\sin q_8\right)^2\right) + \\ & \frac{1}{2}m_{Tot}\dot{q}_2^2 + \frac{1}{2}\left(\begin{array}{l} m_R\dot{q}_3^2 + m_{TC}\left(\dot{q}_3 - \frac{L_{TC}}{2}\dot{q}_7\cos q_7\right)^2 + \\ m_{SB}\left(\dot{q}_3 + \frac{L_{SB}}{2}\dot{q}_8\cos q_8\right)^2 \end{array}\right) + \\ & \frac{1}{2}J_r\dot{q}_4^2 + \frac{1}{2}J_y\dot{q}_5^2 + \frac{1}{2}\left(J_R\dot{q}_6^2 + J_{TC}\left(\dot{q}_6 - \dot{q}_7\right)^2 + J_{SB}\left(\dot{q}_6 - \dot{q}_8\right)^2\right) \end{aligned} \quad (3.10)$$

In the gravitational potential energy equation, the first term accounts for the total system's potential energy in the heave DOF. The next two terms account for the potential energy due to the individual pitch motion of the T-Craft and Sea Base. The

last two terms account for the potential energy in the T-Craft and Sea Base due to the system's collective pitch motion.

$$V_G = m_{Tot} g q_3 - m_{TC} g \frac{L_{TC}}{2} \sin q_7 + m_{SB} g \frac{L_{SB}}{2} \sin q_8 - m_{TC} g \left(L_{TC} + \frac{L_R}{2} \right) \sin q_6 + m_{SB} g \left(L_{SB} + \frac{L_R}{2} \right) \sin q_6 \tag{3.11}$$

$V_S = \sum V_{Sq_i}$, where V_{Sq_i} = the potential energy stored in all springs of the system due to motion in the q_i DOF

$$V_{Sq_3} = \frac{1}{2}\left(4K_{TC3}\right) q_3^2 + \frac{1}{2}\left(4K_{SB3}\right) q_3^2 \tag{3.12}$$

$$V_{Sq_4} = \frac{1}{2}\left(4K_{TC4}\right)\left(\frac{w_{TC}}{2} \sin q_4 \right)^2 + \frac{1}{2}\left(4K_{SB4}\right)\left(\frac{w_{SB}}{2} \sin q_4 \right)^2 \tag{3.13}$$

$$V_{Sq_6} = \frac{1}{2}\left(2K_{TC7}\right) {q_6}^2 + \frac{1}{2}\left(2K_{SB8}\right) {q_6}^2 + \frac{1}{2}\left(2K_{TC7}\right)\left(\frac{L_R}{2} \sin q_6 \right)^2 + \frac{1}{2}\left(2K_{SB8}\right)\left(\frac{L_R}{2} \sin q_6 \right)^2 + \frac{1}{2}\left(2K_{TC3}\right)\left(\left(L_{TC} + \frac{L_R}{2} \right) \sin q_6 \right)^2 + \frac{1}{2}\left(2K_{SB3}\right)\left(\left(L_{SB} + \frac{L_R}{2} \right) \sin q_6 \right)^2 \tag{3.14}$$

$$V_{Sq_7} = \frac{1}{2}\left(2K_{TC7}\right) {q_7}^2 + \frac{1}{2}\left(2K_{TC3}\right) L_{TC} \sin q_7 \tag{3.15}$$

$$V_{Sq_8} = \frac{1}{2}\left(2K_{SB8}\right) {q_8}^2 + \frac{1}{2}\left(2K_{SB3}\right) L_{SB} \sin q_8 \tag{3.16}$$

Generalized Applied Force/Moment Terms from Ocean Waves

Surge: $Q_1 = 0$

Sway: $Q_2 = 0$

Heave: $Q_3 = F_1(t) + F_2(t) + F_3(t) + F_4(t) + F_5(t) + F_6(t) + F_7(t) + F_8(t)$

Roll: $Q_4 = \left[F_1(t) + F_3(t) - F_2(t) - F_4(t)\right]\frac{w_{TC}}{2} + \left[F_5(t) + F_7(t) - F_6(t) - F_8(t)\right]\frac{w_{SB}}{2}$

Yaw: $Q_5 = 0$

Pitch:

$$Q_6 = -\left[F_1(t) + F_2(t)\right]L_{TCR} + \left[F_5(t) + F_6(t) - F_3(t) - F_4(t)\right]\frac{L_R}{2} + \left[F_7(t) + F_8(t)\right]L_{SBR}$$

Pitch (TC joint): $Q_7 = \left[F_1(t) + F_2(t)\right]L_{TC}$

Pitch (SB joint): $Q_8 = \left[F_7(t) + F_8(t)\right]L_{SB}$

where $$F_i = A\sin\left(\omega_o t + \varphi_i\right) + v(t) \qquad (3.17)$$

Defining more variables

$$L_{TCR} = L_{TC} + \frac{L_R}{2}\ ,\ L_{SBR} = L_{SB} + \frac{L_R}{2}$$

J_R, J_{TC}, J_{SB} = Moment of Inertia about the y-axis (pitch DOF) of *Ramp, T-Craft, Sea Base* respectively and after summing define $J_y = J_R + J_{TC} + J_{SB}$

J_r, J_p, J_y = Moment of Inertia of whole system in the roll (about x-axis), pitch (about y-axis), and yaw (about z-axis) DOF respectively

Constructing the Lagrangian (non-linear):

$$
\begin{aligned}
L = & \left\{ \begin{array}{l}
\frac{1}{2}\left(\begin{array}{l} m_R \dot{q}_1^2 + m_{TC} \dot{q}_1^2 + \dot{q}_1 \dot{q}_7 m_{TC} L_{TC} \sin q_7 + m_{TC} \left(\frac{L_{TC}}{2} \dot{q}_7 \sin q_7 \right)^2 + \\ m_{SB} \dot{q}_1^2 - \dot{q}_1 \dot{q}_8 m_{SB} L_{SB} \sin q_8 + m_{SB} \left(\frac{L_{SB}}{2} \dot{q}_8 \sin q_8 \right)^2 \end{array} \right) + \\
\frac{1}{2}\left(\begin{array}{l} m_R \dot{q}_3^2 + m_{TC} \dot{q}_3^2 - \dot{q}_3 \dot{q}_7 L_{TC} \cos q_7 + \left(\frac{L_{TC}}{2} \dot{q}_7 \cos q_7 \right)^2 + \\ m_{SB} \dot{q}_3^2 + \dot{q}_3 \dot{q}_8 L_{SB} \cos q_8 + \left(\frac{L_{SB}}{2} \dot{q}_8 \cos q_8 \right)^2 \end{array} \right) + \\
\frac{1}{2} m_{Tot} \dot{q}_2^2 + \frac{1}{2} J_r \dot{q}_4^2 + \frac{1}{2} J_y \dot{q}_5^2 + \frac{1}{2}\left(\begin{array}{l} J_R \dot{q}_6^2 + J_{TC} \left(\dot{q}_6^2 - 2\dot{q}_6 \dot{q}_7 + \dot{q}_7^2 \right) + \\ J_{SB} \left(\dot{q}_6^2 - 2\dot{q}_6 \dot{q}_8 + \dot{q}_8^2 \right) \end{array} \right)
\end{array} \right\} \\
& - \left\{ \begin{array}{l}
m_{Tot} g q_3 + \left(2K_{TC3} + 2K_{SB3} \right) q_3^2 + \left(K_{TC4} \frac{{w_{TC}}^2}{2} + K_{SB4} \frac{{w_{SB}}^2}{2} \right) \sin^2 q_4 + \\
\left(K_{TC7} + K_{SB8} \right) {q_6}^2 + \left(m_{SB} g L_{SBR} - m_{TC} g L_{TCR} \right) \sin q_6 + \\
\left(K_{TC7} \frac{{L_R}^2}{4} + K_{SB8} \frac{{L_R}^2}{4} + K_{TC3} {L_{TCR}}^2 + K_{SB3} {L_{SBR}}^2 \right) \sin^2 q_6 + \\
\left(K_{TC3} L_{TC} - m_{TC} g \frac{L_{TC}}{2} \right) \sin q_7 + K_{TC7} {q_7}^2 + \\
\left(K_{SB3} L_{SB} + m_{SB} g \frac{L_{SB}}{2} \right) \sin q_8 + K_{SB8} {q_8}^2
\end{array} \right\}
\end{aligned} \tag{3.18}
$$

3.1. **Linearizing the Lagrangian**

Using the trigonometric identity $\sin 2\theta = 2 \sin\theta \cos\theta$ and the first term of the Taylor series expansions of $\sin x$ and $\cos x$ we can "somewhat" linearize the equations, where non-trigonometric non-linearity terms still exist, which will be left to propagate until after computing the Lagrange equations. Once the non-linear equations of motion have been derived one can attempt to linearize the equations of motion even

more or transform the system to first order differential equations and solve the non-linear system using MATLAB. The Lagrangian produces the result in the form $f\left(t, x, \dot{x}, \ddot{x}\right) = 0$.

Taylor series: $\sin x = x - \frac{x^3}{3!} + \frac{x^5}{5!} - \ldots$, $\cos x = 1 - \frac{x^2}{2!} + \frac{x^4}{4!} - \ldots$

$$L_l = \frac{1}{2}\left\{\begin{array}{l} m_{Tot}\dot{q}_1^2 + m_{Tot}\dot{q}_2^2 + J_r\dot{q}_4^2 + J_y\dot{q}_5^2 + m_{TC}L_{TC}\dot{q}_1\dot{q}_7 + \\ m_{TC}\frac{L_{TC}^{\ 2}}{4}\left(\dot{q}_7 q_7\right)^2 - m_{SB}L_{SB}\dot{q}_1\dot{q}_8 + m_{SB}\frac{L_{SB}^{\ 2}}{4}\left(\dot{q}_8 q_8\right)^2 + m_{Tot}\dot{q}_3^2 - \\ \dot{q}_3\dot{q}_7 L_{TC} + \frac{L_{TC}^{\ 2}}{4}\dot{q}_7^2 + L_{SB}\dot{q}_3\dot{q}_8 q_8 + \frac{L_{SB}^{\ 2}}{4}\dot{q}_8^2 + J_R\dot{q}_6^2 + \\ J_{TC}\left(\dot{q}_6^2 - 2\dot{q}_6\dot{q}_7 + \dot{q}_7^2\right) + J_{SB}\left(\dot{q}_6^2 - 2\dot{q}_6\dot{q}_8 + \dot{q}_8^2\right) \end{array}\right\} -$$

$$\left\{\begin{array}{l} m_{Tot}gq_3 + \left(2K_{TC3} + 2K_{SB3}\right)q_3^2 + \left(K_{TC4}\frac{w_{TC}^{\ 2}}{2} + K_{SB4}\frac{w_{SB}^{\ 2}}{2}\right)q_4^2 + \\ \left(m_{SB}gL_{SBR} - m_{TC}gL_{TCR}\right)q_6 + \left(K_{TC3}L_{TC} - m_{TC}g\frac{L_{TC}}{2}\right)q_7 + K_{TC7}q_7^{\ 2} + \\ \left(K_{TC7} + K_{SB8} + K_{TC7}\frac{L_R^{\ 2}}{4} + K_{SB8}\frac{L_R^{\ 2}}{4} + K_{TC3}L_{TCR}^{\ 2} + K_{SB3}L_{SBR}^{\ 2}\right)q_6^{\ 2} + \\ \left(m_{SB}g\frac{L_{SB}}{2} + K_{SB3}L_{SB}\right)q_8 + K_{SB8}q_8^{\ 2} \end{array}\right\} \qquad (3.19)$$

3.2. **Second Order Nonlinear System of Equations of Motion**

1. $m_{Tot}\ddot{q}_1 + \left(\ddot{q}_7 q_7 + \dot{q}_7^2\right)m_{TC}L_{TC}/2 - \left(\ddot{q}_8 q_8 + \dot{q}_8^2\right)m_{SB}L_{SB}/2 = 0$

2. $m_{Tot}\ddot{q}_2 = 0$

3. $m_{Tot}\ddot{q}_3 + \left(\ddot{q}_8 q_8 + \dot{q}_8^2\right)L_{SB}/2 + b_{Tot3}\dot{q}_3 + \left(4K_{TC3} + 4K_{SB3}\right)q_3 + m_{Tot}g = Q_3$

4. $J_r\ddot{q}_4 + \left(w_{TC}^{\ 2}b_{TC3} + w_{SB}^{\ 2}b_{SB3}\right)\dot{q}_4 + \left(K_{TC4}w_{TC}^{\ 2} + K_{SB4}w_{SB}^{\ 2}\right)q_4 = Q_4$

5. $J_y\ddot{q}_5 = 0$

$$J_p\ddot{x}_{16} - J_{TC}\ddot{x}_{17} - J_{SB}\ddot{x}_{18} + \left(\begin{array}{l} 2b_{TC7} + 2b_{SB8} + \frac{L_R^{\,2}}{4}\left(2b_{TC3} + 2b_{SB3}\right) + \\ 2b_{TC3}L_{TCR}^{\,2} + 2b_{SB3}L_{SBR}^{\,2} \end{array}\right)\dot{x}_{16} +$$

6. $$2\left(K_{TC7} + K_{SB8} + K_{TC7}\frac{L_R^{\,2}}{4} + K_{SB8}\frac{L_R^{\,2}}{4} + K_{TC3}L_{TCR}^{\,2} + K_{SB3}L_{SBR}^{\,2}\right)q_6 +$$
$$m_{SB}gL_{SBR} - m_{TC}gL_{TCR} = Q_6$$

$$\ddot{x}_{17}\left(J_{TC} + \frac{L_{TC}^{\,2}}{4} + q_7^2 m_{TC}\frac{L_{TC}^{\,2}}{4}\right) - J_{TC}\ddot{x}_{16} - \ddot{x}_{13}L_{TC}/2 + \left(\ddot{x}_{11}q_7 + \dot{x}_{17}\dot{x}_{17}\right)m_{TC}L_{TC}/2 +$$

7. $$2\dot{x}_{17}q_7 m_{TC}L_{TC}^{\,2}/4 - \dot{x}_{11}\dot{x}_{17}m_{TC}L_{TC}/2 - \dot{x}_{17}^2 q_7 m_{TC}L_{TC}^{\,2}/4 + 2b_{TC7}\left(1 + L_{TC}^{\,2}\right)\ddot{x}_{17} +$$
$$2K_{TC7}q_7 + K_{TC3}L_{TC} - m_{TC}g\frac{L_{TC}}{2} = Q_7$$

$$\ddot{x}_{18}\left(J_{SB} + \frac{L_{SB}^{\,2}}{4} + q_8^2 m_{SB}\frac{L_{SB}^{\,2}}{4}\right) - J_{SB}\ddot{x}_{16} - \left(\ddot{x}_{11}q_8 + \dot{x}_{11}\dot{x}_{18}\right)m_{SB}L_{SB}/2 + 2\dot{x}_{18}q_8 m_{SB}L_{SB}^{\,2}/4 +$$

8. $$\left(\ddot{x}_{13}q_8 + \dot{x}_{13}\dot{x}_{18}\right)L_{SB}/2 + \dot{x}_{11}\dot{x}_{18}m_{SB}L_{SB}/2 - \dot{x}_{18}^2 q_8 m_{SB}L_{SB}^{\,2}/4 - \dot{x}_{13}\dot{x}_{18}L_{SB}/2 - \dot{x}_{18}L_{SB}^{\,2}/4 -$$
$$J_{SB}\left(-\ddot{x}_{16} + \ddot{x}_{18}\right) + 2b_{SB8}\left(1 + L_{SB}^{\,2}\right)\ddot{x}_{18} + 2K_{SB8}q_8 + K_{SB3}L_{SB} + m_{SB}g\frac{L_{SB}}{2} = Q_8$$

The aforementioned 2nd order system of equations is converted to a 1st order system of equations by introducing a change of variables from q to x, as shown below and will be put in the implicit form $f\left(t, x, \dot{x}\right) = 0$.

$$x = \left[x_1 \;\; x_2 \;\; x_3 \;\; x_4 \;\; x_5 \;\; x_6 \;\; x_7 \;\; x_8 \;\; x_9 \;\; x_{10} \;\; x_{11} \;\; x_{12} \;\; x_{13} \;\; x_{14} \;\; x_{15} \;\; x_{16}\right]^T \equiv$$
$$\left[q_1 \;\; \dot{x}_{11} \;\; q_2 \;\; \dot{x}_{12} \;\; q_3 \;\; \dot{x}_{13} \;\; q_4 \;\; \dot{x}_{14} \;\; q_5 \;\; \dot{x}_{15} \;\; q_6 \;\; \dot{x}_{16} \;\; q_7 \;\; \dot{x}_{17} \;\; q_8 \;\; \dot{x}_{18}\right]^T \qquad (3.20)$$

3.3. **First Order Nonlinear System of Equations of Motion**

1. $\dot{x}_1 - x_2 = 0$

2. $m_{Tot}\dot{x}_2 + \left(\dot{x}_{14}x_{13} + x_{13}^2\right)m_{TC}L_{TC}/2 - \left(\dot{x}_{16}x_{15} + x_{16}^2\right)m_{SB}L_{SB}/2 = 0$

3. $\dot{x}_3 - x_4 = 0$

4. $m_{Tot}\dot{x}_4 = 0$

5. $\dot{x}_5 - x_6 = 0$

6. $m_{Tot}\dot{x}_6 + \left(\dot{x}_{16}x_{15} + x_{16}^2\right)L_{SB}/2 + b_{Tot3}x_6 + \left(4K_{TC3} + 4K_{SB3}\right)x_5 + m_{Tot}g - Q_3 = 0$

7. $\dot{x}_7 - x_8 = 0$

8. $J_r\dot{x}_8 + \left(w_{TC}{}^2 b_{TC3} + w_{SB}{}^2 b_{SB3}\right)x_8 + \left(K_{TC4}w_{TC}{}^2 + K_{SB4}w_{SB}{}^2\right)x_7 - Q_4 = 0$

9. $\dot{x}_9 - x_{10} = 0$

10. $J_y\dot{x}_{10} = 0$

11. $\dot{x}_{11} - x_{12} = 0$

$$J_p\dot{x}_{12} - J_{TC}\dot{x}_{14} - J_{SB}\dot{x}_{16} + \left(\begin{array}{l} 2b_{TC7} + 2b_{SB8} + \frac{L_R{}^2}{4}\left(2b_{TC3} + 2b_{SB3}\right) + \\ 2b_{TC3}L_{TCR}{}^2 + 2b_{SB3}L_{SBR}{}^2 \end{array}\right)x_{12} +$$

12. $$2\left(K_{TC7} + K_{SB8} + K_{TC7}\frac{L_R{}^2}{4} + K_{SB8}\frac{L_R{}^2}{4} + K_{TC3}L_{TCR}{}^2 + K_{SB3}L_{SBR}{}^2\right)x_{11} +$$
$$m_{SB}gL_{SBR} - m_{TC}gL_{TCR} - Q_6 = 0$$

13. $\dot{x}_{13} - x_{14} = 0$

$$\dot{x}_{14}\left(J_{TC} + \frac{L_{TC}{}^2}{4} + x_{13}^2\frac{L_{TC}{}^2}{4}m_{TC}\right) - J_{TC}\dot{x}_{12} - \dot{x}_6 L_{TC}/2 + \left(\dot{x}_2 x_{13} + x_2 x_{14}\right)m_{TC}L_{TC}/2 +$$

14. $$2x_{14}x_{13}m_{TC}L_{TC}{}^2/4 - x_2x_{14}m_{TC}L_{TC}/2 - x_{14}^2x_{13}m_{TC}L_{TC}{}^2/4 + 2b_{TC7}\left(1 + L_{TC}{}^2\right)x_{14} +$$
$$2K_{TC7}x_{13} + K_{TC3}L_{TC} - m_{TC}g\frac{L_{TC}}{2} - Q_7 = 0$$

15. $\dot{x}_{15} - x_{16} = 0$

16. $$\ddot{x}_{16}\left(J_{SB}+\frac{L_{SB}^{\ 2}}{4}+x_{15}^{2}\frac{L_{SB}^{\ 2}}{4}m_{SB}\right)-J_{SB}\ddot{x}_{12}-\left(\ddot{x}_{2}x_{15}+x_{2}x_{16}\right)m_{SB}L_{SB}/2+$$
$$2x_{16}x_{15}m_{SB}L_{SB}^{\ 2}/4+\left(\ddot{x}_{6}x_{15}+x_{6}x_{16}\right)L_{SB}/2+x_{2}x_{16}m_{SB}L_{SB}/2-x_{16}^{2}x_{15}m_{SB}L_{SB}^{\ 2}/4-$$
$$x_{6}x_{16}L_{SB}/2-x_{16}L_{SB}^{\ 2}/4-J_{SB}\left(-x_{12}+x_{16}\right)+2b_{SB8}\left(1+L_{SB}^{\ 2}\right)x_{16}+2K_{SB8}x_{15}+$$
$$K_{SB3}L_{SB}+m_{SB}g\frac{L_{SB}}{2}-Q_{8}=0$$

3.4. **Solution to Nonlinear 1st Order System of Equations of Motion**

The solution to the above system of equations is given in Figure 3.1-Figure 3.4. Figure 3.1 and Figure 3.2 show the position and velocity component of each state side by side. Figure 3.3 summarizes all the position states while Figure 3.4 summarizes all the velocity states relative to each other. The solution is visibly comparable to the output of the SimMechanics without quantifying the difference. Note, when programming the system of equations into MATLAB the sinusoidal force terms (3.17) used to construct the generalized applied force terms above did not include the additive noise term. Including the noise outputted an error message and didn't allow the simulation to complete.

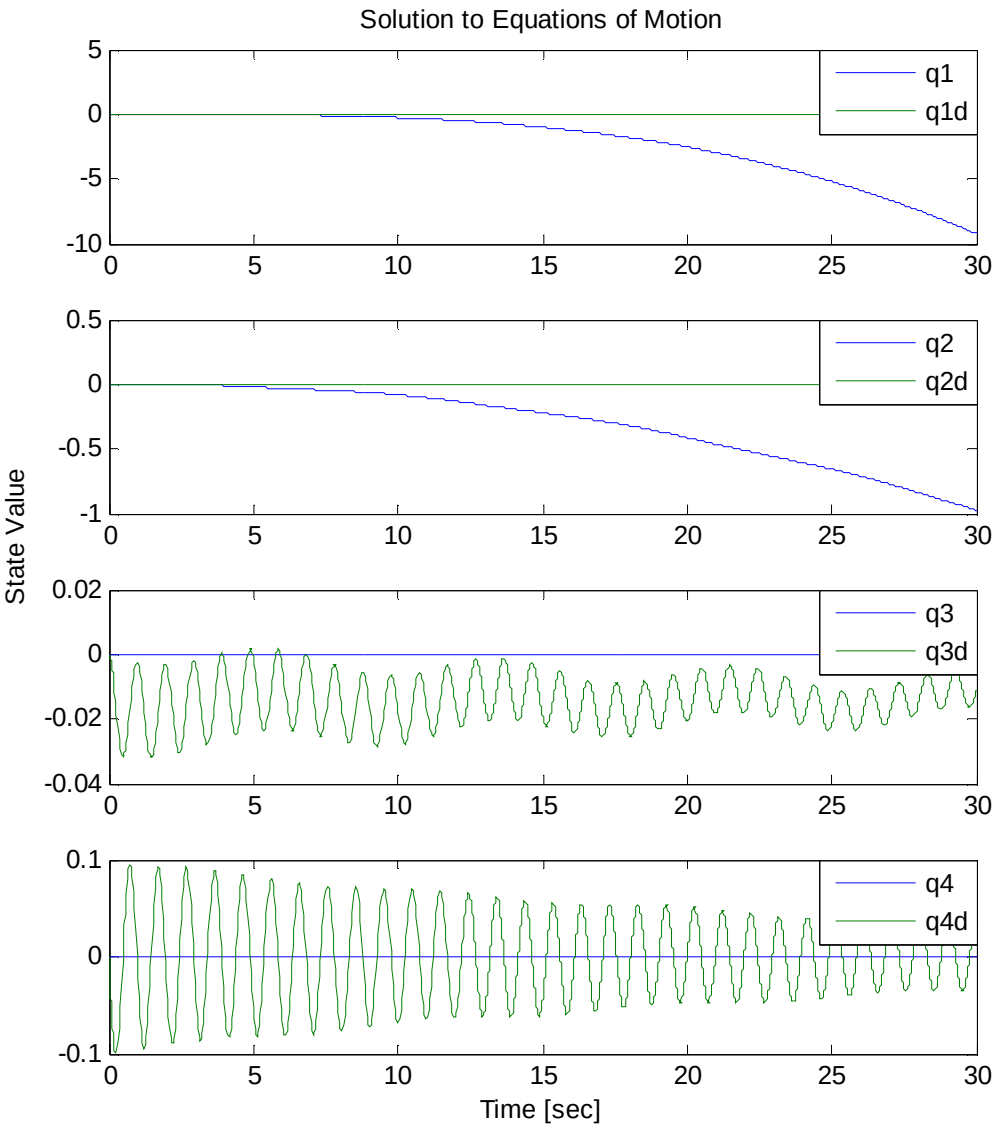

Figure 3.1: Solution to Equations of Motion for $q_1 - q_4$

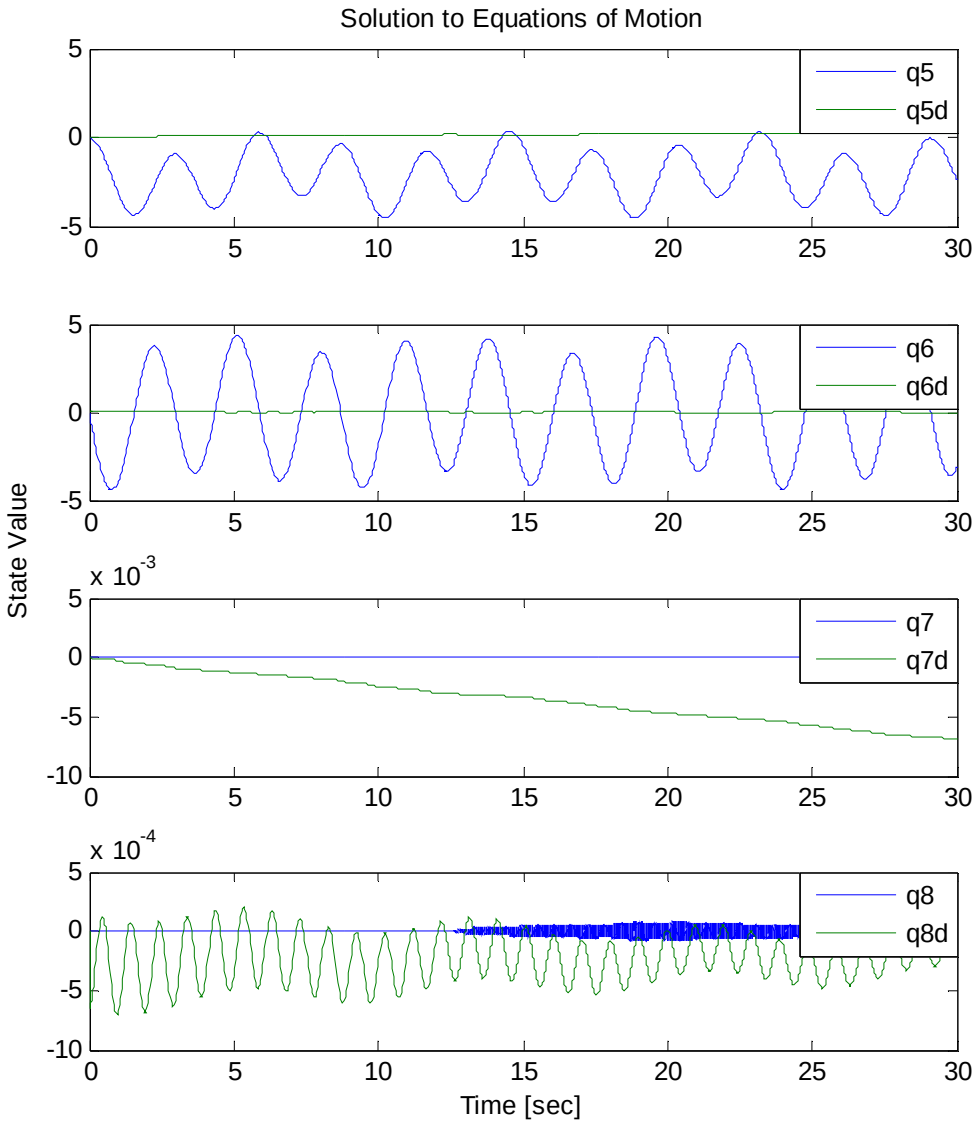

Figure 3.2: Solution to Equations of Motion for $q_5 - q_8$

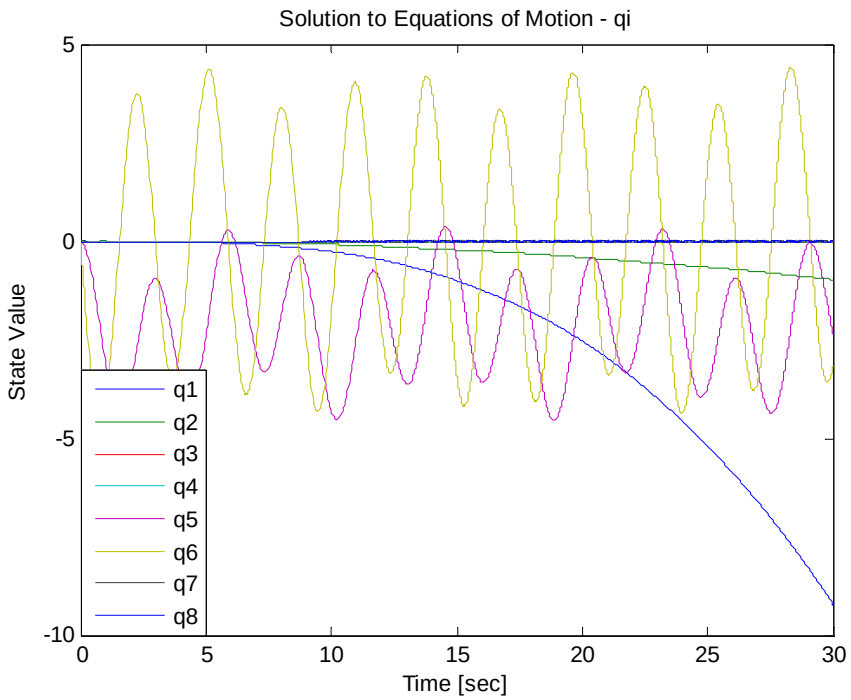

Figure 3.3: Summary of Position States

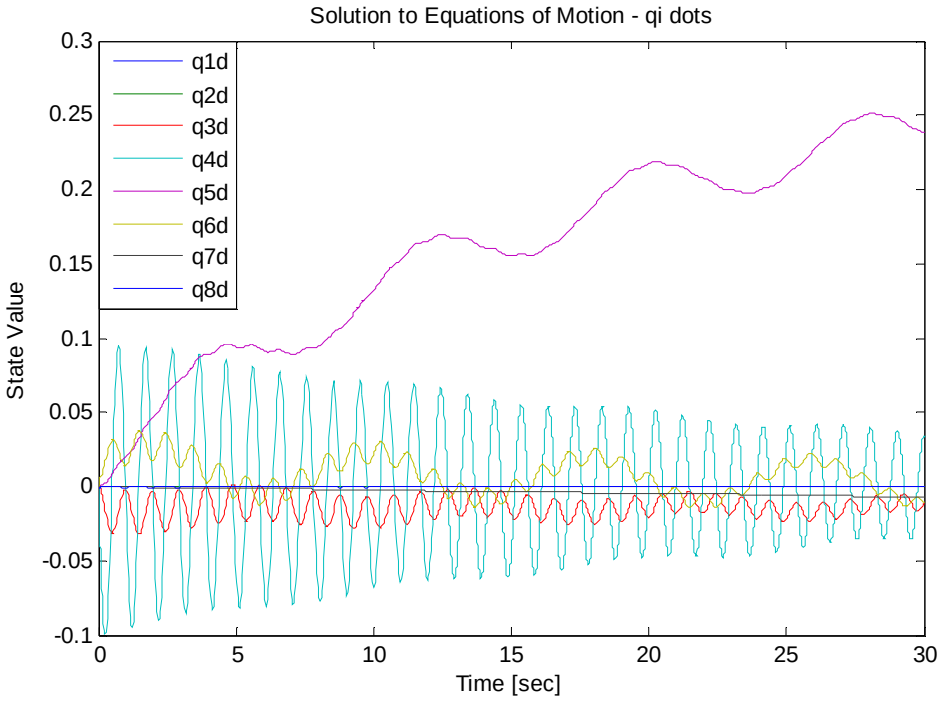

Figure 3.4: Summary of Velocity States

Chapter 4. Extremum Seeking

Extremum Seeking is a non-model based tool to find local extremum in relevant situations. The algorithm presupposes that a local minimum exists in the plant and by filtering, demodulating, integrating and perturbing the output which is then fed back into the plant, over time, the output will converge to an optimal value. A more detailed proof of this algorithm can be found in Ariyur and Krstic [1]. The uniqueness of the ship system in regards to its applicability to extremum seeking is that an added perturbation signal is unnecessary in the ES loop; rather the inherent oscillatory behavior of the ship motion in the ocean waves suffices for its implementation. In the usual implementation of ES the system is driven to equilibrium stabilization. Due to the fact that the ship system will indefinitely oscillate in an ocean environment, the ES algorithm is used to minimize the amplitude of the limit cycle inherent in this system. The joint type that is used in the ES simulations is Pitch Joint. The parameter chosen to optimize is the pitch angle of the ramp, which is fed into the amplitude detector block and then to construct the cost.

4.1. Amplitude Detector Block

The additional component in the ES loop in the limit cycle application is the amplitude detector block (ADB). This consist of running the desired oscillatory signal through a high pass filter to eliminate the DC component, square the filtered signal to separate the amplitude term from the unwanted high frequency components, and finally run the resulting signal through a low pass filter in order to output just the

amplitude term. The main assumption is: the limit cycle frequency, ω_o, is much greater than the cutoff frequency of the high and low pass filters. This technique was adapted from Ariyur and Krstic [1]. In its application to the ship system the detector block is shown in Figure 4.1.

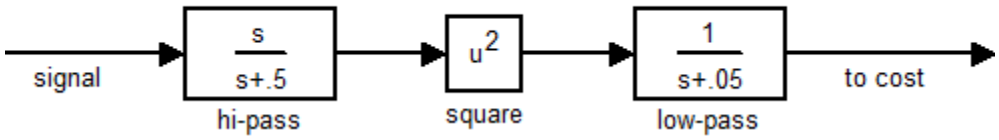

Figure 4.1: Amplitude detector block components

Figure 4.2 shows the pitch and roll power spectrums of the limit cycle for the ramp where the main frequency component lies at $\omega_o = 0.785$ rad/s for both signals corresponding to the ocean wave model modal frequency for SS 4. However, the pitch angle spectrum also includes frequencies around 2.2 and 2.5 rad/s. The additional components in the pitch angle are due to the fact that the two vessels experience slightly different frequencies in heave motion. This fact directly influences the pitch angle position and thus frequency components. Since there is no separate roll DOF in the pitch joint model, the whole system oscillates with the same frequency in roll, hence the single dominant frequency. The frequency content does not change with varying ramp length and wave heading angle, but the magnitude of the frequencies do. The results from Figure 4.2 correspond to ramp length = 10 m and α = 45 degrees. The resulting ADB output is fed into the cost and into the rest of the ES loop. For a successful seek, the amplitude of the inputted signal will decrease to its minimum value once the parameters are optimized with respect to the given cost.

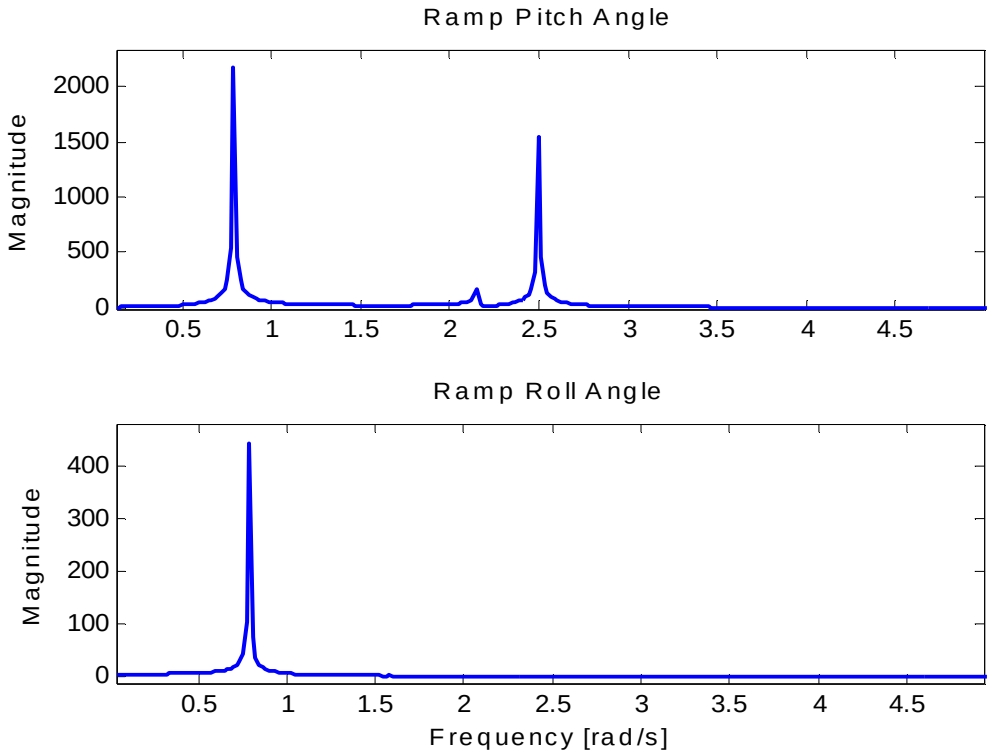

Figure 4.2: Frequency Content of Ramp's Pitch and Roll Positions

The cost is constructed using the signal that is output from the amplitude extraction block then multiplied by an exponential penalty function on the ramp length that peaks around a specified neighborhood of values.

$$Cost = S \times 1.003^{R^2} \tag{4.1}$$

where S is the signal amplitude term from the ADB and R is the ramp length. Upon implementation of the single parameter (ramp length) optimization problem the signal chosen to drive the cost is the pitch angle between the T-Craft and ramp. The reason for not including the roll signal in the cost is because increasing the ramp length does not show any influence on the roll motion and therefore its inclusion in the cost would be inconsequential in regards to the ES loop objective of finding a local

minimum. However, in the multiple parameter optimization problem, both the roll and pitch signals can be used in constructing the cost. In other words, the wave heading angle influenced the roll experienced by the system, while the ramp length influenced the pitch, proving their worthiness of inclusion in the cost.

Forming the cost plots a priori provides an ad hoc estimate of the locations of extremum, which automatically gives the optimal values for the ramp length and heading angle. Three dimensional cost plots were generated based on the Pitch Joint SimMechanics model through a series of simulations where the ramp length and wave heading angle were varied from 5 to 30 meters and $-\pi/2$ to $\pi/2$ radians respectively. During each simulation the ramp length and heading angle were fixed and the maximum of the absolute value of the pitch and roll signals were recorded. This was done until every combination of ramp length and heading angle was accounted for. The plots of Figure 4.3 show the cost value for the corresponding ramp length and heading angle without and with a penalty on ramp length for the pitch only joint case. The next two figures show the cost for the PR-Joint and PRY-Joint respectively. As shown in the left plot of the P-Joint case, the cost decreases as the ramp length increases; this makes sense intuitively. If the heave motions of two vessels stay constant, and the distance between the vessels increases, the ramp angle amplitudes will clearly decrease. Increasing the ramp length until the desired angle amplitudes are achieved is impractical and therefore a penalty function is included to prevent the ramp length from tracking to an infinitely long value. The inclusion of the penalty function creates a more pronounced and convex cost plot and therefore facilitates the

ES algorithm to tracking to a certain ramp length value while minimizing the ramp angle amplitudes as much as possible.

The penalty function is an exponential raised to the square of the ramp length and multiplied by the sum of the maximum pitch and maximum roll angle amplitudes. The constants a1 and a2 serve as weights to give either DOF a greater influence on the cost. In this investigation both weights were set to one. In all the joint cases considered, the cost plots were mostly symmetric about the zero degree line with a slightly smaller cost value in the negative region compared to the positive region. This negative wave heading angle corresponds to the waves first hitting the Sea Base and then propagating towards the T-Craft. Having the penalty function multiply the original cost effectively preserved the ramp length's influence on the cost as seen in the post washout filter signal as shown in Figure 4.8. For an additive penalty on the ramp length there were insignificant differences in the post washout filter signal and lead to the conclusion that the tracked values did not optimize over the ramp length.

In the P-Joint case, we can use the cost plot above to get an estimate of the optimal value for ramp length and wave heading angle for the penalty function used. In Figure 4.6 the two relevant side views of the cost plot are shown, making the minimum values clearly visible. The minimum ramp length lies between 10 and 15 meters, while the minimum heading angle lies between -20 and -30 degrees. The goal of the extremum seeking algorithm is to make the two parameters considered converge to the aforementioned neighborhood of values to minimize the cost.

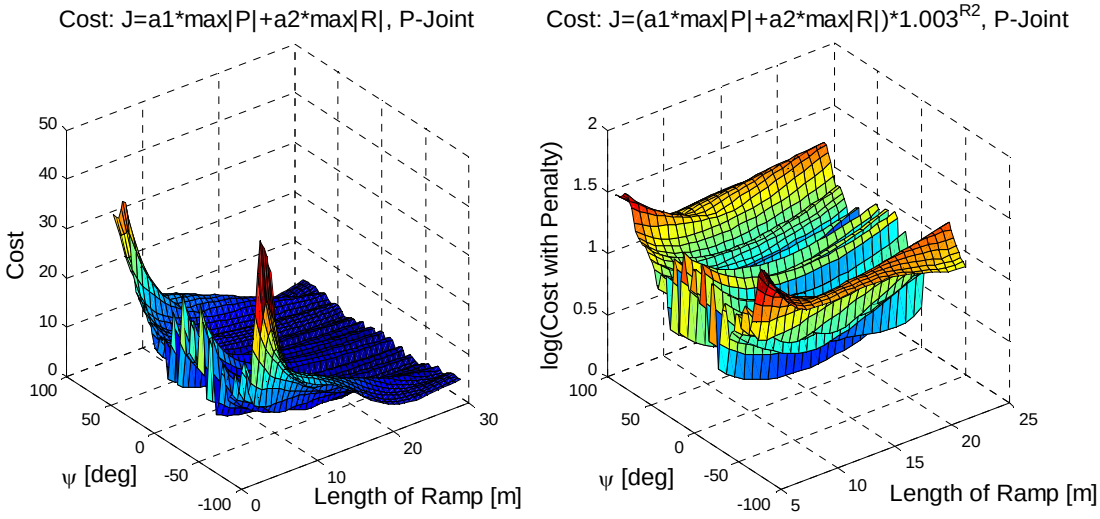

Figure 4.3: Cost Plot without penalty (left) and with penalty (right) for P-Joint

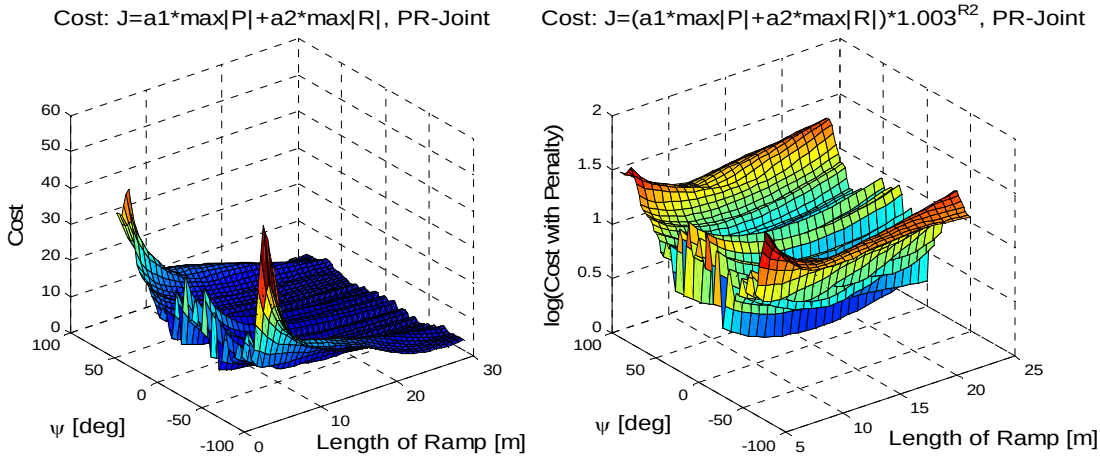

Figure 4.4: Cost Plot without penalty (left) and with penalty (right) for PR-Joint

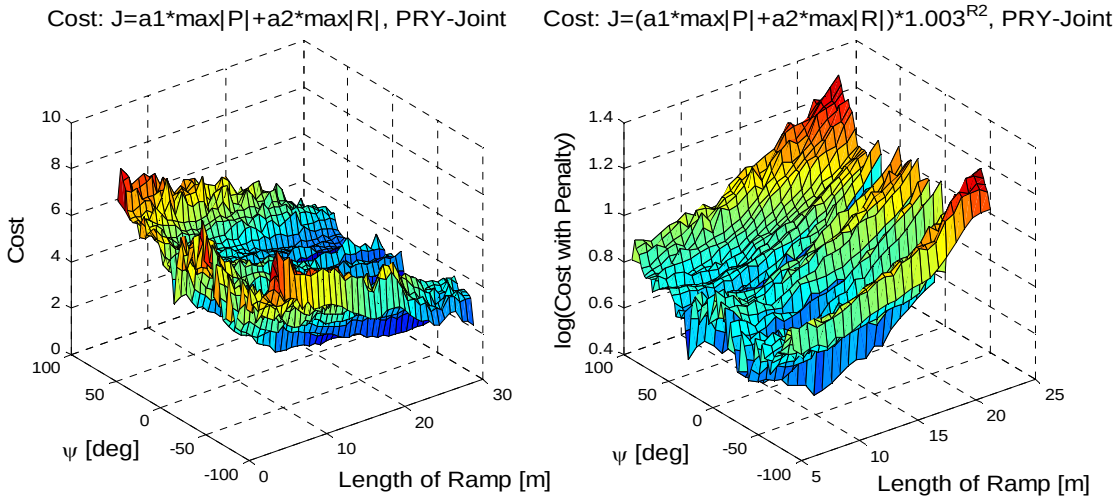

Figure 4.5: Cost Plot without penalty (left) and with penalty (right) for PRY-Joint

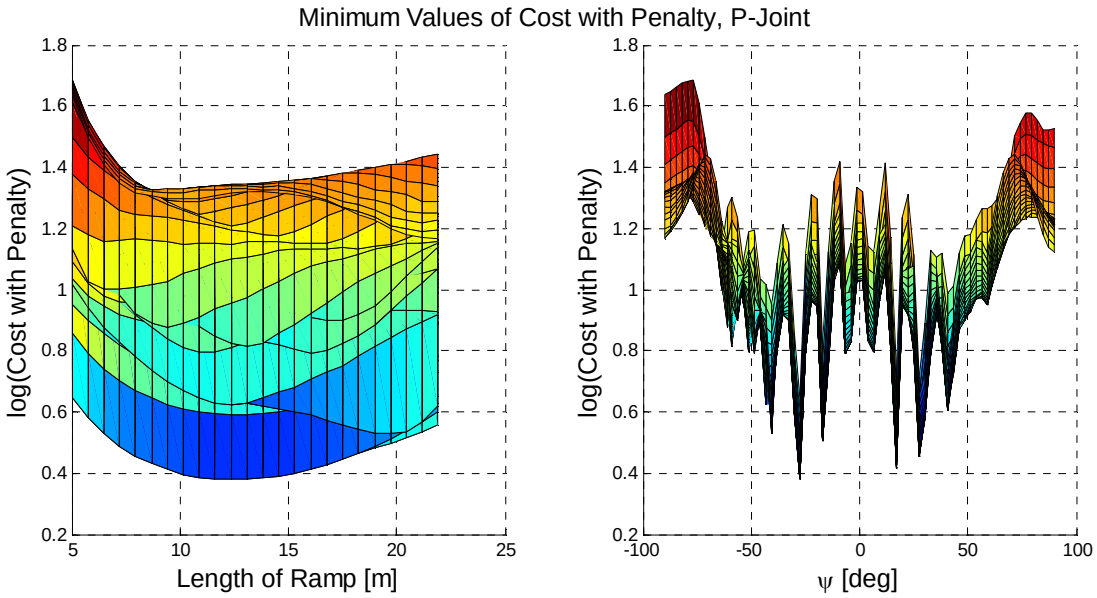

Figure 4.6: Minimum Values View of Cost with Penalty, P-Joint

4.2. ES Loop and Results for Single Parameter Seeking

The next matter of discussion will be the details of the ES loop when applied to this system and the results that follow. As shown in Figure 4.7, following the ADB the ES loop consists of a washout filter, demodulation signal, integrator, gain and then a low-pass filter. The resulting signal is fed into the actuators to extend the ramp. This process is repeated until the signal reaches its extremum value on the cost and the parameter values are optimized. The washout filter acts as a high-pass filter and kills the DC component of the incoming signal. The demodulation works under the assumption the incoming signal is fairly sinusoidal, which is valid in this case. Demodulating with a sine wave returns a convenient form of the signal after applying the necessary trigonometric identities, which isolates the desired term corresponding to the error between estimate and minimum value. The low pass filter acts to prevent the ramp from extending and contracting too quickly and rather promotes smooth

actuation. Once the ramp length reaches a steady value, the inherent oscillations can be eliminated by a dead zone block after the integrator in the ES loop to further smooth the actuation.

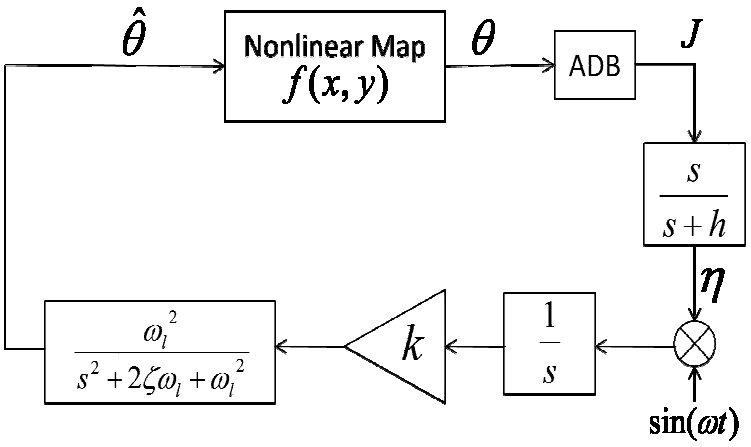

Figure 4.7: ES loop for single parameter seeking

The results shown in Figure 4.8 are obtained when using the following values for the constants in the ES loop $P = 1.003,\ h = 10,\ \omega = 1$ rad/s, $k = -5,\ \omega_l = 0.03$ rad/s, $\zeta = 1$.

In practice it is convenient to find internal measurable signals of the system to use for demodulation. For example, the following signals were used as the demodulation: T-Craft heave, Sea Base heave, pitch angle between T-Craft and ramp, angular velocity and angular acceleration. The oscillatory behavior of these signals is beneficial for the ES loop to work properly. Although these substitutions may promote convergence there exists some offset in the final ramp length convergence that varies with the demodulating signal chosen. Also, the phase delay that the demodulating

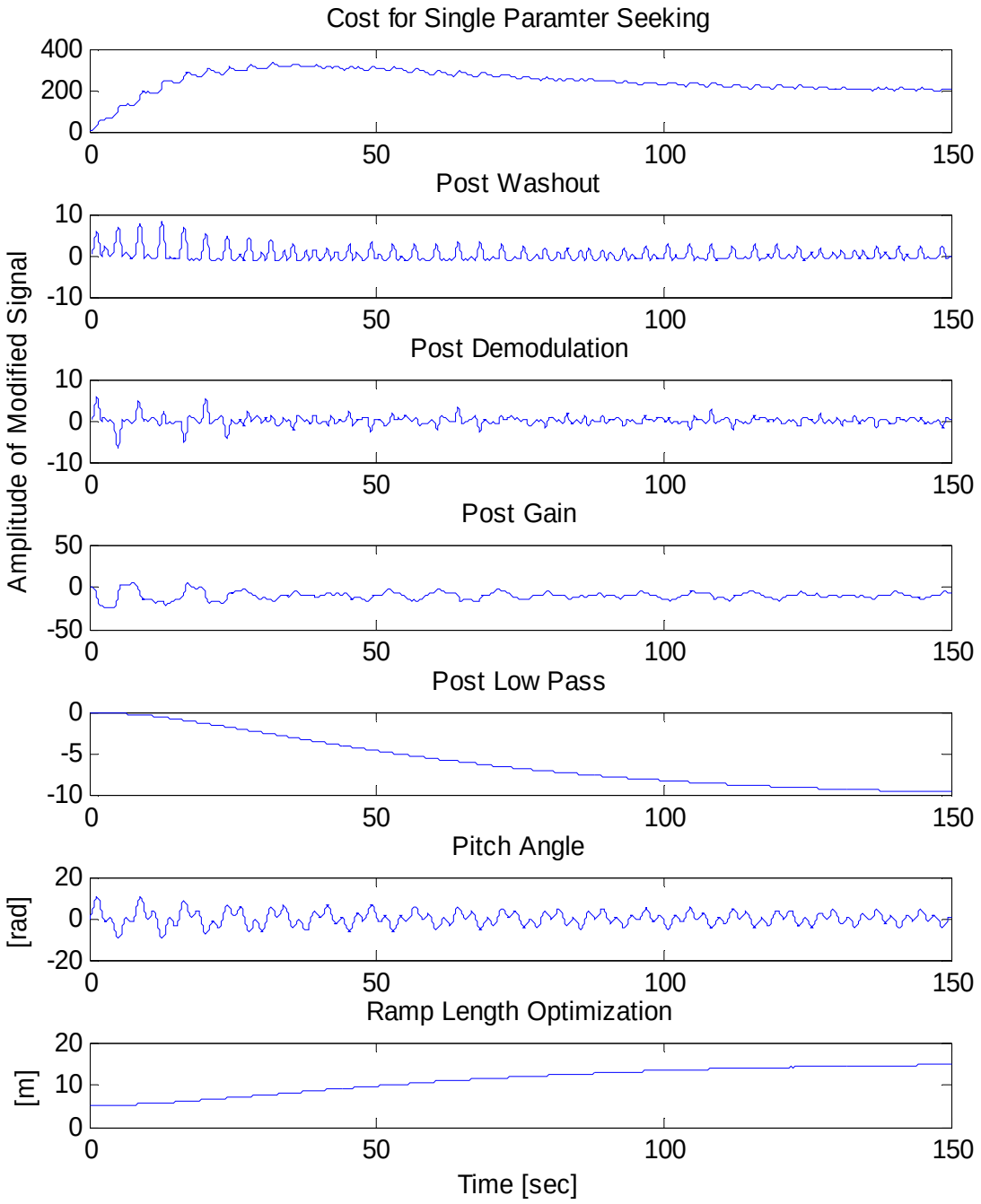

Figure 4.8: Summary of Results for Single Parameter Seeking

signal enters the ES loop is a crucial parameter that influences the success of the extremum seeking. Table 4.1 summarizes the demodulating signals, their respective phases and the ramp length convergence value. The cost associated with these results

is formed by adding the ramp length penalty (instead of multiplying) to the signal amplitude. Although the cost function has been improved by multiplying the terms, these results show the strategy one needs to find a proper demodulating signal. The initial ramp length is 25 m with a heading angle of 90 degrees.

Table 4.1: Summary of demodulation results for α = 90□

Demodulation Signal	Phase [sec]	Final ramp length [m]
Sine	0	35
T-Craft Heave	5	37
Sea Base Heave	3	37
Angular Position	7	34
Angular Velocity	14.1	33
Angular Acceleration	10.1	33

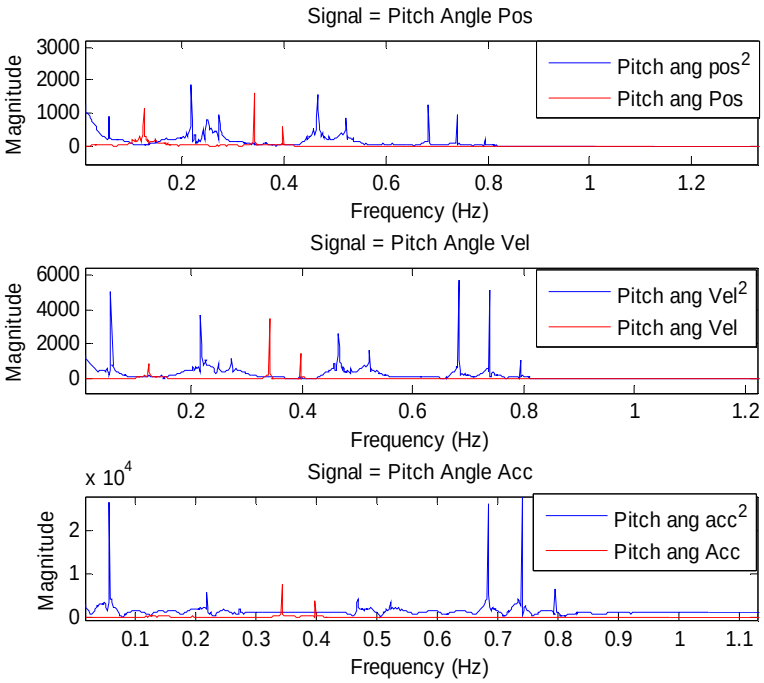

Figure 4.9: Spectrums of signals from pitch joint

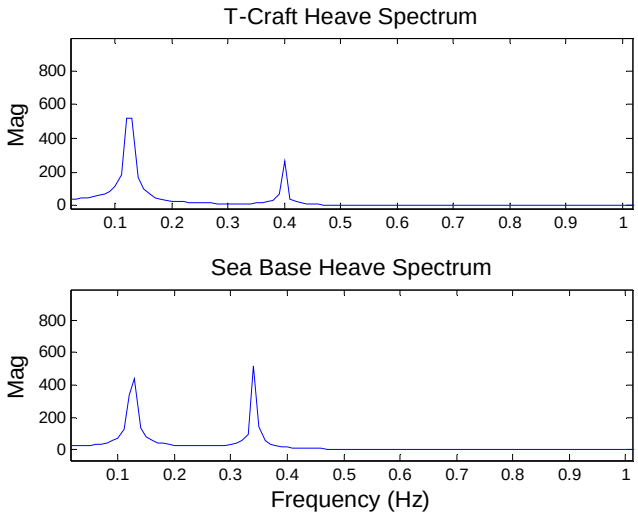

Figure 4.10: Spectrum of T-Craft and Sea Base heave signal

4.3. **Results for Multiple Parameter Seeking**

Modifying the ES loop for the single parameter case allows us to add another variable to optimize. In addition to optimizing the ramp length, the ES loop is designed to optimize the orientation of the system with respect to the ocean wave heading angle, α. Figure 4.11 shows the general components of the ES loop for multiple parameter seeking, with the constant values given as $h_1 = 0.02,\ h_2 = 10,\ l = 1,\ P = 1.003,\ \omega_1 = \omega_2 = 1.04,\ k_1 = -1, k_2 = -0.09, \omega_l = 0.01, \zeta = 30$.

The ships were configured in a bow to stern orientation connected by a pitch jointed ramp. Figure 4.12 shows the results of a system beginning at a heading angle of 60 degrees and an initial ramp length of 5 meters. The heading angle settles to 28.5 degrees while the ramp settles to 11.5 meters as predicted by the cost plots.

The pitch oscillations are effectively reduced from initial amplitude of 15 degrees to just over 5 degrees throughout the simulation. Figure 4.13 shows the pitch

angle evolution with no ES tuning (top) and its reduction while using the ES algorithm (bottom). These results show that extremum seeking effectively reduces the pitch angle in the joint by finding the optimal ramp length and heading angle.

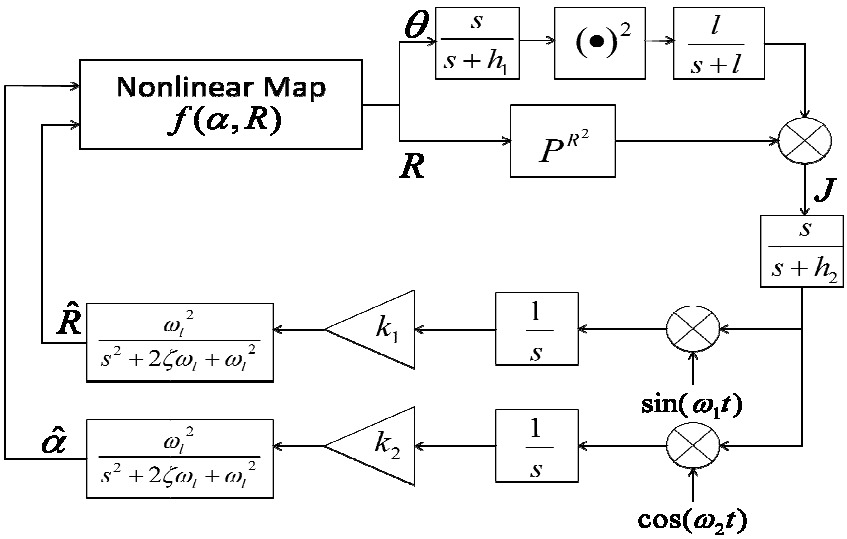

Figure 4.11: ES loop for multiple parameter seeking

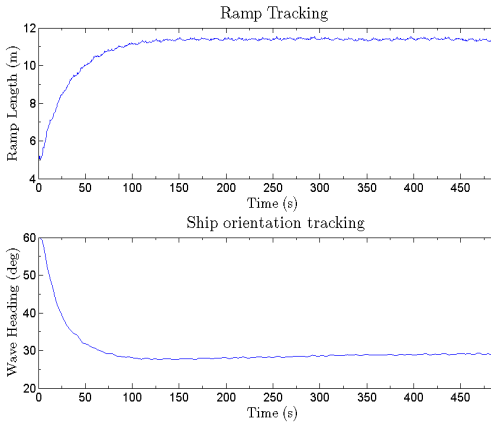

Figure 4.12: Multiple Parameter ES

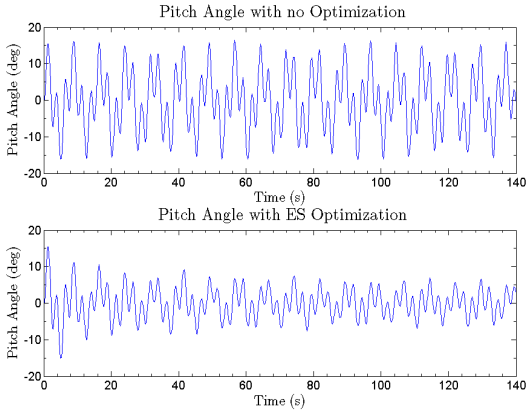

Figure 4.13: Pitch angle reduction during ES

Chapter 5. Passive Control with Shock Absorbers

The goal of the passive control investigation is to mimic automotive shock absorbers with springs and dampers. This reduces the angle amplitudes between the ramp and each vessel. We investigate three joint cases of the cargo transfer system with these passive control techniques. The three types of joints are: pitch joint (P-joint), pitch-roll joint (PR-joint), and pitch-roll-yaw joint (PRY-joint). The same initial conditions are used in each simulation. The ramp length is 5 meters and the wave front angle, (α), is 45 degrees. We use a damping coefficient of 100 Nms/deg in all cases. This magnitude is fixed to provide minimal impact on angle amplitude that instead will vary with spring rates.

In the PRY-joint case, we introduce springs in the roll and yaw DOFs to stabilize the system. Otherwise, the two ships end up crashing during the simulation. In the PRY-Joint case, the T-Craft's (TC) roll and yaw spring rates are $1x10^2$ Nm/deg and $1x10^6$ Nm/deg respectively, and the Sea-Base's (SB) roll and yaw rates are $1x10^5$ Nm/deg and $1x10^6$ Nm/deg respectively. We consider these spring rates minimum order of magnitude values to maintain stability and name them the uncontrolled case. The controlled case refers to the increased spring rate beyond the uncontrolled case in the PRY-joint. For the other joint cases the control case refers simply to the present of the absorbers. In each joint case, we ground the Sea-Base in the surge and sway directions to improve system stability.

We first simulate the system with no spring/damper absorber on either joint in order to get an estimate of the baseline angle amplitude values during a stable limit

cycle (except for the PRY-joint case as mentioned above). This is the open loop response. In this series of simulations we measure the following variables: roll, pitch, yaw angles, and the difference in heave between the two ships. The difference in heave measurement is calculated using the absolute value of the distance between the center of gravity of the T-Craft and Sea-Base. Due to the ships' different inertial and buoyancy properties their z-direction position is not necessarily going to be equal. The relative distance between the centers of gravity of the two ships directly relates to the pitch angle oscillations. If the difference in heave decreases in magnitude, the pitch angle amplitude will decrease accordingly. The open loop simulation results for the three cases for the TC and SB joint angles and heave are summarized on the first row of Figure 5.1, Figure 5.2, and Figure 5.3 respectively.

We then simulate the system applying a spring/damper absorber to the TC joint that is analogous to position and velocity feedback. For the pitch only case, we only use one spring/damper pair. We use two for the pitch-roll case and three for the pitch-roll-yaw case, one for each DOF. During the simulations the following measurements are taken: TC joint angles (pitch, roll, and yaw), difference in heave between the two ships and passive control effort (torque from spring/damper). The results are summarized in the second rows of Figure 5.1, Figure 5.3 and first row of Figure 5.4 respectively. In case of absorber failure, the control effort data can be used for the actuator requirements to provide the necessary torque for stability.

Finally, we simulate the system applying a spring/damper to the SB joint. The results of the angles, passive control effort and difference in heave and from the

controlled SB joint case are summarized in the second rows of Figure 5.2, Figure 5.3 and third row of Figure 5.4 respectively.

5.1. **Results**

A summary of all the results is given in Figure 5.1-Figure 5.5. Figure 5.1 summarizes the TC joint maximum angles of the open-loop and controlled system for the three joint cases. Figure 5.2 summarizes the SB joint maximum angles of the open-loop and controlled system for the three joint cases. Figure 5.3 summarizes the heave difference for the three cases using no control, TC joint control, and SB joint control. Figure 5.4 summarizes the passive control effort for the three cases using TC joint control and SB joint control. Figure 5.5 summarizes the ramp angles for all the cases and absorber arrangements considered. In the bar graphs the abscissa correspond to the three joint cases considered, namely P-joint, PR-joint, and PRY-joint respectively and the ordinate the corresponding angle or distance magnitude. The angle and distance evolution with time for each simulation is given in the appendix.

TC Joint Summary

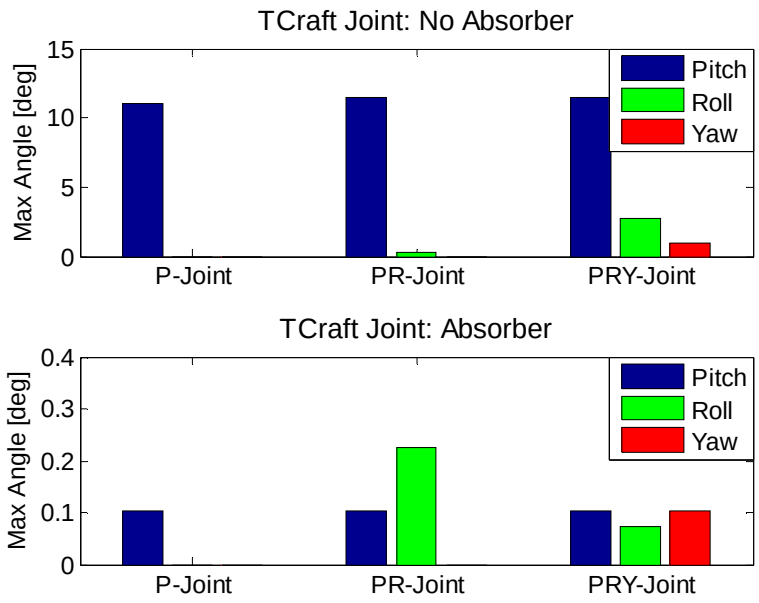

Figure 5.1: TC Joint Angles Summary

SB Joint Summary

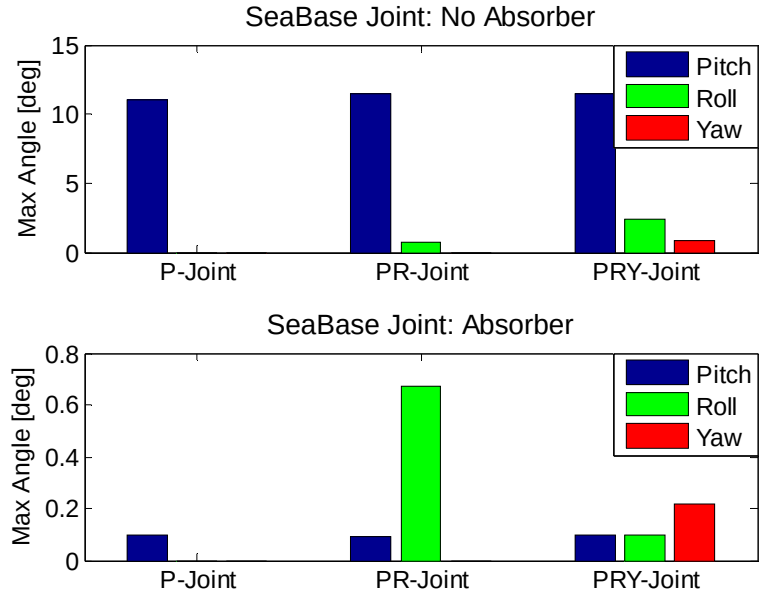

Figure 5.2: SB Joint Angles Summary

Heave Summary

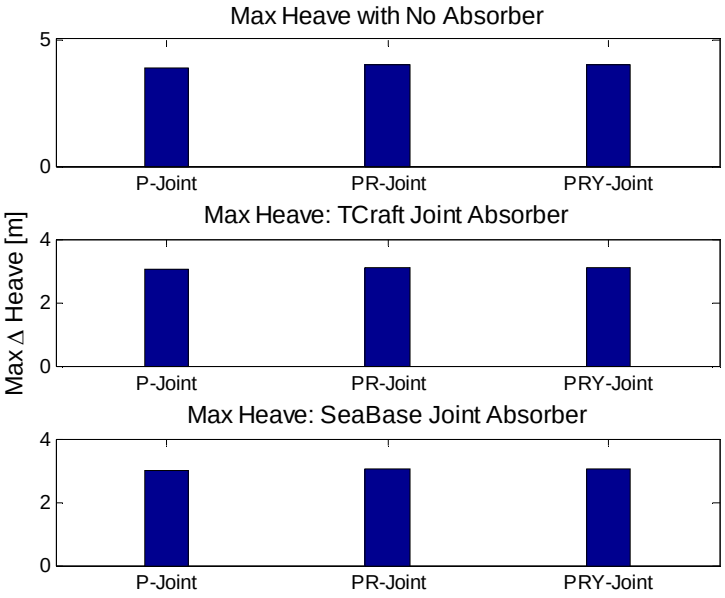

Figure 5.3: Heave Summary for No Absorber, TC Joint Absorber, and SB Joint Absorber

Passive Control Effort Summary for TC and SB Joint

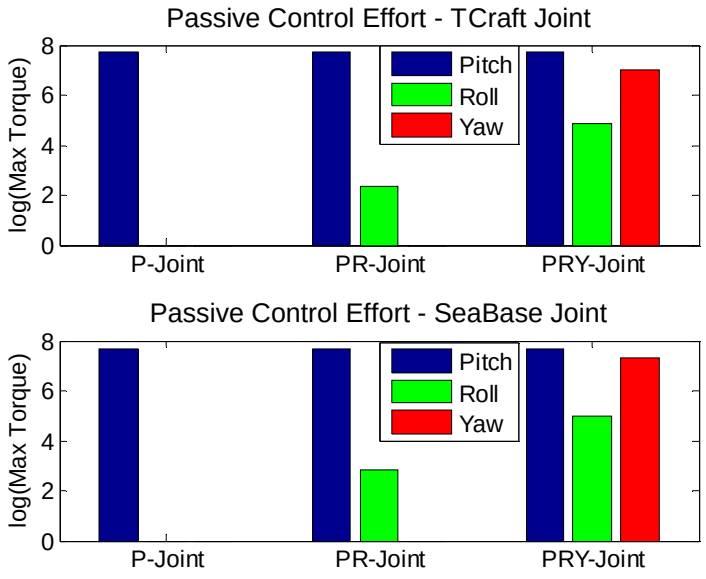

Figure 5.4: Passive Control Effort Summary

5.2. **Discussion of Joint Angles**

The above results summarize the motion at the joints for the various cases mentioned with and without shock absorbers. The open loop simulations show, for each of the cases in both the TC and SB joints, that the pitch angle oscillated between about ± 10 degrees. In the PR-joint case, the TC and SB joints experienced a roll angle oscillation of 0.34 and 0.89 degrees respectively. Any difference in TC and SB angle oscillations may be due to their different dimensions, inertial properties and the Sea-Base being grounded in the surge and sway directions while the T-Craft was not. In the PRY-joint case, the TC and SB *roll* angles were 2.93 and 2.76 degrees respectively, and their respective *yaw* angles were 1.14 and 1.09 degrees. The *yaw* angle oscillations in both joints are significantly more sensitive. These DOFs have a higher tendency to become unstable, and therefore require larger spring rate in the joints for stabilization. Increasing the spring rate in the *yaw* DOF decreases its influence on the behavior of the system, hence closely mirroring the PR-joint case, which has a desired stable system response. Furthermore, increasing the spring rate of the *roll* DOF makes the system response closely mirror the P-joint case, which also has a stable response.

The heave summary plots in Figure 5.3 show the improved performance between the open and closed loop simulations. With no absorbers the average delta heaves between the T-Craft and Sea-Base are 3.89 m, 4.01 m, and 4.00 m for the P-joint, PR-joint, and PRY-joint cases respectively; for an absorber on the TC joint the delta heaves are 3.03 m, 3.07 m, 3.07 m for each case respectively; for an absorber on

the SB joint the delta heaves are 3.02 m, 3.07 m, 3.07 m for each case respectively. The important point to see from these results is the decrease of about 1 m in delta heave between the uncontrolled and controlled simulations, which primarily affects the pitch angle, reducing it a few degrees.

The results of the controlled simulations show an improvement in the amplitude of angle oscillations for each of the DOFs as shown in Figure 5.1 and Figure 5.2. The amount of reduction depends on the spring constant chosen. An arbitrary constant was chosen in the effective order of magnitude range for the simulations to show a reduction in angle amplitudes. For all three controlled cases the *pitch* angle was reduced to about ±0.10 degrees for both the TC and SB joints with a gain value of $K_{pitch} = -5x10^{8}$. In the controlled PR-joint case the roll angle oscillation reduced to about ±0.21 and ± 0.59 degrees for the TC and SB joints respectively with a gain value of $K_{roll} = -1x10^{3}$. The smaller gain value implies less torque is experienced in the *roll* DOF. In the controlled PRY-joint case the *roll* angle oscillation is ±0.06 and ± 0.10 degrees for the TC and SB joints respectively with a gain value of $K_{roll} = -1x10^{6}$, and the *yaw* angle oscillation was ±0.10 and ± 0.22 degrees for the TC and SB joints respectively with a gain value of $K_{yaw} = -1x10^{8}$. Comparing the PR-joint to the PRY-joint we see that the addition of the *yaw* DOF significantly influences the gain tuning by a few orders of magnitude to reach a similar steady state value for the roll angle in the PR-joint case. As assumed the complexity and unpredictability of the response grows with the amount of DOFs.

5.3. **Discussion of Ramp Angles**

Another relevant set of values to look at is the ramp angles since the above joint data misses some crucial information. For example, in each of the joint cases, the only measured angle is the allowed DOF(s). In the pitch joint case, only the pitch angle is measured while the roll and yaw angle amplitudes of the ramp are unmeasured. If the ramp's roll DOF is unstable, it can be considered unobservable in the above joint measurements and would not be known if we only rely on the joint angle measurements. Measuring the ramp angles directly eliminates this problem. Figure 5.5 summarizes the ramp angles for each of the three cases and for four various scenarios, namely: no absorbers used in joints, an absorber on the T-Craft joint, an absorber on the Sea Base joint, and an absorber on both joints. Matching our intuition, the ramp angles are mostly maximal when no absorbers are used (with two exceptions as seen in figure), and mostly minimal when both joints have absorbers. The addition of each DOF creates unintuitive reactions in angle amplitudes. For example, when no absorber is used the roll angle is minimum in the PR-joint case and greater in the P- and PRY-joint case for no apparent reason. A future endeavor is to tune the dampers using extremum seeking in order to reduce the angles amplitudes even further.

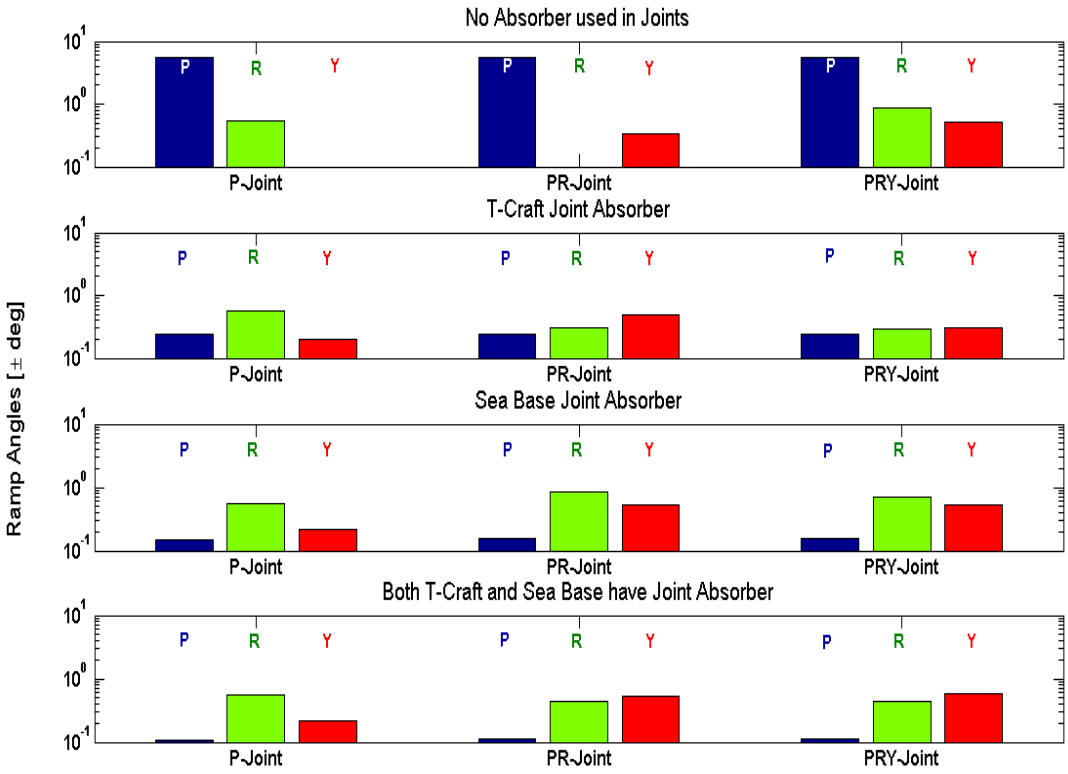

Figure 5.5: Summary of Max Ramp Angles

5.4. **Weight, Dimensions and Cost**

The rotary damper concept used in the absorber design exists on the market where one vendor is Efdyn and has a product with model number LD4 Dashpot. The product has dimensions 0.24 x 0.24 x 0.23 m, a damping rate of 4,000 Nms/rad (~70 Nms/deg), a weight of 17 Kg and cost of $4,400 each. A more feasible design will have greater dimensions and damping rate by a few orders of magnitude, but for the sake of proof of concept these values are sufficient.

In designing the springs one is constrained by the industry maximum values. The maximum wire diameter dimension is 3 inches and wire length before wound of 40 feet. The vendor MW Industries can make a spring with rate $5x10^9$ Nm/rad that

weighs about 160 Kg. Using the Hooke's law applied to a torsion spring one can design the spring by altering the relevant variables. One way to design the spring is to first define the torque (T) at a given deflection (F□) requirement, then approximate the design bending stress (S_b) from average service curves, then use the equations in (5.1) which are valid for round wire to determine the wire diameter, spring diameter and body length. Other wire options are square and rectangular wire.

$$d = \sqrt[3]{\frac{10.18T}{S_b}}, \quad T = \frac{Ed^4F^o}{4000ND}, \quad N = \frac{Ed^4F^o}{4000TD} \tag{5.1}$$

where E is elastic modulus of wire material, d diameter of wire, D outer diameter of spring cross section and N is number of active coils.

Chapter 6. Ship Roll Stabilizing Gyroscope

The technology of ship stabilizing gyroscopes emerged in the early 1900's and became more popular during the 1990's for stabilizing roll motions of low speed ocean vessels. Otto Schick of Hamburg, Germany was the first to use a pendulous gyroscope with a break device at the precession axis in 1903 to reduce the roll motion of a ship. Since then an active type was invented by Elmer A. Sperry where an actuator controlled the precession moment to counteract the moment from roll due to the ocean waves.

A gyroscope is a device that allows its flywheel to move about all three rotary degrees of freedom. If any of the output gimbals is in a fixed configuration then the gyroscope's flywheel will resist rotating in the corresponding DOF and will introduce a precession torque acting on the mounted body. When this gyroscopic resistance force exists the device is called a control moment gyroscope (CMG) or a rate gyroscope. CMG devices are commonly used in attitude control of spacecraft, aircraft and are adapted in ship systems, such as in military, luxury yachts, and ferry applications where low forward speed and roll stabilization is important. The effectiveness of a roll stabilizing gyroscope is a function of vessel displacement (the weight of a volume of water displaced by the vessel), transverse metacentric height, vessel speed, heading angle of waves and sea state. These devices typically comprise 1-5% of the vessel displacement to provide a various range of degrees in roll angle reduction. It is proposed that an anti-roll gyroscope mounted on the T-Craft can reduce

its roll angle amplitude and hence facilitate safely transferring cargo to it from the Sea Base through an interconnected ramp.

The basic elements of a control moment gyroscope are the flywheel, the inner and outer gimbals, and the motor that spins the flywheel. The most effective CMGs only have one gimbal, resulting in a total of two DOF for the flywheel with the precession torque acting in the direction of the third DOF. Let us define three axes of gyroscopic motion namely: spin, input and output axes. The axle upon which the flywheel rotates defines the spin axis. Each gimbal provides one degree of rotational freedom, which will define the motions along the input and output axes. The input axis is defined by the axis where an external torque is applied to the flywheel. Torque applied at the input axis brings forth the phenomenon of precession at the output axis. In roll stabilization applications, the spin axis corresponds to the z-axis on the body-fixed reference frame of an ocean vessel [3]; the input axis is the x-axis where roll occurs and is typically a fixed gimbal; the output axis is the y-axis where precession occurs and is a free gimbal. Figure 6.1 summarizes the orientation of these axes with respect to the T-Craft. The flywheel is designed to have a large moment of inertia about the spin axis in order to create the gyroscope effect of resisting roll motions.

Tilting the flywheel about the input axis while it spins, changes its angular momentum, consequently creating a precession torque acting on the output axis, which through active control is utilized to stabilize roll motion. For instance, in a typical control moment gyroscope for ships, if the flywheel lies on the z-axis of a vessel, and the spin is counterclockwise an angular momentum is created about the positive z-axis and is equal to $H = I_f \omega_f$, where ω_f is the spin rate of the flywheel in rad/s and I_f is

its moment of inertia about the spin axis in kgm^2. When a torque is applied to the flywheel at the input axis perpendicular to the spin axis, due to roll motion of the vessel, a torque perpendicular to both of these axes is created in the flywheel resulting in precession, an oscillatory motion about the y-axis of the gyroscope and thus creates a precession torque that acts internally to the ship system. The precession torque or Gyroscopic Reaction Moment (GRM) is given by

$$\tau_p = \omega_p \times H \Rightarrow \omega_p \times I_f \omega_f \tag{6.1}$$

where ω_p is the precession rate in rad/s and H is the angular momentum of the flywheel about the spin axis. Since the roll of the ship occurs on the x-axis and is orthogonal to the spin axis, the cross product becomes an ordinary multiplication. Typically, a gyro controller is used to regulate the precession torque rate by sending commands to a hydraulic brake generating an opposing torque on the y-axis of equal order of magnitude to transfer this internal precession torque to an external torque that acts on the hull of the vessel and will be addressed below. At this point there are effectively two sources of torque acting on the gyroscope despite the roll moment, namely the torque from the spinning flywheel on the z-axis and the torque from the hydraulic break on the y-axis. These two perpendicular torques cause the desired anti-roll torque required along the x-axis on the ship's hull to oppose the natural roll motion of the ship.

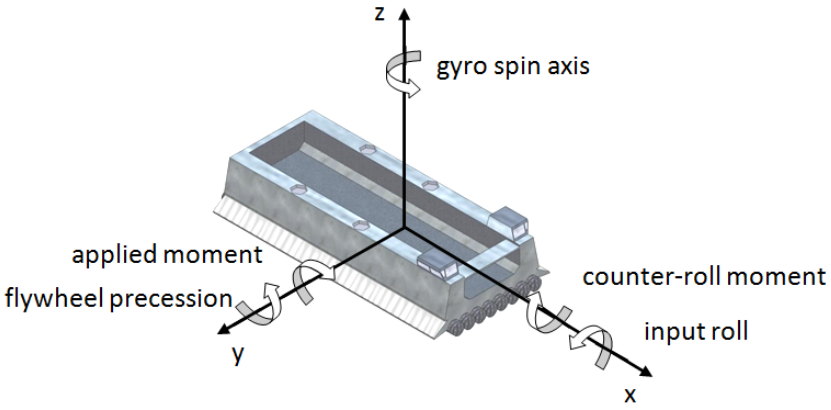

Figure 6.1: T-Craft with body fixed coordinates and axes of gyroscope

6.1. Design of the Gyroscope's Flywheel

The initial step in designing an effective roll stabilizing gyroscope is to determine the vessel's rolling moment and roll period while floating in flat water. It is assumed that the vessel rolls under constant displacement, meaning the ship neither loses nor adds loads. For small angles of roll a vessel's rolling moment is approximated by $M_R = \Delta \overline{GM}_R \sin\phi$ where Δ is the displacement (equal to the vessel weight force) and $\overline{GM}_R$ is the metacentric height about the roll axis, and when multiplied by $\sin\phi$ expresses the perpendicular distance from the center of gravity to the line of action of the new buoyancy force. Since the buoyancy force always acts perpendicular to the waterline, as the ship rolls ϕ degrees the waterline rotates ϕ degrees, the center of buoyancy moves toward the ship's submerged section and creates a new metacentric height. This new metacentric height is the point of intersection of the old and new buoyancy force line of actions. Carrying over the assumption of small roll angles extends the assumption that the metacentric height

stays relatively constant during roll and therefore the original metacentric height is used in computing the vessel's rolling moment. Figure 6.2, although not to scale, shows the location of these variables relative to each other on a transverse section of a half cylinder. The buoyant force labeled B causes the restoring moment when the vessel rolls.

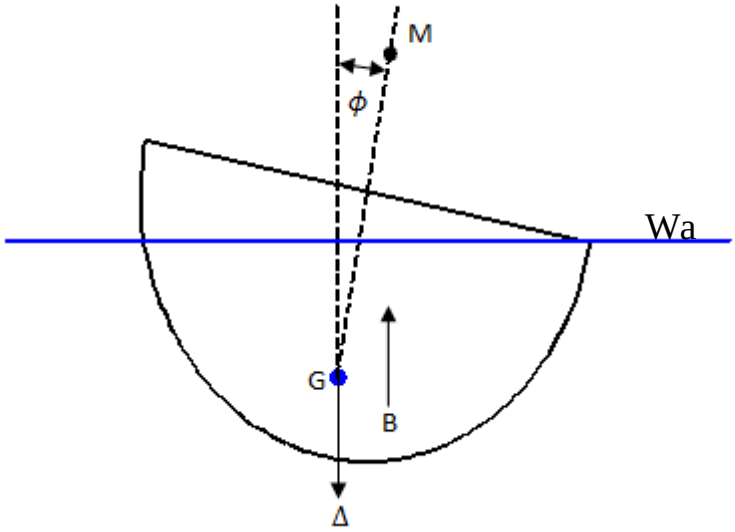

Figure 6.2: Vessel parameters during roll motion

It is assumed that a quasi-static roll angle of one degree suffices for the stabilization requirement. Thus, the T-Craft's roll moment becomes $M_R = 9,370\,\text{kNm}$. The designed gyroscope will create an equal and opposite moment on the vessel hull attempting to eliminate the roll motion. The three design parameters for the gyroscope become the flywheel's moment of inertia, its angular spin velocity and its controlled precession rate. The precession rate is designed to be in the neighborhood of the vessel's natural roll frequency, which given above by $\omega_\phi = \sqrt{g\,\overline{GM}_R}\,/\,i_r$ and equals about 3 rad/s for the T-Craft. The flywheel spin rate is set to

$\omega_f = 10,000\,\text{rpm} = 1,047\,\text{rad/s}$ to comply with existing industry specs, thus requiring the gyroscope flywheel to have a minimum moment of inertia of

$$I_{f\min} = \frac{M_R}{\omega_p \omega_f} \Rightarrow \frac{9,370 kNm}{\left(3\frac{rad}{s}\right)\left(1047\frac{rad}{\text{s}}\right)} = 2,940\,\text{kg m}^2 \qquad (6.2)$$

If steel is used to make the flywheel and its shape is a cylindrical tube as shown in Figure 6.3 with moment of inertia about the spin axis as $I_f = \frac{1}{2} m_f \left(r_2^2 - r_1^2\right)$ it would have the dimensions shown in Table 6.1. Given that the resulting moment of inertia for the cylindrical tube shape of 3,453 Kgm^2 is greater than the minimum flywheel inertia introduces the flexibility to vary the spin angular velocity in compensation.

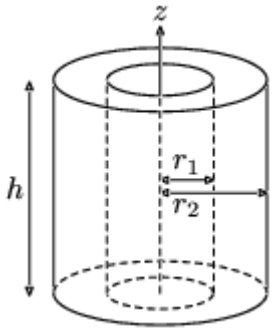

Figure 6.3: Cylindrical Tube

Table 6.1: Designed parameters of Gyroscope Flywheel

Metric	Value
Density of steel [kg/m^3]	7850
Inner radius, r_1 [m]	0.6
Outer radius, r_2 [m]	0.8
Height, h [m]	1
Mass, m_f [kg]	6,905
Moment of Inertia, I_f [kgm^2]	3,453

6.2. **Equations of Motion of the Gyroscope**

In deriving the equations of motion of the gyroscope we start by considering a rigid body that rotates in 3-dimensions and invoke the dynamical law: *The time rate of change of the angular momentum of a rigid body rotating about any axis is equal to the moment of the applied external forces about the same axis* [4].

$$\frac{d\mathbf{H}}{dt} = \mathbf{M} = M_x\mathbf{i} + M_y\mathbf{j} + M_z\mathbf{k} \tag{6.3}$$

If the time rate of change equals zero, it expresses the law of Conservation of Angular Momentum. On a fixed *O-XYZ* coordinate system, the above law for a moving rigid body, in component form with respect to the fixed coordinate system looks as follows

$$\begin{aligned} \frac{dH_x}{dt} + H_z\omega_y - H_y\omega_z &= M_x \\ \frac{dH_y}{dt} + H_x\omega_z - H_z\omega_x &= M_y \\ \frac{dH_z}{dt} + H_y\omega_x - H_x\omega_y &= M_z \end{aligned} \tag{6.4}$$

If the axes *OX*, *OY*, *OZ* coincide with the principal axes of inertia of the body, then

$$H_x = J_R\omega_x,\ H_y = I_y\omega_y,\ H_z = I_z\omega_z \tag{6.5}$$

where J_R is the moment of inertia of the ship about the roll axis. Since the gyroscope is constrained in this DOF, making its angular velocity zero, we choose to

model the roll of the ship instead of the trivial roll motion of the gyroscope. Furthermore, if the body is dynamically symmetrical about the vertical z-axis ($I_x = I_y$) the equations of motion of a rigid body about a fixed point simplify to (6.6).

$$\begin{aligned} I_x \frac{d\omega_x}{dt} + \left(I_z - I_y\right)\omega_y\omega_z &= M_x \\ I_y \frac{d\omega_y}{dt} + \left(I_x - I_z\right)\omega_x\omega_z &= M_y \\ I_z \frac{d\omega_z}{dt} + \left(I_x - I_y\right)\omega_x\omega_y &= M_z \end{aligned} \tag{6.6}$$

Equations (6.4) and (6.6) are known as *Euler's Dynamical Equations* and was used above to design the flywheel of the gyroscope letting $d\mathrm{H}/dt = 0$.

6.3. **Active-Type (Sperry) Gyroscope Stabilizer**

To arrive at the final form of the equations of motion for the gyroscope, the *Euler's Dynamical Equations* need to be adapted to correspond with the gyroscopic parameters using the form of (6.4). Each variable is projected onto the inertial *O-XYZ* coordinate system by performing the flowing transformations

$$\omega_{x'} = -\dot{\phi}\cos\theta,\ \omega_{y'} = \dot{\theta},\ \omega_{z'} = -\dot{\phi}\sin\theta \tag{6.7}$$

Hence

$$H_{x'} = -J_R\dot{\phi}\cos\theta,\ H_{y'} = I_y\dot{\theta},\ H_{z'} = I_f\left(\omega_f - \dot{\phi}\sin\theta\right) = I_f\omega_f \tag{6.8}$$

Since $\dot{\phi}$ and θ are assumed to be small. Differentiating in time gives

$$\frac{dH_{x'}}{dt} = -J_R\left(\ddot{\phi}\cos\theta - \dot{\phi}\dot{\theta}\cos\theta\right) = -J_R\ddot{\phi}\cos\theta,\ \frac{dH_{y'}}{dt} = I_y\ddot{\theta},\ \frac{dH_{z'}}{dt} = 0 \qquad (6.9)$$

Plugging in these expressions and making the assumption that $\cos\theta = 1$ readily forms the following equations, which describe the ships motion about its roll axis and the gyroscope's motion about its precession axis.

Ship Roll Motion $$J_R\ddot{\phi} + K\dot{\phi} - I_f\omega_f\dot{\theta} + \Delta\overline{GM}_R\phi = M_R \qquad (6.10)$$

Gyroscope Precession Motion $$I_{gy}\ddot{\theta} + I_f\omega_f\dot{\phi} = -N \qquad (6.11)$$

where I_{gy} denotes the moment of inertia of the gyroscope's flywheel along the y-axis, N denotes the variable control moment provided by the gyroscope's actuators along the precession axis, and K denotes the skin friction between water and the ship's hull. Since this variable moment is controlled through the rolling of the ship, one would think it is reasonable to assume that the applied precession moment is proportional to the angular velocity of the ship's roll. This stabilizing action will supplement the gyroscope's flywheel moment to oppose the ship's rolling. This assumption leads to the result that setting $N = Q\dot{\phi}$, where Q denotes a positive constant, can reduce the roll as much as desired provided the angular momentum $I_f\omega_f$ is sufficiently large. This assumption only holds true when the ship's course is a straight line or when the course curves in the same direction as the spin of the flywheel. Given the known fact that a Sperry stabilizer works for courses in any direction another relationship must be found.

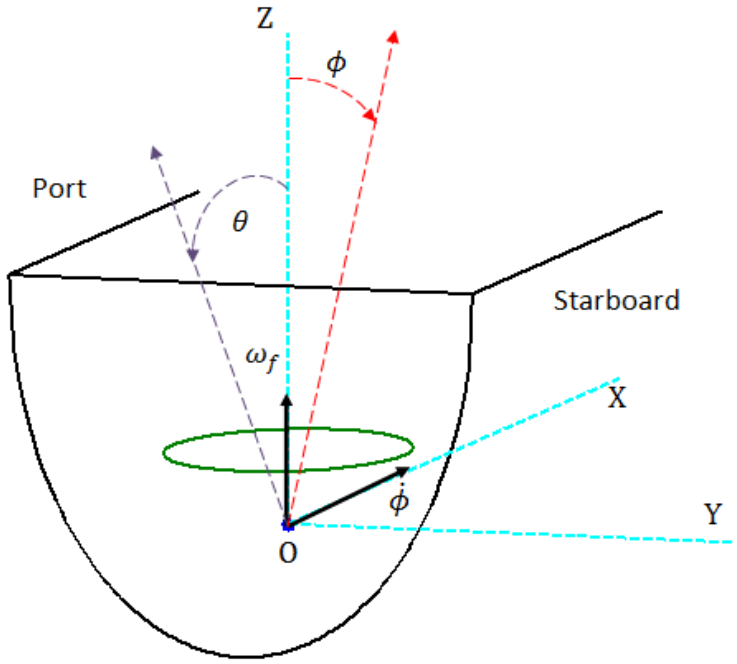

Figure 6.4: Degrees of freedom of gyroscope mounted on T-Craft

Another approach is proposed and Figure 6.4 is used to visualize the argument. If the controlled precession moment acts in the negative y-direction, making θ negative and clockwise (looking from starboard) and given that the flywheel's moment acts along the positive z-axis, a positive roll ϕ can be quenched. In other words, if the ship's roll angular velocity is positive, the gyro's precession angular velocity must be negative to produce an opposing roll moment. This fact leads to the relationship $\dot{\theta} = -m\dot{\phi}$, where m is a positive constant, holds for any course curves direction, and acts as a linear state-feedback controller term. The controlled moment about the precession axis is now assumed to depend on time, denoted by $R(t)$ and can be computed once ϕ is found. The above equations are now replaced by the following

Ship Roll Motion $$J_R\ddot{\phi} + K\dot{\phi} - I_f\omega_f\dot{\theta} + \Delta\overline{GM}_R\phi = M_W \tag{6.12}$$

Gyroscope Precession Motion $$I_{gy}\ddot{\theta} + I_f \omega_f \dot{\phi} = R(t) \tag{6.13}$$

Linear state feedback controller $$\dot{\theta} = -m\phi \tag{6.14}$$

where $M_W = g\Delta\overline{GM}_R \frac{2\pi\zeta_o}{\lambda}\sin(\omega_W t)$ is the ocean wave moment on the roll axis.

Solving for the roll variable ϕ

To solve for ϕ we begin by plugging the linear controller into the ship roll motion equation, making it purely a function of ϕ

$$J_R\ddot{\phi} + (K + I_f \omega_f m)\dot{\phi} + \Delta\overline{GM}_R\phi = M_W \tag{6.15}$$

Since it is reasonable to assume the solution is periodic, we let $\phi = ae^{rt}$, then plug it into the above equation and divide by ae^{rt} to produce the characteristic equation below for the homogenous solution

$$J_R r^2 + (K + I_f \omega_f m)r + \Delta\overline{GM}_R = 0 \tag{6.16}$$

Solving for r gives

$$r = \frac{-(K + I_f \omega_f m) \pm i\sqrt{4J_R\Delta\overline{GM}_R - (K + I_f \omega_f m)^2}}{2J_R} \tag{6.17}$$

The square root term must be imaginary since we know that the solution will naturally oscillate. Plugging r into the assumed solution produces the following result

$$\phi = \exp\left[-\frac{\left(K + I_f \omega_f m\right)t}{2J_R}\right]\left(c_1 \sin \delta t + c_1 \cos \delta t\right) \tag{6.18}$$

where

$$\delta = \frac{\sqrt{4J_R \Delta\overline{GM}_R - \left(K + I_f \omega_f m\right)^2}}{2J_R}$$

From the exponent term of ϕ it is clear that the gyroscopic moment assists in making the damping more rapid. To find the particular solution we let

$$\phi = P_1 \sin \omega_W t + P_2 \cos \omega_W t \tag{6.19}$$

then compute its first and second derivatives with respect to time, plug them into the characteristic equation and set equal to the ocean wave moment. The results are given below in (6.20).

$$\begin{gathered}\left(\Delta\overline{GM}_R - J_R\omega_W^2\right)P_1 - \omega_W\left(K + I_f\omega_f m\right)P_2 = g\Delta\overline{GM}_R\frac{2\pi\zeta_o}{\lambda} \\ \omega_W\left(K + I_f\omega_f m\right)P_1 + \left(\Delta\overline{GM}_R - J_R\omega_W^2\right)P_2 = 0\end{gathered} \tag{6.20}$$

Solving for P_1 and P_2 gives

$$\begin{aligned}P_1 &= \frac{g\Delta\overline{GM}_R\frac{2\pi\zeta_o}{\lambda}\left(\Delta\overline{GM}_R - J_R\omega_W^2\right)}{\left(\Delta\overline{GM}_R - J_R\omega_W^2\right)^2 + \omega_W^2\left(K + I_f\omega_f m\right)^2} \\ P_2 &= \frac{-g\Delta\overline{GM}_R\frac{2\pi\zeta_o}{\lambda}\omega_W\left(K + I_f\omega_f m\right)}{\left(\Delta\overline{GM}_R - J_R\omega_W^2\right)^2 + \omega_W^2\left(K + I_f\omega_f m\right)^2}\end{aligned} \tag{6.21}$$

These constants give a particular solution of

$$\phi = \frac{g\Delta\overline{GM}_R \dfrac{2\pi\zeta_o}{\lambda}}{\left(\Delta\overline{GM}_R - J_R\omega_W^2\right)^2 + \omega_W^2\left(K + I_f\omega_f m\right)^2}\begin{bmatrix}\left(\Delta\overline{GM}_R - J_R\omega_W^2\right)\sin\omega_W t + \\ \omega_W\left(K + I_f\omega_f m\right)\cos\omega_W t\end{bmatrix}$$

and is simplified to

$$\boxed{\begin{aligned}\phi(t) &= \frac{g\Delta\overline{GM}_R \dfrac{2\pi\zeta_o}{\lambda}}{\sqrt{\left(\Delta\overline{GM}_R - J_R\omega_W^2\right)^2 + \omega_W^2\left(K + I_f\omega_f m\right)^2}}\sin\left(\omega_W t - \gamma\right) \\ \gamma &= \tan^{-1}\frac{\omega_W\left(K + I_f\omega_f m\right)}{\Delta\overline{GM}_R - J_R\omega_W^2}\end{aligned}} \qquad (6.22)$$

From the above solution to the roll motion it is evident that the roll amplitude can be decreased by increasing the gyroscope's angular momentum $I_f\omega_f$, either by spinning it faster or increasing its moment of inertia.

To find the controlled moment about the precession axis $R(t)$, we compute $\dot{\phi}$, then $\dot{\theta}$, differentiating gives $\ddot{\theta}$, then solve for $R(t)$ from the precession motion equation.

$$\dot{\phi} = \frac{\omega_W g\Delta\overline{GM}_R \dfrac{2\pi\zeta_o}{\lambda}}{\sqrt{\left(\Delta\overline{GM}_R - J_R\omega_W^2\right)^2 + \omega_W^2\left(K + I_f\omega_f m\right)^2}}\cos\left(\omega_W t - \gamma\right) \qquad (6.23)$$

$$\dot{\theta} = \frac{-m\omega_W g\Delta\overline{GM}_R \dfrac{2\pi\zeta_o}{\lambda}}{\sqrt{\left(\Delta\overline{GM}_R - J_R\omega_W^2\right)^2 + \omega_W^2\left(K + I_f\omega_f m\right)^2}}\cos\left(\omega_W t - \gamma\right) \qquad (6.24)$$

$$\ddot{\theta} = \frac{m\omega_W^2 g\Delta\overline{GM}_R \frac{2\pi\zeta_o}{\lambda}}{\sqrt{\left(\Delta\overline{GM}_R - J_R\omega_W^2\right)^2 + \omega_W^2\left(K + I_f\omega_f m\right)^2}}\sin\left(\omega_W t - \gamma\right) \tag{6.25}$$

$$R(t) = \omega_W g\Delta\overline{GM}_R \frac{2\pi\zeta_o}{\lambda}\left[\frac{\left(I_{gy}m\omega_W\right)^2 + \left(I_f\omega_f\right)^2}{\left(\Delta\overline{GM}_R - J_R\omega_W^2\right)^2 + \omega_W^2\left(K + I_f\omega_f m\right)^2}\right]^{\frac{1}{2}}\sin\left(\omega_W t - \gamma + \beta\right)$$

$$\beta = \tan^{-1}\frac{I_f\omega_f}{I_{gy}m\omega_W} \tag{6.26}$$

The periodic nature of the controlled moment gives credence to its desire to track the roll motion and produce a stabilizing moment to counteract the roll as it occurs in real time. The only difference between the two motions is the phase by the angle β, which since the numerator will dominate is likely to be near 90 degrees.

6.4. **Gyroscope Simulation Results**

For the control gyroscope simulation, the ship system was modeled as half cylinders, the gravity and buoyancy forces as a second order spring-mass-damper system and the wave model as a sum of linear waves weighted by frequency according to the PM Spectrum for SS 4. Table 6.2 shows the parameter values from the above results and the simulation. The simulation result shows that the gyroscope design complies with the original roll angle amplitude stability requirement of 1 degree. The controller gain value required to reach this stability threshold is $m = 7,000$ and translates into an upper bound of 400 kNm for the precessional moment that the gyroscope must output.

Figure 6.5 shows the simulation results of the roll angle evolution with time while the gyro is off and while it is on. The gyroscope's effectiveness at reducing the T-Craft's roll amplitude is clearly observed. Figure 6.6 shows the controlled precession moment of the gyroscope, which somewhat resembles the shape of the roll evolution while the gyro is off. Note on Figure 6.6 the time scale starts at 100 seconds since that is when the gyro turns on.

Table 6.2: Gyroscope Control Parameters

Metric	Value
Gain, $\boldsymbol{m}$	7,000
Gamma, $\boldsymbol{\gamma}$ [deg]	0.49
Beta, $\boldsymbol{\beta}$ [deg]	16
Gyro Off Max Roll, $\boldsymbol{\phi}$ [deg]	89
Gyro On Max Roll, $\boldsymbol{\phi}$ [deg]	1
Max Control Effort, $\boldsymbol{R(t)}$ [kNm]	400

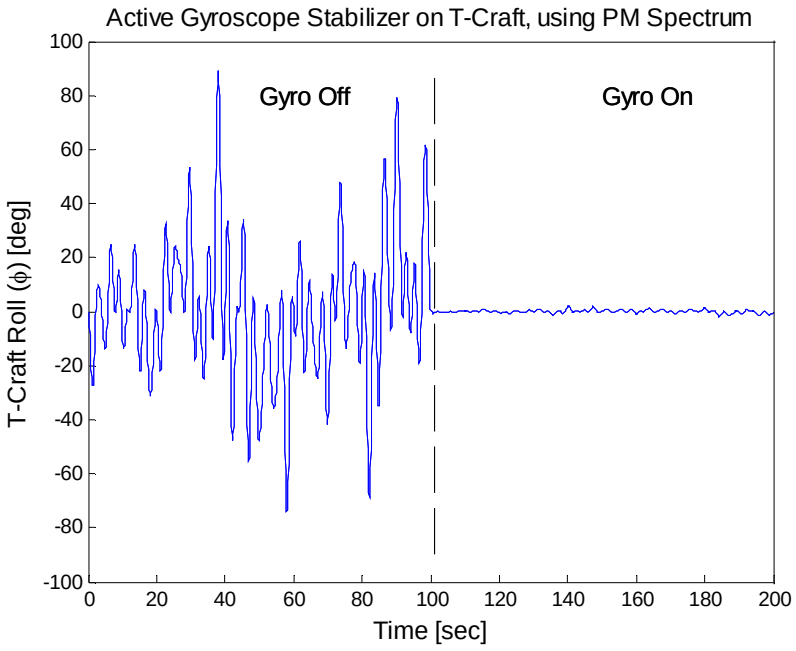

Figure 6.5: Simulation of gyroscope reducing roll angle

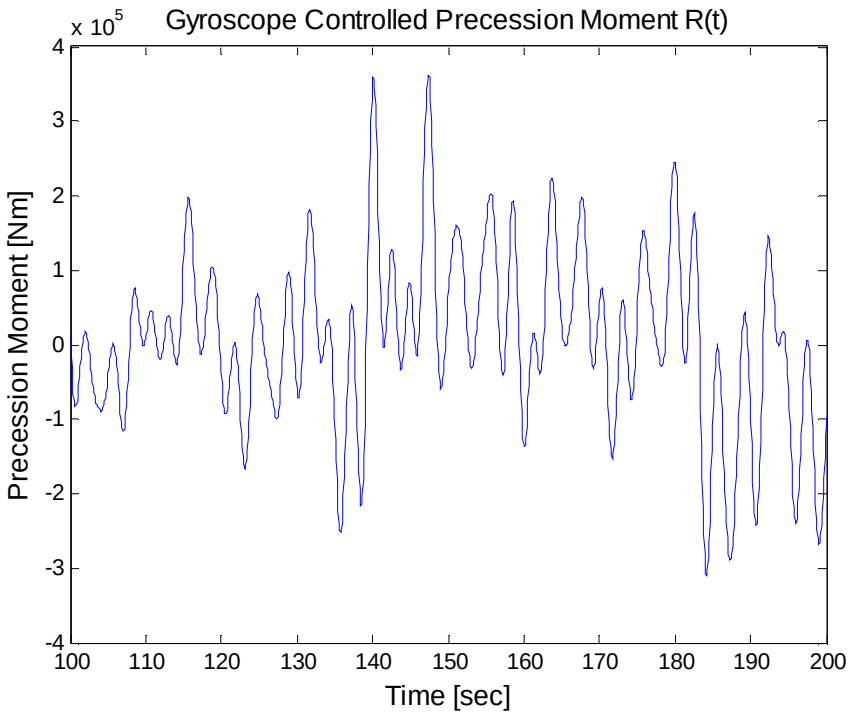

Figure 6.6: Controlled Precession Moment

6.5. **Dimensions and Power Requirements**

Comparing the upper bound of 400 kNm for the precessional moment to the current industry maximum torque output of about 6,000 kNm in roll stabilizers demonstrates the feasibility of the stabilizing gyroscope concept. The vendor ShipDynamics[1] sells a gyro with model number GYR256 with maximum torque

[1] Ship Dynamics Spec Sheet http://www.shipdynamics.com/assets/public/File/Gyro%20size%20range_PDF%20version_R6000h_2009-07-07.pdf

output about the x-axis of 5,005.1 kNm. The dimensions of this model are $l \times w \times h = 5.9 \times 3.0 \times 3.3$ m, weighs 100.3 metric tons and requires 9 motors with 30kW each of power. Based on the half cylinder ship model it is proposed that two gyro's of the GYR256 model will suffice for the T-Craft application and can be installed in the multiple transverse configuration. The gyroscope unit can be mounted anywhere on the vessel, longitudinally, transversely or multiple transversely. Since the metacentric height greatly influences the gyro requirements and given that the metacentric height in the model is a really conservative estimate being an order of magnitude greater than common ship metacentric heights, the actual gyro size and power for the T-Craft will be less than proposed here.

6.6. **Extremum Seeking on Gyroscope Parameters**

Due to the various tunable parameters in the design of a control moment gyroscope, it is a good candidate to apply extremum seeking and optimize the parameters for a given cost function. The tunable parameters are: flywheel moment of inertia, spin speed and precession rate. As an initial effort a cost plot is constructed to show the dependence of the roll amplitude on flywheel moment of inertia and spin rate as shown in the left plot of Figure 6.7 similar to what is shown above in the left plots of Figure 4.3-Figure 4.5. Since the behavior of the cost gradually decreases with increasing inertia and spin rate, a penalty function in parabolic form as shown in equation (6.27) is additively introduced to the cost to make it more convex to produce the right plot of Figure 6.7. In equation (6.27) the minimum values are given as $\omega_f^* = 1000,\ I_f^* = 4000$ which after applying the ES algorithm should be the values the

flywheel's spin rate and moment of inertia respectively converge towards. An analogous scenario where the moment of inertia changes is when an ice skater extends his arms inward and outward while spinning to influence the spin rate. A similar concept can be applied to the flywheel design to allow for a certain range of inertias and thus spin rates to choose from that can be used to optimize over per sea state.

$$Penalty = \frac{50}{1500^2}\left(\omega_f^* - 1000\right)^2 + \frac{2}{1500^2}\left(I_f^* - 4000\right)^2 \tag{6.27}$$

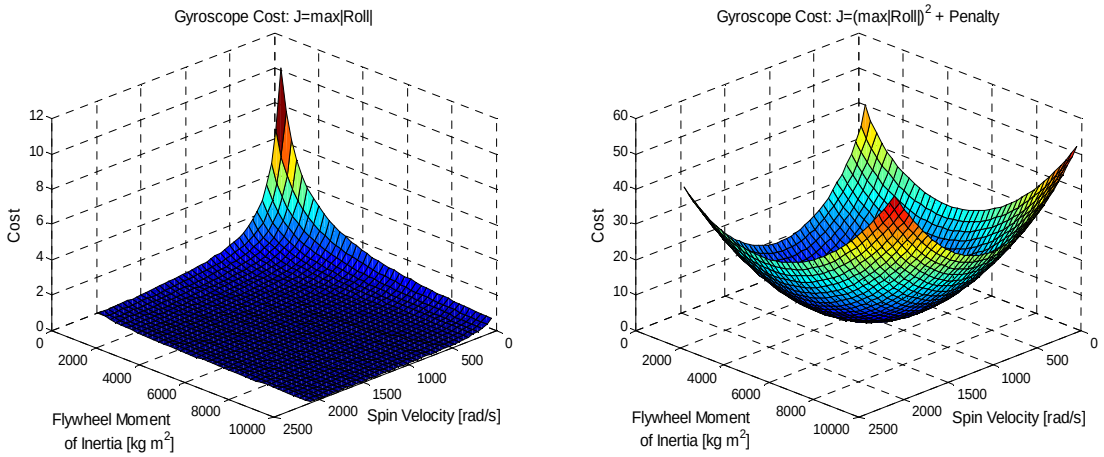

Figure 6.7: Gyroscope cost without (left) and with (right) penalty function

The ES application concept to optimize the gyroscope parameters is depicted in Figure 6.8 as a Simulink block diagram. Essentially it solves the roll differential equation of an ocean vessel coupled with the gyroscope controller and updates the flywheel's moment of inertia and spin rate per times step as influenced by the multi-parameter ES loop. An amplitude extraction block as in Figure 4.1 is included in this application, the roll signal is then introduced to the penalty, then through the ES loop then back into the equations of roll motion.

The ES tuning of gyroscope parameters concept still needs more work to be fully implementable. For instance, the cost function form should be modified to tailor to quick parameter value convergence and whether it is added or multiplied to the roll amplitude signal should also be explored.

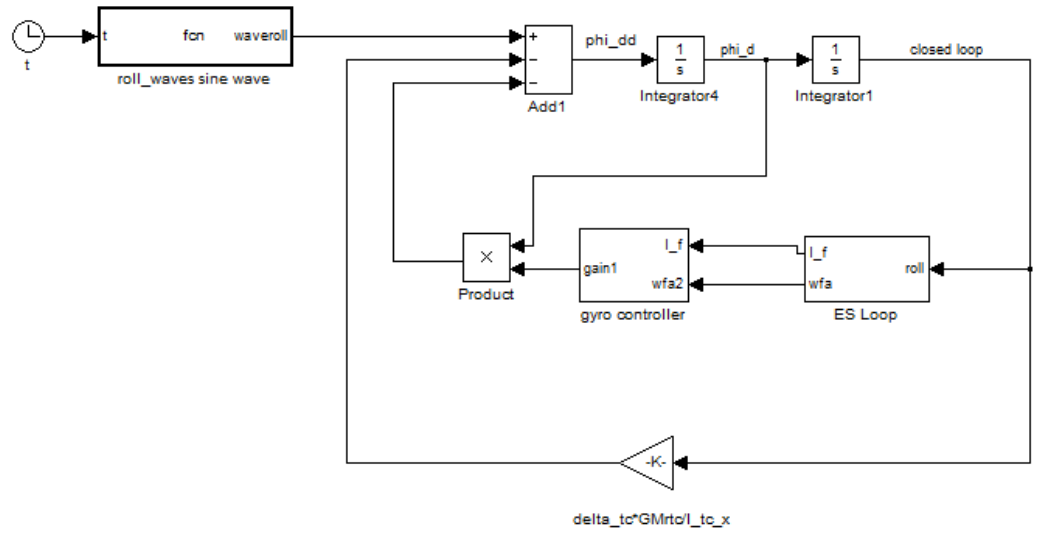

Figure 6.8: Simulink block diagram of ES on gyroscope parameters

Chapter 7. Future Work

Some of the control methods explored throughout the thesis can be expanded upon to improve performance and possibly cost of design. The passive control method of applying shock absorbers can be improved by tuning the damper values using extremum seeking. The concept exists in the automotive industry in the form of magnetorheological dampers, which change their damping coefficient by exposing the inner fluid to a magnetic field. Actively modifying the dampers is great for adapting to the different sea state characteristics and allows for a more robust control design. This is another application of extremum seeking that has not been previously explored. Using extremum seeking to tune the gyroscope parameter values is also an unsolved problem that can prove to be a robust tool for ship stabilization.

Other methods to investigate in further research for stabilizing the T-Craft is heave and pitch control using inflatable skirts beneath the hull. Since the T-Craft may be a catamaran vessel (double hull), this is a likely control option. Also, installing water tanks to create an opposing moment to the roll motion can assist in reducing the roll amplitude of the T-Craft. In this application, each hull can be designed to act a tank where a sufficiently powerful water pump is used to transfer the fluid between the tanks.

There are many methods that exist in controlling and stabilizing ships at sea and many that don’t exist yet. In this thesis some of these methods were explained, simulated and results documented. It is dependent on further research to prove the feasibility of these other control design concepts.

Appendix

A 1. Time Plots from Passive Control Investigation

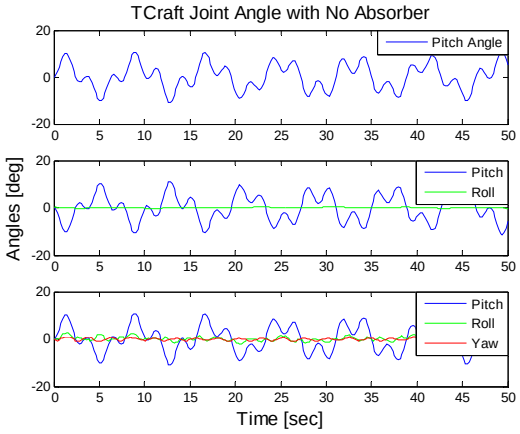

Figure A.1: TC Joint: Angles with No Absorber

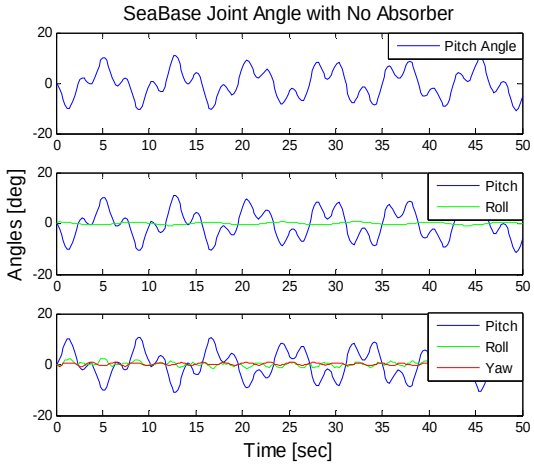

Figure A.2: SB Joint: Angles with No Absorber

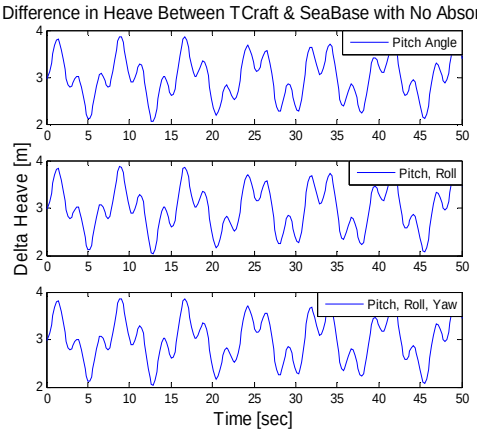

Figure A.3: Delta Heave with No Absorber

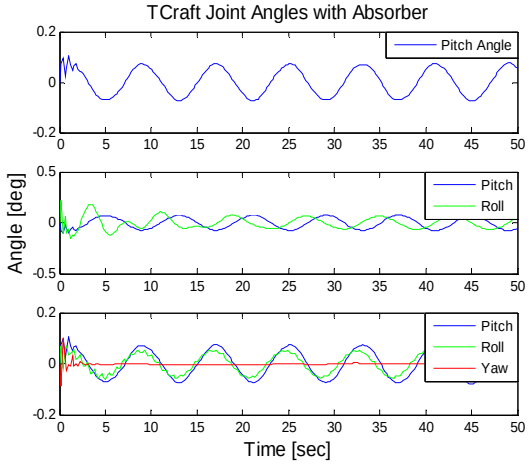

Figure A.4: TC Joint: Angles with Absorber

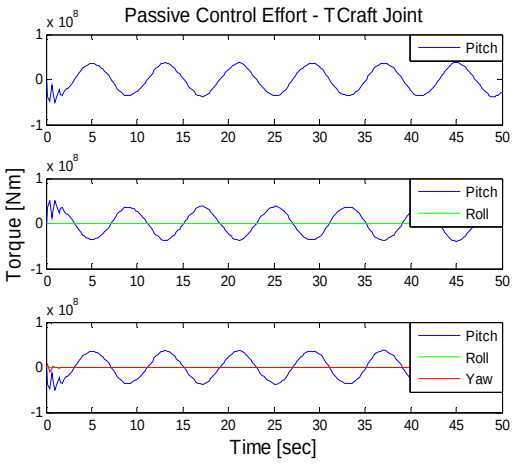

Figure A.5: TC Joint: Passive Control Effort

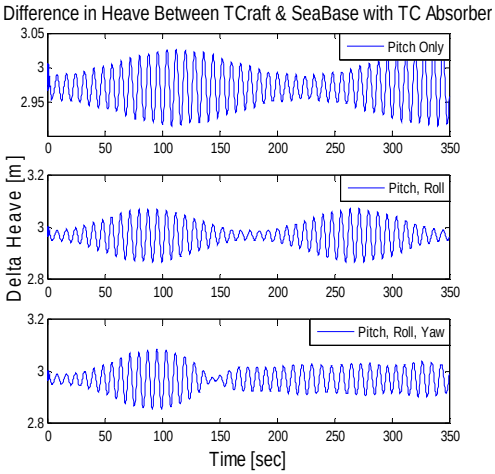

Figure A.6: TC Joint with Absorber: Delta Heave

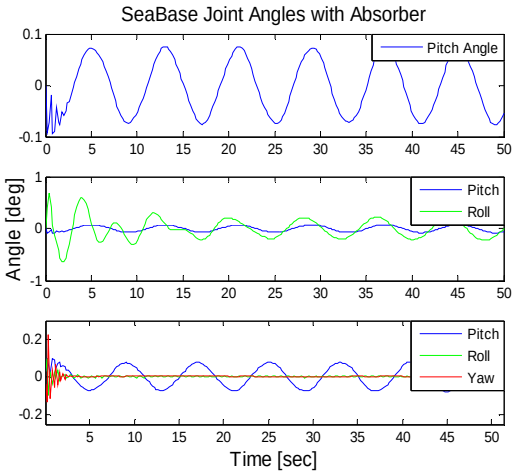

Figure A.7: SB Joint: Angles with Absorber

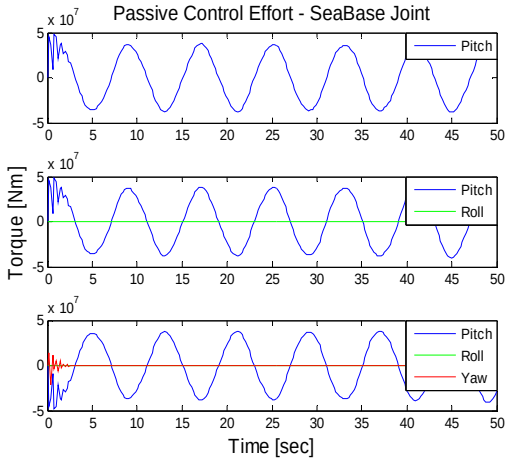

Figure A.8: SB Joint: Passive Control Effort

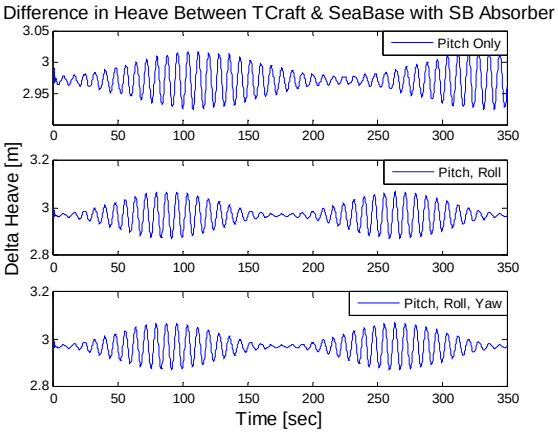

Figure A.9: SB Joint with Absorber: Delta Heave

A 2. MATLAB initialization script for SimMechanics model

```
%The following program is a general-purpose m-file to initialize
variables in the Simulink/SimMechanics two ship and ramp models.
rtime=150;
srate=15;
alpha_init=pi/4;
fs=13;      %font size
g=9.806;    %m/s^2

%Sea Base mass + dimensions
m_sb= 45359237;   %kg   50,000 tons
L_sb= 200;        %m
r_sb= 15;         %m
w_sb= 2*r_sb;
delta_sb=m_sb*g;  %weight of water displaced by TC =displacement

%T-craft mass + dimensions
m_tc= 2721554.22; %kg(1000kg=1metric ton=tonne)
L_tc= 40;         %m
r_tc= 8;          %m
w_tc= 2*r_tc;
delta_tc=m_tc*g;%weight of water displaced by TC =displacement

%Ramp mass + dimensions
%Assume Steel Ramp
rho_steel= 7850;  %kg/m^3 density of steel
L_ramp= 5;        %m   82.021 feet
w_ramp= 4;        %m   13.1234 feet
h_ramp= 0.0508;   %m   2 inches
V_ramp= L_ramp*w_ramp*h_ramp;
m_ramp= rho_steel*V_ramp;

%Moment of Inertia Tensor of Ship
%Assume Ship is modeled as half cylinder
```

```
% Ixx= (1/2 - 16/(9pi^2))*mr^2
% Iyy= 1/4*mr^2 + 1/2*(mL^2)
% Izz= (1/4 - 16/(9pi^2))*mr^2 + 1/12*(mL^2)

% Moment of Inertia of SeaBase through CG CS
I_sb= [(1/2- 16/(9*pi^2))*m_sb*r_sb^2 0 0;...
        0 (1/4-16/(9*pi^2))*m_sb*r_sb^2 + (1/12)*m_sb*L_sb^2 0;...
        0 0 (1/4)*m_sb*r_sb^2 + (1/12)*m_sb*L_sb^2 ];

%Moment of Inertia of T-craft through CG CS
I_tc= [(1/2- 16/(9*pi^2))*m_tc*r_tc^2 0 0;...
        0 (1/4-16/(9*pi^2))*m_tc*r_tc^2 + (1/12)*m_tc*L_tc^2 0;...
        0 0 (1/4)*m_tc*r_tc^2 + (1/12)*m_tc*L_tc^2];

%Moment of Inertia Tensor of Ramp
%Assume Ramp is modeled as a thin rectangular prism
%      [ 1/12mw^2  0       0  ]
%   I= [ 0  1/12m(w^2+L^2) 0  ]
%      [ 0         0 1/12mL^2 ]

%Moment of Inertia of Ramp through CG CS
I_ramp= [(1/12)*m_ramp*(w_ramp^2) 0 0; 0
(1/12)*m_ramp*((w_ramp^2)+(L_ramp^2)) 0; 0 0
(1/12)*m_ramp*(L_ramp^2)];

%Draught Information
T_tc= 1/4*r_tc;
T_sb= 1/2*r_sb;
%Waterplane Area
Aw_tc= 2*L_tc*sqrt(r_tc^2-(r_tc-T_tc)^2);
Aw_sb= 2*L_sb*sqrt(r_sb^2-(r_sb-T_sb)^2);
%Density of sea water and gravity
rho= 1025;  %kg/m^3

%Wave Information
%8 seconds in between waves
time= 8;           %s
f= 1/time;         %linear frequency Hz
omega= 2*pi*f;     %angular frequency rad/s
zetaknot=1;        %wave amplitude
A_tc= rho*g*Aw_tc*zetaknot; %Wave Force Amplitude for TC in Heave
A_sb= rho*g*Aw_sb*zetaknot; %Wave Force Amplitude for SB in Heave

%Assume there is 125 ft between wave peaks
lambda= 38.1;    %125 ft

%Metacentric Heights
%Roll Motions
GMrsb=(r_sb-(2/3*r_sb^3*((sin(acos((r_sb-
T_sb)/r_sb))^3))/(r_sb^2*acos((r_sb-T_sb)/r_sb)-(r_sb-
T_sb)*sqrt(r_sb^2-(r_sb-T_sb)^2)))+...
    (((L_sb*w_sb^3)/12)/(L_sb*(r_sb^2*acos((r_sb-T_sb)/r_sb)-(r_sb-
T_sb)*sqrt(r_sb^2-(r_sb-T_sb)^2))))-(r_sb-((4*r_sb)/(3*pi))));
```

```
GMrtc=(r_tc-(2/3*r_tc^3*((sin(acos((r_tc-
T_tc)/r_tc))^3))/(r_tc^2*acos((r_tc-T_tc)/r_tc)-(r_tc-
T_tc)*sqrt(r_tc^2-(r_tc-T_tc)^2)))+...
    (((L_tc*w_tc^3)/12)/(L_tc*(r_tc^2*acos((r_tc-T_tc)/r_tc)-(r_tc-
T_tc)*sqrt(r_tc^2-(r_tc-T_tc)^2))))-(r_tc-((4*r_tc)/(3*pi))));

%Pitch Motions
GMpsb=(0.5*T_sb+(((w_sb*L_sb^3)/12)/(L_sb*(r_sb^2*acos((r_sb-
T_sb)/r_sb)-(r_sb-T_sb)*sqrt(r_sb^2-(r_sb-T_sb)^2))))-r_sb/2);
GMptc=(0.5*T_tc+(((w_tc*L_tc^3)/12)/(L_tc*(r_tc^2*acos((r_tc-
T_tc)/r_tc)-(r_tc-T_tc)*sqrt(r_tc^2-(r_tc-T_tc)^2))))-r_tc/2);

%Account for the difference in forces
eta_rolltc= (rho*Aw_tc)/(m_tc);
eta_rollsb= (rho*Aw_sb)/(m_sb);

eta_pitchtc= (rho*Aw_tc)/(m_tc);
eta_pitchsb= (rho*Aw_sb)/(m_sb);
%Spring Contstant to SImulate Gravity and Buoyancy
P3tc= rho*g*Aw_tc;  %Heave Motions
P3sb= rho*g*Aw_sb;
R1sb= g*m_sb*GMrsb*eta_rollsb; %Roll Motions
R1tc= g*m_tc*GMrtc*eta_rolltc;
R2sb= g*m_sb*GMpsb*eta_pitchsb; %Pitch Motions
R2tc= g*m_tc*GMptc*eta_pitchtc;

%Damping Coefficients
b=0.01;
BP3tc= b;        %Heave
BP3sb= b;
BR1tc= 2*m_tc*((w_tc/(2*sqrt(3)))^2)*b;  %Roll
BR1sb= 2*m_sb*((w_sb/(2*sqrt(3)))^2)*b;
BR2tc= 2*m_tc*((L_tc/(2*sqrt(3)))^2)*b;  %Pitch
BR2sb= 2*m_sb*((L_sb/(2*sqrt(3)))^2)*b;
```

A 3. Pierson-Moskowitz ocean model script

```
%% Pierson Moskowitz Spectrum of Ocean Waves
run Research_Project_Data_updating_phi
wend=3;
w=linspace(0,wend,wend*50);
H1=1.875;   % for sea state 4 (Moderate) Hs = 1.25-2.5 m
A=8.1e-3*9.806^2;
B1=3.11/H1^2;
S1=A*w.^(-5).*exp(-B1*w.^(-4)); %SS4

% Plotting the wave with time
N=100;    % # of waves added together
dw=w(2);
t=linspace(0,rtime,rtime*srate);
wave_ss4(1,:)=zeros(1,length(t));%initialize wave vector
tot_wave=zeros(1,length(t));
```

```
for i=2:N
    wave_ss4(i,:)=sqrt(2*S1(i)*dw).*sin(w(i)*t+2*pi*rand);
%individual sine waves
    tot_wave=tot_wave+wave_ss4(i,:);  %vector of wave amplitudes
end
```

A 4. Passive Control Script

```
%Initializations of Damping/Spring Constants
RPJD=1e2;   %Right Pitch Joint Damper
RRJD=1e2;
RYJD=1e2;
RRK=1e5;    %Right Roll Spring Constant for PRY Joint Case, No
Control
RYK=1e6;    %Right Yaw Spring Constant for PRY Joint Case, No Control
LPJD=1e2;   %Left Pitch Joint Damper
LRJD=1e2;
LYJD=1e2;
LRK=1e2;
LYK=1e6;
run Research_Project_Data_updating_phi

rtime=50;
L_ramp=5;
phi_init=pi/4;
%% No Control & No Damper, SeaBase and TCraft Joint
%TCraft not grounded
j=1; %1,2,3 are for SB Joint, 4,5,6 TC Joint
fz=13;
%pitch only
        sim  Simulation_Pitch_UC
        figure(1)
        subplot(3,1,1),plot(tout, RPA(:,2))
        title('SeaBase Joint Angle with No Absorber','FontSize',fz)
        legend('Pitch Angle')

        figure(2)
        heave1=abs(abs(TCraftZ(:,2))-abs(SeaBaseZ(:,2)));
        subplot(3,1,1),plot(tout, heave1)
        title('Difference in Heave Between TCraft & SeaBase with No
Absorber','FontSize',fz)
        legend('Pitch Angle')

        figure(3)
        subplot(3,1,1),plot(tout, LPA(:,2))
        title('TCraft Joint Angle with No Absorber','FontSize',fz)
        legend('Pitch Angle')

        maxLA_P(j)=max(abs(LPA(:,2)));
        maxRA_P(j)=max(abs(RPA(:,2)));
        maxheave(j)=max(abs(TCraftZ(:,2)-SeaBaseZ(:,2)));
```

```
%Extract angles from Rotation Matrices
N=length(Rot_r(:,1));
    for i=1:N
        theta_r(i) = asind(-Rot_r(i,7));                    % Pitch
        psi_r(i) = asind(Rot_r(i,4)/cosd(theta_r(i)));      % Yaw
        phi_r(i) = asind(Rot_r(i,8)/cosd(theta_r(i)));      % Roll
    end

sim  Simulation_Pitch_Roll_UC
        figure(1)
        subplot(3,1,2),plot(tout, RPA(:,2),tout,RRA(:,2),'g')
        legend('Pitch','Roll')
        ylabel('Angles [deg]','FontSize',fz)

        figure(2)
        heave1=abs(abs(TCraftZ(:,2))-abs(SeaBaseZ(:,2)));
        subplot(3,1,2),plot(tout, heave1)
        ylabel('Delta Heave [m]','FontSize',fz)
        legend('Pitch, Roll')

        figure(3)
        subplot(3,1,2),plot(tout, LPA(:,2),tout,LRA(:,2),'g')
        legend('Pitch','Roll')
        ylabel('Angles [deg]','FontSize',fz)

        maxLA_PR(j)=max(abs(LPA(:,2)));
        maxLA_PR(j+1)=max(abs(LRA(:,2)));

        maxRA_PR(j)=max(abs(RPA(:,2)));
        maxRA_PR(j+1)=max(abs(RRA(:,2)));
        maxheave(j+1)=max(abs(TCraftZ(:,2)-SeaBaseZ(:,2)));

i=3;    %pitch roll yaw

        sim  Simulation_Pitch_Roll_Yaw_UC
        figure(1)
        subplot(3,1,3),plot(tout,
RPA(:,2),tout,RRA(:,2),'g',tout,RYA(:,2),'r')
        legend('Pitch','Roll','Yaw')
        xlabel('Time [sec]','FontSize',fz)

        figure(2)
        heave1=abs(abs(TCraftZ(:,2))-abs(SeaBaseZ(:,2)));
        subplot(3,1,3),plot(tout, heave1)
        xlabel('Time [sec]','FontSize',fz)
        legend('Pitch, Roll, Yaw')

        figure(3)
        subplot(3,1,3),plot(tout,
LPA(:,2),tout,LRA(:,2),'g',tout,LYA(:,2),'r')
        legend('Pitch','Roll','Yaw')
        xlabel('Time [sec]','FontSize',fz)
```

```
        maxLA_PRY(j)=max(abs(LPA(:,2)));
        maxLA_PRY(j+1)=max(abs(LRA(:,2)));
        maxLA_PRY(j+2)=max(abs(LYA(:,2)));

        MaxLAngles(1:3,1:3)=[maxLA_P(1)          0       0
%Pitch Only                  maxLA_PR(1)  maxLA_PR(2)     0
%Pitch, Roll                 maxLA_PRY(1) maxLA_PRY(2) maxLA_PRY(3)];
%Pitch, Roll, Yaw
        maxRA_PRY(j)=max(abs(RPA(:,2)));
        maxRA_PRY(j+1)=max(abs(RRA(:,2)));
        maxRA_PRY(j+2)=max(abs(RYA(:,2)));
        maxheave(j+2)=max(abs(TCraftZ(:,2)-SeaBaseZ(:,2)));
        MaxRAngles(1:3,1:3)=[maxRA_P(1)          0        0
%Pitch Only                  maxRA_PR(1)  maxRA_PR(2)      0
%Pitch, Roll                 maxRA_PRY(1) maxRA_PRY(2) maxRA_PRY(3)];
%Pitch, Roll, Yaw

        MaxHeave_RLJ = [maxheave(1) maxheave(2) maxheave(3)];
%max heave for no control on either TC/SB joint

%% With Control SB Joint%%%%%%%%%%%%%%%%%%%%%%%%%%%%%%%%%%%%
j=1; %1,2,3 Right Joint, 4,5,6 Left Joint

sim  Simulation_Pitch_RC

    figure(1),subplot(3,1,1),plot(tout, RPA(:,2))
    title('SeaBase Joint Angles with Absorber','FontSize',fz)
    legend('Pitch Angle')

    figure(2), subplot(3,1,1),plot(tout, R_Pitch_feedback(:,2))
    title('Passive Control Effort - SeaBase Joint','FontSize',fz)
    legend('Pitch')

    figure(3)
    heave1=abs(TCraftZ(:,2)-SeaBaseZ(:,2)); %Pos=Tcraft is above SB,
Neg=Tcraft is below SB
    subplot(3,1,1),plot(tout, heave1)
    title('Difference in Heave Between TCraft & SeaBase with SB
Absorber','FontSize',fz)
    legend('Pitch Only')

    maxRA_P(j)=max(abs(RPA(:,2)));
    maxheave(j)=max(abs(TCraftZ(:,2)-SeaBaseZ(:,2)));
    maxRTor_P(j)=max(abs(R_Pitch_feedback(:,2)));

sim  Simulation_Pitch_Roll_RC

    figure(1),subplot(3,1,2),plot(tout, RPA(:,2),tout,RRA(:,2),'g')
    ylabel('Angle [deg]','FontSize',fz)
    legend('Pitch','Roll')

    figure(2), subplot(3,1,2),plot(tout, R_Pitch_feedback(:,2),tout,
R_Roll_feedback(:,2),'g')
```

```
    ylabel('Torque [Nm]','FontSize',fz)
    legend('Pitch','Roll')

    figure(3)
    heave1=abs(abs(TCraftZ(:,2))-abs(SeaBaseZ(:,2)));
    subplot(3,1,2),plot(tout, heave1)
    ylabel('Delta Heave [m]','FontSize',fz)
    legend('Pitch, Roll')

    maxRA_PR(j)=max(abs(RPA(:,2)));
    maxRA_PR(j+1)=max(abs(RRA(:,2)));
    maxheave(j+1)=max(abs(TCraftZ(:,2)-SeaBaseZ(:,2)));
    maxRTor_PR(j)=max(abs(R_Pitch_feedback(:,2)));
    maxRTor_PR(j+1)=max(abs(R_Roll_feedback(:,2)));

sim  Simulation_Pitch_Roll_Yaw_RC

    figure(1),subplot(3,1,3), plot(tout,
RPA(:,2),tout,RRA(:,2),'g',tout,RYA(:,2),'r')
    xlabel('Time [sec]','FontSize',fz)
    legend('Pitch','Roll','Yaw')

    figure(2), subplot(3,1,3),plot(tout, R_Pitch_feedback(:,2),tout,
R_Roll_feedback(:,2),'g',tout, R_Yaw_feedback(:,2),'r')
    xlabel('Time [sec]','FontSize',fz)
    legend('Pitch','Roll','Yaw')

    figure(3)
    heave1=abs(abs(TCraftZ(:,2))-abs(SeaBaseZ(:,2)));
    subplot(3,1,3),plot(tout, heave1)
    xlabel('Time [sec]','FontSize',fz)
    legend('Pitch, Roll, Yaw')

    maxRA_PRY(j)=max(abs(RPA(:,2)));
    maxRA_PRY(j+1)=max(abs(RRA(:,2)));
    maxRA_PRY(j+2)=max(abs(RYA(:,2)));
    maxheave(j+2)=max(abs(TCraftZ(:,2)-SeaBaseZ(:,2)));

    maxRTor_PRY(j)=max(abs(R_Pitch_feedback(:,2)));
    maxRTor_PRY(j+1)=max(abs(R_Roll_feedback(:,2)));
    maxRTor_PRY(j+2)=max(abs(R_Yaw_feedback(:,2)));

    MaxRAngles(1:3,4:6)=[maxRA_P(1)          0         0
%Pitch Only             maxRA_PR(1)  maxRA_PR(2)      0
%Pitch, Roll            maxRA_PRY(1) maxRA_PRY(2) maxRA_PRY(3)];
%Pitch, Roll, Yaw

   MaxHeave_RJC = [maxheave(1) maxheave(2) maxheave(3)];
   MaxRightTorque=[maxRTor_P(1)          0           0
%Pitch Only        maxRTor_PR(1)  maxRTor_PR(2)      0
%Pitch, Roll       maxRTor_PRY(1) maxRTor_PRY(2) maxRTor_PRY(3)];
%Pitch, Roll, Yaw
```

```
%% With Control: TC Joint%%%%%%%%%%%%%%%%%%%%%%%%%%%%%%%%%%%%
j=1; %1,2,3 Right Joint, 4,5,6 Left Joint

sim  Simulation_Pitch_LC

    figure(1),subplot(3,1,1),plot(tout, LPA(:,2))
    title('TCraft Joint Angles with Absorber','FontSize',fz)
    legend('Pitch Angle')

    figure(2), subplot(3,1,1),plot(tout, L_Pitch_feedback(:,2))
    title('Passive Control Effort - TCraft Joint','FontSize',fz)
    legend('Pitch')

    figure(3)
    heave1=abs(TCraftZ(:,2)-SeaBaseZ(:,2)); %Pos=Tcraft is above SB,
Neg=Tcraft is below SB
    subplot(3,1,1),plot(tout, heave1)
    title('Difference in Heave Between TCraft & SeaBase with TC
Absorber','FontSize',fz)
    legend('Pitch Only')

    maxLA_P(j)=max(abs(LPA(:,2)));
    maxheave(j)=max(abs(TCraftZ(:,2)-SeaBaseZ(:,2)));
    maxLTor_P(j)=max(abs(L_Pitch_feedback(:,2)));
sim  Simulation_Pitch_Roll_LC
    figure(1),subplot(3,1,2),plot(tout, LPA(:,2),tout,LRA(:,2),'g')
    ylabel('Angle [deg]','FontSize',fz)
    legend('Pitch','Roll')
    figure(2), subplot(3,1,2),plot(tout, L_Pitch_feedback(:,2),tout,
L_Roll_feedback(:,2),'g')
    ylabel('Torque [Nm]','FontSize',fz)
    legend('Pitch','Roll')
    figure(3)
    heave1=abs(abs(TCraftZ(:,2))-abs(SeaBaseZ(:,2)));
    subplot(3,1,2),plot(tout, heave1)
    ylabel('Delta Heave [m]','FontSize',fz)
    legend('Pitch, Roll')
    maxLA_PR(j)=max(abs(LPA(:,2)));
    maxLA_PR(j+1)=max(abs(LRA(:,2)));
    maxLTor_PR(j)=max(abs(L_Pitch_feedback(:,2)));
    maxLTor_PR(j+1)=max(abs(L_Roll_feedback(:,2)));
    maxheave(j+1)=max(abs(TCraftZ(:,2)-SeaBaseZ(:,2)));
sim  Simulation_Pitch_Roll_Yaw_LC
    figure(1),subplot(3,1,3), plot(tout,
LPA(:,2),tout,LRA(:,2),'g',tout,LYA(:,2),'r')
    xlabel('Time [sec]','FontSize',fz)
    legend('Pitch','Roll','Yaw')
    figure(2), subplot(3,1,3),plot(tout, L_Pitch_feedback(:,2),tout,
L_Roll_feedback(:,2),'g',tout, L_Yaw_feedback(:,2),'r')
    xlabel('Time [sec]','FontSize',fz)
    legend('Pitch','Roll','Yaw')
    figure(3)
    heave1=abs(abs(TCraftZ(:,2))-abs(SeaBaseZ(:,2)));
    subplot(3,1,3),plot(tout, heave1)
```

```
    xlabel('Time [sec]','FontSize',fz)
    legend('Pitch, Roll, Yaw')
    maxLA_PRY(j)=max(abs(LPA(:,2)));
    maxLA_PRY(j+1)=max(abs(LRA(:,2)));
    maxLA_PRY(j+2)=max(abs(LYA(:,2)));

    maxLTor_PRY(j)=max(abs(L_Pitch_feedback(:,2)));
    maxLTor_PRY(j+1)=max(abs(L_Roll_feedback(:,2)));
    maxLTor_PRY(j+2)=max(abs(L_Yaw_feedback(:,2)));
    maxheave(j+2)=max(abs(TCraftZ(:,2)-SeaBaseZ(:,2)));
    MaxLAngles(1:3,4:6)=[maxLA_P(1)          0         0
%Pitch Only              maxLA_PR(1)  maxLA_PR(2)     0
%Pitch, Roll             maxLA_PRY(1) maxLA_PRY(2) maxLA_PRY(3)];
%Pitch, Roll, Yaw
    MaxHeave_LJC = [maxheave(1) maxheave(2) maxheave(3)]; %maximum
heave for the 3 cases using control on TC joint
                  MaxLeftTorque=[maxLTor_P(1)          0          0
%Pitch Only                      maxLTor_PR(1)  maxLTor_PR(2)     0
%Pitch, Roll           maxLTor_PRY(1) maxLTor_PRY(2) maxLTor_PRY(3)];
%Pitch, Roll, Yaw
```

A 5. Active gyroscope simulation script

```
%% Active type (Sperry) Stabilizing Gyroscope Soln. to Eq. of Motion
t=linspace(0,rtime,rtime*5);
fs=12;
% run PM_Spectrum
% using PM Spectrum waves of SS4
wfa=1.0472e3;
m=7000;%linear controller gain, u = -mx
gam=atan(omega*(K+I_f(3,3)*wfa*m)/(delta_tc*GMrtc-
I_tc(1,1)*omega^2));
phi_on =
g*delta_tc*GMrtc*2*pi*tot_wave(length(t)/2+1:end)/lambda/sqrt((delta_
tc*GMrtc-I_tc(1,1)*omega^2 )^2+(omega*(K+I_f(3,3)*wfa*m))^2 ).*
sin(omega*t(length(t)/2+1:end)-gam) ;

% computing the controlled precession moment - R(t) = control effort
beta=atan((I_f(3,3)*wfa)/(I_f(1,1)*m*omega));
r=omega*g*delta_tc*GMrtc*2*pi*tot_wave(length(t)/2+1:end)/lambda
*sqrt(((I_f(1,1)*m*omega)^2+(I_f(3,3)*wfa )^2)/((delta_tc*GMrtc-
I_tc(1,1)*omega^2)^2+(omega^2*(K+I_f(3,3)*wfa*m)^2))).*
sin(omega*t(length(t)/2+1:end)-gam+beta);

%turning off the gyro, ang velocity=0
wfa=0;
gam=atan(omega*(K+I_f(3,3)*wfa*m)/(delta_tc*GMrtc-
I_tc(1,1)*omega^2));
phi_off =
g*delta_tc*GMrtc*2*pi*tot_wave(length(t)/2+1:end)/lambda/sqrt((delta_
tc*GMrtc-I_tc(1,1)*omega^2 )^2+(omega*(K+I_f(3,3)*wfa*m))^2 ).*
sin(omega*t(1:length(t)/2)-gam) ;
phi_gyro=[phi_off phi_on]*180/pi;
```

```
%Roll Reduction using gyroscope
figure(1)
hold on
plot(t,phi_gyro), title('Active Gyroscope Stabilizer on T-Craft,
using PM Spectrum','fontsize',fs)
xlabel('Time [sec]','fontsize',fs)
ylabel('T-Craft Roll ( \phi) [deg]','fontsize',fs)
text(.25*tend,80,'Gyro Off','fontsize',fs)
text(.75*tend,80,'Gyro On','fontsize',fs)
line([tend/2+1 tend/2+1],[-90 90],'LineStyle','--','Color','k')

%Precession moment R(t)
figure(2)
plot(t(length(t)/2+1:end),r), title('Gyroscope Controlled Precession
Moment R(t)','fontsize',fs)
xlabel('Time [sec]','fontsize',fs)
ylabel('Precession Moment [Nm]','fontsize',fs)
```

Bibliography

[1] K. B. Ariyur, M. Krstic. *Real-Time Optimization by Extremum-Seeking Control*. John Wiley & Sons, New York, 2003

[2] A. Biran. *Ship Hydrostatics and Stability*. Oxford: Butterworth-Heinemann, MA, 2003

[3] T. I. Fossen. *Guidance and Control of Ocean Vehicles*. John Wiley & Sons, New York, 1994

[4] J.B. Scarborough. *The Gyroscope, Theory and Applications.* Interscience Publications, New York, 1958

[5] Goldstein, Herbert. *Classical Mechanics 2nd edition*. Reading, Massachusetts: Addison-Wesley Publishing Company, 1980

[6] Oonk, Stephen H., "Wave-Induced Motion of Ramp-Interconnected Craft", (MS thesis, University of California San Diego, 2008).

[7] Carlson, Harold. *Spring Designer's Handbook.* Marcel Dekker, Inc., New York, 1987